



HAL
open science

Measurement of the production and lepton charge asymmetry of W bosons in Pb+Pb collisions at $\sqrt{s_{\text{NN}}} = 2.76$ TeV with the ATLAS detector

G. Aad, S. Albrand, J. Brown, J. Collot, S. Crépé-Renaudin, B. Dechenaux, P.A. Delsart, C. Gabaldon, M.H. Genest, J.Y. Hostachy, et al.

► To cite this version:

G. Aad, S. Albrand, J. Brown, J. Collot, S. Crépé-Renaudin, et al.. Measurement of the production and lepton charge asymmetry of W bosons in Pb+Pb collisions at $\sqrt{s_{\text{NN}}} = 2.76$ TeV with the ATLAS detector. European Physical Journal C: Particles and Fields, 2015, 75 (1), pp.23. 10.1140/epjc/s10052-014-3231-6 . in2p3-01056937

HAL Id: in2p3-01056937

<https://hal.in2p3.fr/in2p3-01056937>

Submitted on 3 Jun 2021

HAL is a multi-disciplinary open access archive for the deposit and dissemination of scientific research documents, whether they are published or not. The documents may come from teaching and research institutions in France or abroad, or from public or private research centers.

L'archive ouverte pluridisciplinaire **HAL**, est destinée au dépôt et à la diffusion de documents scientifiques de niveau recherche, publiés ou non, émanant des établissements d'enseignement et de recherche français ou étrangers, des laboratoires publics ou privés.



Distributed under a Creative Commons Attribution 4.0 International License



CERN-PH-EP-2014-156

Submitted to: EPJ C

Measurement of the production and lepton charge asymmetry of W bosons in Pb+Pb collisions at $\sqrt{s_{NN}} = 2.76$ TeV with the ATLAS detector

The ATLAS Collaboration

Abstract

A measurement of W boson production in lead-lead collisions at $\sqrt{s_{NN}} = 2.76$ TeV is presented. It is based on the analysis of data collected with the ATLAS detector at the LHC in 2011 corresponding to an integrated luminosity of 0.14 nb^{-1} and 0.15 nb^{-1} in the muon and electron decay channels, respectively. The differential production yields and lepton charge asymmetry are each measured as a function of the average number of participating nucleons $\langle N_{\text{part}} \rangle$ and absolute pseudorapidity of the charged lepton. The results are compared to predictions based on next-to-leading-order QCD calculations. These measurements are, in principle, sensitive to possible nuclear modifications to the parton distribution functions and also provide information on scaling of W boson production in multi-nucleon systems.

Measurement of the production and lepton charge asymmetry of W bosons in Pb+Pb collisions at $\sqrt{s_{\text{NN}}} = 2.76$ TeV with the ATLAS detector

The ATLAS Collaboration

Received: date / Accepted: date

Abstract A measurement of W boson production in lead-lead collisions at $\sqrt{s_{\text{NN}}} = 2.76$ TeV is presented. It is based on the analysis of data collected with the ATLAS detector at the LHC in 2011 corresponding to an integrated luminosity of 0.14 nb^{-1} and 0.15 nb^{-1} in the muon and electron decay channels, respectively. The differential production yields and lepton charge asymmetry are each measured as a function of the average number of participating nucleons $\langle N_{\text{part}} \rangle$ and absolute pseudorapidity of the charged lepton. The results are compared to predictions based on next-to-leading-order QCD calculations. These measurements are, in principle, sensitive to possible nuclear modifications to the parton distribution functions and also provide information on scaling of W boson production in multi-nucleon systems.

1 Introduction

Studies of particle production in the high-density medium created in ultra-relativistic heavy-ion collisions have been previously conducted at the Relativistic Heavy Ion Collider (RHIC) at Brookhaven National Laboratory [1–4] and have been extended to larger centre-of-mass energies at the Large Hadron Collider (LHC) at CERN [5, 6]. These collisions provide access to a phase of nuclear matter at high temperature and low baryon density called quark-gluon plasma (QGP), in which the relevant degrees of freedom are quarks and gluons [7–11]. In a QGP, high-energy partons transfer energy to the medium through multiple interactions and gluon radiation, resulting in a modification of the parton shower of jets (jet-quenching). This effect is consistent with the measurements of high transverse momentum (p_{T})

charged hadron yields [12–16], inclusive jets [17] and dijets with asymmetric transverse energies (E_{T}) [18–20].

Electroweak bosons ($V = \gamma, W, Z$) provide additional ways to study partonic energy loss in heavy-ion collisions. They do not interact strongly with the medium, thus offering a means to calibrate the energy of jets in V -jet events. At sub-TeV centre-of-mass energies, the only viable candidates for playing this role are photons [21]. However at higher energies, heavy gauge bosons (W^{\pm} and Z) are also produced in relatively high abundance, introducing an additional avenue for benchmarking in-medium modifications to coloured probes. This potential has already been realised in lead-lead (Pb+Pb) collisions in previous ATLAS [22] and CMS [23–25] publications, where it was observed that electroweak boson production rates scale linearly with the number of binary nucleon-nucleon collisions.

Moreover, in principle, electroweak bosons are an excellent tool for studying modifications to parton distribution functions (PDFs) in a multi-nucleon environment. To leading-order, $W^{+}(W^{-})$ bosons are primarily produced by interactions between a $u(d)$ valence quark and a $\bar{d}(\bar{u})$ sea quark. The rapidity of the W boson is primarily determined by the momentum fractions, x , of the incoming partons. Therefore, information about the PDF can be extracted by measuring the charge asymmetry as a function of the pseudorapidity¹ of charged leptons produced from W decays.

¹ The ATLAS detector uses a right-handed coordinate system with the nominal Pb+Pb interaction point at its centre. The z -axis is along the beam pipe. The x -axis points from the interaction point toward the centre of the ring and the y -axis points upward. Cylindrical coordinates (r, ϕ) are used in the transverse plane with ϕ being the azimuthal angle around the z -axis. The pseudorapidity is defined in terms of the polar angle θ as $\eta = -\ln(\tan \theta/2)$.

The charge asymmetry is defined in terms of the differential production yields for $W \rightarrow \ell\nu_\ell$ ($\ell = \mu, e$), $dN_{W \rightarrow \ell\nu_\ell}/d\eta_\ell$:

$$A_\ell(\eta_\ell) = \frac{dN_{W^+ \rightarrow \ell^+\nu_\ell}/d\eta_\ell - dN_{W^- \rightarrow \ell^-\bar{\nu}_\ell}/d\eta_\ell}{dN_{W^+ \rightarrow \ell^+\nu_\ell}/d\eta_\ell + dN_{W^- \rightarrow \ell^-\bar{\nu}_\ell}/d\eta_\ell} \quad (1)$$

where η_ℓ is the pseudorapidity of the charged lepton and the W boson production yields are determined in the kinematic phase space used to select $W \rightarrow \ell\nu_\ell$ events. This observable has been used to study PDFs in binary nucleon systems such as pp collisions at the LHC [26–28] and $p\bar{p}$ collisions at the Tevatron [29, 30]. However, its utility in nuclear systems has only recently been explored with a limited set of experimental data [25].

Although the method for measuring the charge asymmetry in Pb+Pb is essentially identical to that in pp , the distributions themselves are not expected to be identical. In pp collisions, the overall production rate of W^+ bosons is larger than that of W^- bosons as a result of the larger fraction of u valence quarks relative to d valence quarks in the colliding system. On the other hand, in Pb+Pb collisions, the nuclei contain 126 neutrons and 82 protons. Thus, pp interactions make up only $\approx 15\%$ of the total number of nucleon–nucleon interactions, whereas neutron–neutron (nn) and proton–neutron (pn) combinations contribute $\approx 37\%$ and $\approx 48\%$, respectively. Consequently, a marked difference is expected in the lepton charge asymmetry between Pb+Pb and pp collisions.

Prior to this analysis, the only published charge asymmetry measurement in heavy–ion collisions was reported by the CMS collaboration [25] with an integrated luminosity of $7.3 \mu\text{b}^{-1}$ using the $W \rightarrow \mu\nu_\mu$ channel in Pb+Pb collisions at $\sqrt{s_{\text{NN}}} = 2.76 \text{ TeV}$. The measurement presented here uses a dataset from 2011, which corresponds to an integrated luminosity of 0.14 and 0.15 nb^{-1} for the muon and electron channels, respectively. In addition, the $W \rightarrow e\nu_e$ decay mode is employed for the first time in a heavy–ion environment.

The paper is organised as follows: a brief overview of the ATLAS detector and trigger is given in Sect. 2. A description of the simulated event samples used in the analysis is provided in Sect. 3. The criteria for selecting Pb+Pb events are presented in Sect. 4. This is followed by a description of muon and electron reconstruction and signal candidate selection in Sect. 5. The background estimations are presented in Sect. 6. A discussion of the procedure for correcting the signal yields is presented in Sect. 7. The systematic uncertainties and the combination of the two channels are described in Sect. 8, and the W boson production yields, measured as a function of the mean number of inelastically interacting nucleons $\langle N_{\text{part}} \rangle$ and $|\eta_\ell|$, are discussed in Sect. 9. A differential measurement of the lepton charge asymmetry as a function of $|\eta_\ell|$ is also presented. These results are com-

pared to predictions at next–to–leading order (NLO) [31–33] in QCD, both with and without nuclear corrections. The former is represented by the EPS09 PDF [34]. Section 10 provides a brief summary of the results.

2 The ATLAS detector

ATLAS [35], one of four large LHC experiments, is well equipped to carry out an extensive heavy–ion program. The inner detector (ID) comprises a precision tracking system that covers a pseudorapidity range $|\eta| < 2.5$. The ID consists of silicon pixels, silicon microstrips, and a transition radiation tracker (TRT)² consisting of cylindrical drift tubes and operates within a 2 T axial magnetic field supplied by a superconducting solenoid.

Due to the high occupancy in heavy–ion events, tracks of charged particles are reconstructed using only the silicon pixels and microstrips. No information from the TRT is used in this analysis, and henceforth ID tracks will refer to those tracks that are reconstructed without this detector component.

Outside the solenoid, highly segmented electromagnetic (EM) and hadronic sampling calorimeters cover the region $|\eta| < 4.9$. The EM calorimetry is based on liquid–argon (LAr) technology and is divided into one barrel ($|\eta| < 1.475$, EMB) and two end–cap ($1.375 < |\eta| < 3.2$, EMEC) components. The transition region between the barrel and end–cap calorimeters is located within the pseudorapidity range $1.37 < |\eta| < 1.52$. The hadronic calorimeter is based on two different detector technologies: steel absorber interleaved with plastic scintillator covering the barrel ($|\eta| < 1.0$) and extended barrels ($0.8 < |\eta| < 1.7$) and LAr hadronic end–cap calorimeters (HEC) located in the region $1.5 < |\eta| < 3.2$. A forward calorimeter (FCal) that uses LAr as the active material is located in the region $3.1 < |\eta| < 4.9$. On the inner face of the end–cap calorimeter cryostats, a minimum–bias trigger scintillator (MBTS) is installed on each side of the ATLAS detector, covering the pseudorapidity region $2.1 < |\eta| < 3.8$.

The outermost sub–system of the detector is a muon spectrometer (MS) that is divided into a barrel region ($|\eta| < 1.05$) and two end–cap regions ($1.05 < |\eta| < 2.7$). Precision measurements of the track coordinates and momenta are provided by monitored drift tubes (MDTs), cathode strip chambers (CSCs), and three sets of air–core superconducting toroids with coils arranged in an eight–fold symmetry that provide on average 0.5 T in the azimuthal plane.

The zero–degree calorimeters (ZDCs) [36] are located symmetrically at $z = \pm 140 \text{ m}$ and cover $|\eta| > 8.3$. In Pb+Pb collisions the ZDCs primarily measure spectator neutrons from the colliding nuclei.

² The TRT provides tracking information up to $|\eta| < 2$.

The ATLAS detector also includes a three-level trigger system [37]: level one (L1) and the software-based High Level Trigger (HLT), which is subdivided into the Level 2 (L2) trigger and Event Filter (EF). Muon and electron triggers are used to acquire the data analysed in this paper.

The trigger selection for muons is performed in three steps. Information is provided to the L1 trigger system by the fast-response resistive plate chambers (RPCs) in the barrel ($|\eta| < 1.05$) and thin gap chambers (TGCs) in the end-caps ($1.05 < |\eta| < 2.4$). Both the RPCs and TGCs are part of the MS. Information from L1 is then passed to the HLT, which reconstructs muon tracks in the vicinity of the detector region reported by the L1 trigger. The L2 trigger performs a fast reconstruction of muons using a simple algorithm, which is then further refined at the EF by utilising the full detector information as in the offline muon reconstruction software.

The trigger selection for electrons is performed using a L1 decision based on electromagnetic energy depositions in trigger towers of $\Delta\phi \times \Delta\eta = 0.1 \times 0.1$ formed by EM calorimeter cells within the range $|\eta| < 2.5$. The electron trigger algorithm identifies a region of interest as a trigger tower cluster for which the transverse energy (E_T) sum from at least one of the four possible pairs of nearest neighbour towers exceeds a specified E_T threshold.

3 Monte Carlo samples

Simulated event samples are produced using the Monte Carlo (MC) method and are used to estimate both the signal and background components. The response of the ATLAS detector is simulated using GEANT4 [38, 39]. The samples used throughout this paper are summarised in Table 1. Each signal process and most of the background processes are embedded into minimum-bias (MB) heavy-ion events from data recorded in the same run periods as the data used to analyse W boson production. Events from the $Z \rightarrow \mu^+ \mu^-$ channel are embedded into HIJING [40] – a widely used heavy-ion simulation that reproduces many features of the underlying event [17].

The production of W bosons and its decay products are modelled with the POWHEG [41] event generator, which is interfaced to PYTHIA8 [42] in order to model parton showering and fragmentation processes. These samples use the CT10 [43] PDF set and are used to estimate the signal selection efficiency and to provide predictions from theory. In order to account for the isospin of the nucleons, separate samples of pp , pn , and nn events are generated and combined in proportion to their corresponding collision frequency in Pb+Pb collisions. Only pp simulations are used to model background processes (discussed in detail in Sect. 6) since these channels are not sensitive to isospin effects.

Table 1 Signal and background simulated event samples used in this analysis. $W \rightarrow \ell\nu_\ell$ events include all nucleon combinations, whereas background processes use only pp simulations. The variable \hat{p}_T is the average p_T of the two outgoing partons involved in the hard-scattering process evaluated before modifications from initial- and final-state radiation. Details for each sample are given in the text.

Physics process	Generator	PDF set
$W \rightarrow \mu\nu_\mu$	POWHEG+PYTHIA8	CT10
$W \rightarrow e\nu_e$	POWHEG+PYTHIA8	CT10
Dijet ($17 < \hat{p}_T < 140$ GeV)	PYTHIA6	MRST LO*
$Z \rightarrow \mu^+ \mu^-$	PYTHIA6	MRST LO*
$Z \rightarrow e^+ e^-$	POWHEG+PYTHIA8	CT10
$W \rightarrow \tau\nu_\tau \rightarrow \mu\nu_\mu\nu_\tau\nu_\tau$	PYTHIA6	MRST LO*
$W \rightarrow \tau\nu_\tau \rightarrow e\nu_e\nu_\tau\nu_\tau$	POWHEG+PYTHIA8	CT10

Background samples are generated for muons with PYTHIA6 using the MRST LO* PDF set [44] and for electrons with POWHEG using the CT10 PDF set. At the level of the precision of the background estimation, no significant difference is expected between the PYTHIA6 and POWHEG generators. The background contribution to the muon channel from heavy-flavour is modelled using simulated dijet samples with average final-state parton energies \hat{p}_T in the range 17–140 GeV. Tau decays from $W \rightarrow \tau\nu_\tau$ events are treated using either TAUOLA [45] or PYTHIA8 for final states involving muons or electrons, respectively. Final-state radiation from QED processes is simulated by PHOTOS [46].

4 Event selection

4.1 Centrality definition

Pb+Pb collision events are selected by imposing basic requirements on the beam conditions and the performance of each sub-detector. In order to select MB hadronic Pb+Pb collisions, a hit on each side of the MBTS system with a time coincidence within 3 ns is required for each collision. In addition, each event is required to have a reconstructed vertex with at least three associated high-quality tracks [47] compatible with the beam-spot position. These requirements select MB hadronic Pb+Pb collisions in the data with an efficiency of $(98 \pm 2)\%$ with respect to the total non-Coulombic inelastic cross-section [5]. After accounting for the selection efficiency and prescale factors imposed by the trigger system during data taking [48], approximately 1.03×10^9 Pb+Pb events are sampled (denoted by N_{events} hereafter).

Each event is categorised into a specific centrality class defined by selections on FCal ΣE_T , the total transverse energy deposited in the FCal and calibrated to the EM energy scale [47]. Centrality classes in heavy-ion events represent the percentiles of the total inelastic non-Coulombic Pb+Pb cross-section. This reflects the overlap volume between the

colliding nuclei and allows for selection of various collision geometries in the initial state.

The FCal ΣE_T is closely related to the mean number of inelastically interacting nucleons $\langle N_{\text{part}} \rangle$ and mean number of binary collisions $\langle N_{\text{coll}} \rangle$ through the Glauber formalism [49]. $\langle N_{\text{part}} \rangle$ and $\langle N_{\text{coll}} \rangle$ are monotonic functions of the collision impact parameter and are correlated with the FCal ΣE_T of each Pb+Pb collision [5]. $\langle N_{\text{coll}} \rangle$ can also be expressed as the product of the average nuclear thickness function $\langle T_{AA} \rangle$ and the total inelastic pp cross-section (64 ± 5 mb at $\sqrt{s} = 2.76$ TeV [50]). In this paper, events are separated into five centrality classes: 0–5%, 5–10%, 10–20%, 20–40%, and 40–80% with the most central interval (0–5%) corresponding to the 5% of events with the largest FCal ΣE_T . The $\langle N_{\text{coll}} \rangle$ estimation in the 80–100% class suffers from high experimental uncertainties, and therefore, this centrality class is not considered in the analysis. Table 2 presents $\langle N_{\text{part}} \rangle$ and $\langle N_{\text{coll}} \rangle$ for each centrality class along with their relative systematic uncertainties (see Sect. 8). Since a single participant can interact inelastically with several nucleons in a collision, the uncertainty in $\langle N_{\text{part}} \rangle$ is less than that of the corresponding $\langle N_{\text{coll}} \rangle$ in each centrality class.

Table 2 Average number of participating nucleons (N_{part}) and binary collisions (N_{coll}) for the centrality classes used in this analysis alongside their relative uncertainties.

Centrality [%]	$\langle N_{\text{part}} \rangle$	$\delta \langle N_{\text{part}} \rangle$ [%]	$\langle N_{\text{coll}} \rangle$	$\delta \langle N_{\text{coll}} \rangle$ [%]
0–5	382	0.5	1683	7.7
5–10	330	0.9	1318	7.5
10–20	261	1.4	923	7.4
20–40	158	2.6	441	7.3
40–80	46	6.0	78	9.4
0–80	140	4.7	452	8.5

4.2 Trigger selection

$W \rightarrow \mu\nu_\mu$ candidates are selected using single muon triggers with a requirement on the minimum transverse momentum of 10 GeV in the HLT. Two types of single muon triggers are used: one that requires a muon in coincidence with a total event transverse energy – measured in the calorimeter at L1 – above 10 GeV and another which requires a muon in coincidence with a neutral particle at $|\eta| > 8.3$ in the ZDCs. This combination of triggers maximises the efficiency for events across all centrality classes. The muon trigger efficiencies are evaluated using high-quality single muons reconstructed from MB events and range from 89.3% to 99.6%, depending on $|\eta_\mu|$ and the centrality of the event from which the muon originated.

Candidate events for $W \rightarrow e\nu_e$ are selected using only the hardware-based L1 trigger, i.e. without use of the HLT. The L1 calorimeter trigger selects photon and electron candidates in events where the transverse energy in an EM cluster of trigger towers exceeds 14 GeV. The efficiency is evaluated using a tag-and-probe method that utilises $Z \rightarrow e^+e^-$ events selected using the criteria from Ref. [22]. This gives an efficiency of 99.6% for electrons with $E_T > 25$ GeV and $|\eta| < 2.47$ – excluding the transition region – with a negligible centrality dependence.

4.3 Transverse momentum imbalance, p_T^{miss}

Previous W boson analyses in ATLAS [26] have used the event momentum imbalance in the plane transverse to the beam axis (E_T^{miss}) as a proxy for the true neutrino p_T . Traditionally, these analyses reconstruct the E_T^{miss} using contributions from energy deposits in the calorimeters and muons reconstructed in the MS [51]. In minimum bias events, no genuine missing energy is expected, and the resolution of the two E_T^{miss} components ($\sigma_x^{\text{miss}}, \sigma_y^{\text{miss}}$) is measured directly from reconstructed quantities in the data by assuming the true E_x^{miss} and E_y^{miss} are zero. The resolution is estimated from the width of the E_x^{miss} and E_y^{miss} distributions. In heavy-ion collisions, soft particle production is much higher than in pp collisions, thereby resulting in an increased number of particles that do not reach the calorimeter or seed a topocluster. Consequently, the resolution in the E_T^{miss} observed in the data using calorimeter cells is at the level of 45 GeV in the most central heavy-ion events. Therefore, this analysis employs a track-based calculation proposed in Ref. [25] that provides a four-fold improvement in resolution relative to the calorimeter-based method. The event momentum imbalance using this approach is defined as the negative vector sum of all high-quality ID tracks [47] with $p_T > 3$ GeV:

$$\mathbf{p}^{\text{miss}} = - \sum_{i=1}^{N_{\text{tracks}}} \mathbf{p}_i^{\text{track}}, \quad (2)$$

where $\mathbf{p}_i^{\text{track}}$ is the momentum vector of the i^{th} ID track, and N_{tracks} represents the total number of ID tracks in the event. The magnitude of the transverse component p_T^{miss} and azimuthal angle ϕ^{miss} are calculated from the transverse components (p_x^{miss} and p_y^{miss}) of the resultant vector. The lower track p_T threshold is chosen based on that which gives the best resolution in the p_T^{miss} while still including a sufficient number of tracks in the vector summation.

The transverse mass of the charged lepton and neutrino system is defined as

$$m_T = \sqrt{2p_T^\ell p_T^{\text{miss}} (1 - \cos \Delta\phi_{\ell, p_T^{\text{miss}}})}, \quad (3)$$

where $\Delta\phi_{\ell, p_T^{\text{miss}}}$ is the difference between the direction of the charged lepton and p_T^{miss} vector in the azimuthal plane.

5 Signal candidate reconstruction and selection

5.1 Muon reconstruction

Muon reconstruction in ATLAS consists of separate tracking in the ID and MS. In this analysis, tracks reconstructed in each sub-system are combined using the χ^2 -minimisation procedure described in Ref. [52]. These combined muons are required to satisfy selection criteria that closely follow those used in the Z boson analysis in Pb+Pb data [22]. To summarise, these criteria include a set of ID hit requirements in the pixel and SCT layers of the ID, a selection on the transverse and longitudinal impact parameters ($|d_0|$ and $|z_0|$), and a minimum requirement on the quality of the muon track fit. Additional selection criteria specific to W bosons are discussed below.

Decays-in-flight from pions and kaons contribute a small background fraction in this analysis. They are reduced by requiring the difference between the ID and MS muon p_T measurements (corrected for the mean energy loss due to interactions with the material between the ID and MS) to be less than 50% of the p_T measured in the ID. Decays-in-flight are further reduced by locating changes in the direction of the muon track trajectory. This is performed using a least-squares track fit that includes scattering angle parameters accounting for multiple scattering between the muon and detector material. Scattering centers are allocated along the muon track trajectory from the ID to MS, and decays are identified by scattering angle measurements much greater than the expectation value due to multiple scattering [53].

In order to reduce the multi-jet contribution, a track-based isolation of the muon is imposed. The tracks are taken from a cone radius $\Delta R = \sqrt{(\Delta\eta)^2 + (\Delta\phi)^2} = 0.2$ around the direction of the muon. The muon is considered isolated if the sum of the transverse momenta of ID tracks ($\sum p_T^{\text{ID}}$) with $p_T > 3$ GeV – excluding the muon p_T itself – is less than 10% of the muon p_T . In this paper, the quantity $\sum p_T^{\text{ID}}/p_T$ is referred to as the muon isolation ratio. Based on MC studies, the isolation requirement is estimated to reject 50–70% of muons in QCD multi-jet events, depending on the centrality class, while retaining at least 95% of signal candidates.

5.2 Electron reconstruction

In order to reconstruct electrons in the environment of heavy-ion collisions, the energy deposits from soft particle production due to the underlying event (UE) must be subtracted, as they distort calorimeter-based observables.

The two-step subtraction procedure, described in detail in Ref. [17], is applied. It involves calculating a per-event average UE energy density that excludes contributions from jets and EM clusters and accounts for effects from elliptic flow modulation on the UE. The residual deposited energies stem primarily from three sources: photons/electrons, jets and UE fluctuations (including higher-order flow harmonics). After the UE background subtraction, a standard ATLAS electron reconstruction and identification algorithm [54, 55] for heavy-ions is used – the only difference between this algorithm and the one used in pp collisions is that the TRT is not used. The algorithm is designed to provide various levels of background rejection and high identification efficiencies over the full acceptance of the ID system.

The electron identification selections are based on criteria that use calorimeter and tracking information and are optimised in bins of η and E_T . Patterns of energy deposits in the first layer of the EM calorimeter, track quality variables, and a cluster-track matching criterion are used to select electrons. Selection criteria based on shower shape information from the second layer of the EM calorimeter and energy leakage into the hadronic calorimeters are used as well. Background from charged hadrons and secondary electrons from conversions are reduced by imposing a requirement on the ratio of cluster energy to track momentum. Electrons from conversions are further reduced by requiring at least one hit in the first layer of the pixel detector.

A calorimeter-based isolation variable is also imposed. Calorimeter clusters are taken within $\Delta R = 0.25$ around the candidate electron cluster. An electron is considered isolated if the total transverse energy of calorimeter clusters – excluding the candidate electron cluster – is less than 20% of the electron E_T . In this paper, the quantity $\sum E_T^{\text{calo}}/E_T$ is referred to as the electron isolation ratio. The isolation requirement was studied in each centrality class and retains, on average, 92% of signal candidates while rejecting 42% of electrons from QCD multi-jet events.

5.3 W boson candidate selection

W boson production yields are measured in a fiducial region defined by:

$$\begin{aligned} W \rightarrow \mu\nu_\mu: & \quad p_T^\mu > 25 \text{ GeV}, \quad 0.1 < |\eta_\mu| < 2.4, \\ & \quad p_T^\nu > 25 \text{ GeV}, \quad m_T > 40 \text{ GeV}; \\ W \rightarrow e\nu_e: & \quad p_T^e > 25 \text{ GeV}, \quad |\eta_e| < 2.47, \\ & \quad \text{excluding } 1.37 < |\eta_e| < 1.52, \\ & \quad p_T^\nu > 25 \text{ GeV}, \quad m_T > 40 \text{ GeV}. \end{aligned}$$

In the MS, a gap in chamber coverage is located at $|\eta_\mu| < 0.1$ that allows for services to the solenoid magnet, calorimeters, and ID, and therefore, this region is excluded.

The most forward bin boundary is determined by the acceptance of the muon trigger chambers. In the electron analysis, the calorimeter transition region at $1.37 < |\eta_e| < 1.52$ is excluded. The lower limit on the m_T is imposed to further suppress background events that satisfy the lepton p_T and p_T^{miss} requirements.

In the muon channel, the background contribution from $Z \rightarrow \mu^+\mu^-$ decays is suppressed by rejecting muons from opposite-charge pairs that have an invariant mass greater than 66 GeV. These events are selected by requiring that one muon in the pair has $p_T > 25$ GeV and passes the quality requirements in Sect. 5.1 and the other muon in the pair satisfies a lower p_T threshold of 20 GeV. In principle, this method allows for the possibility of accepting events with more than one W boson. However, only one event in the data was found where two muons satisfy all signal selection requirements. This selection vetoes 86% of muons produced from Z bosons while retaining over 99% of W boson candidates. The 14% of background muons that satisfy the selection criteria is attributable to instances where the second muon from the Z boson decay is produced outside the ID acceptance or has $p_T < 20$ GeV.

In the electron channel, the $Z \rightarrow e^+e^-$ background contribution is suppressed by rejecting events with more than one electron satisfying the identification requirements from Sect. 5.2. This selection retains over 99% of signal events while rejecting 23% of Z boson candidates. Events surviving the selection are attributable to instances where the second electron from the Z boson decay is either produced outside the ID acceptance (26%) or does not pass the relatively tight electron identification requirements (74%).

After applying all selection criteria, 3348 W^+ and 3185 W^- candidates are detected in the muon channel. In the electron channel, 2893 W^+ and 2791 W^- candidates are observed.

6 Background estimation

The main backgrounds to the $W \rightarrow \ell\nu_\ell$ channel arise from lepton production in electroweak processes and semileptonic heavy-flavour decays in multi-jet events. The former include $W \rightarrow \tau\nu_\tau \rightarrow \ell\nu_\ell\nu_\tau\nu_\tau$ events and $Z \rightarrow \ell^+\ell^-$ events, where one lepton from the Z boson is emitted outside the ID acceptance and produces spurious p_T^{miss} . Other sources of background that are considered include $Z \rightarrow \tau\tau$ events, in which at least one tau decays into a muon or electron, and $t\bar{t}$ events, in which at least one top quark decays semileptonically into a muon or electron. These two background sources are negligible ($<0.5\%$) and are not taken into account in this analysis.

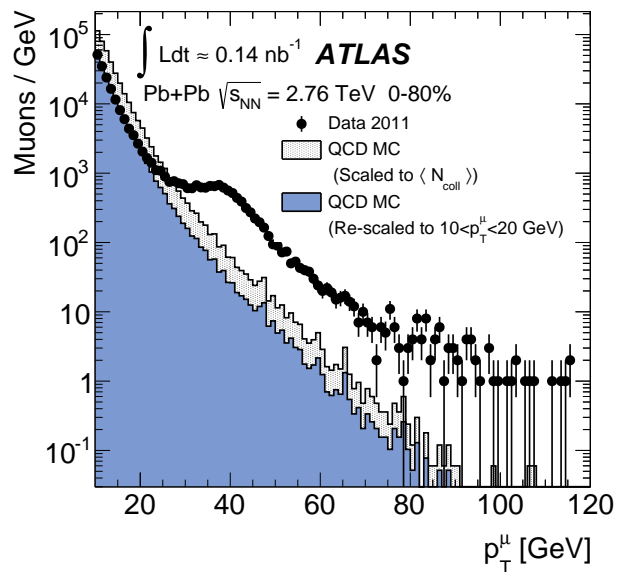


Fig. 1 Muon transverse momentum distribution in the data (points) before applying the signal selection requirements. The p_T distribution of QCD multi-jet processes from the MC simulation is also shown in the same figure. The shaded histogram is scaled to $\langle N_{\text{coll}} \rangle$ and the solid histogram is rescaled to match the data in a control region $10 < p_T^\mu < 20$ GeV. The background fraction from QCD multi-jet processes is determined from the number of muons in the MC surviving the final selection criteria.

6.1 $W \rightarrow \mu\nu_\mu$ channel

In the muon channel, the total number of background events from QCD multi-jet processes is estimated using a partially data-driven method. The dijet muon yields per Pb+Pb event in the MC simulation are normalised to the pp cross-section and scaled by the number of binary collisions and Pb+Pb events in the data. The resulting distribution is represented by the shaded histogram in Fig. 1. To take into account jet energy-loss in the medium, the MC distribution is rescaled to the data in a control region dominated by QCD multi-jet events in the range $10 < p_T^\mu < 20$ GeV (solid histogram). This scale factor is on average 0.4 over all $|\eta_\mu|$ intervals and centrality classes. As a cross-check, the shape of the rescaled QCD multi-jet background distribution was compared to that of a control sample consisting of anti-isolated muons from the data. They are found to agree well, confirming that the distributions in Fig. 1 are an accurate representation of the multi-jet background in the data. The number of expected QCD multi-jet events is determined by extrapolating the rescaled MC distribution from the control region to the signal p_T^μ region above 25 GeV. The fraction of background events in the data is then calculated from the ratio of the number of QCD multi-jet events surviving final selection in the MC and the number of W candidates in the data. This is performed as function of η_μ and centrality. The back-

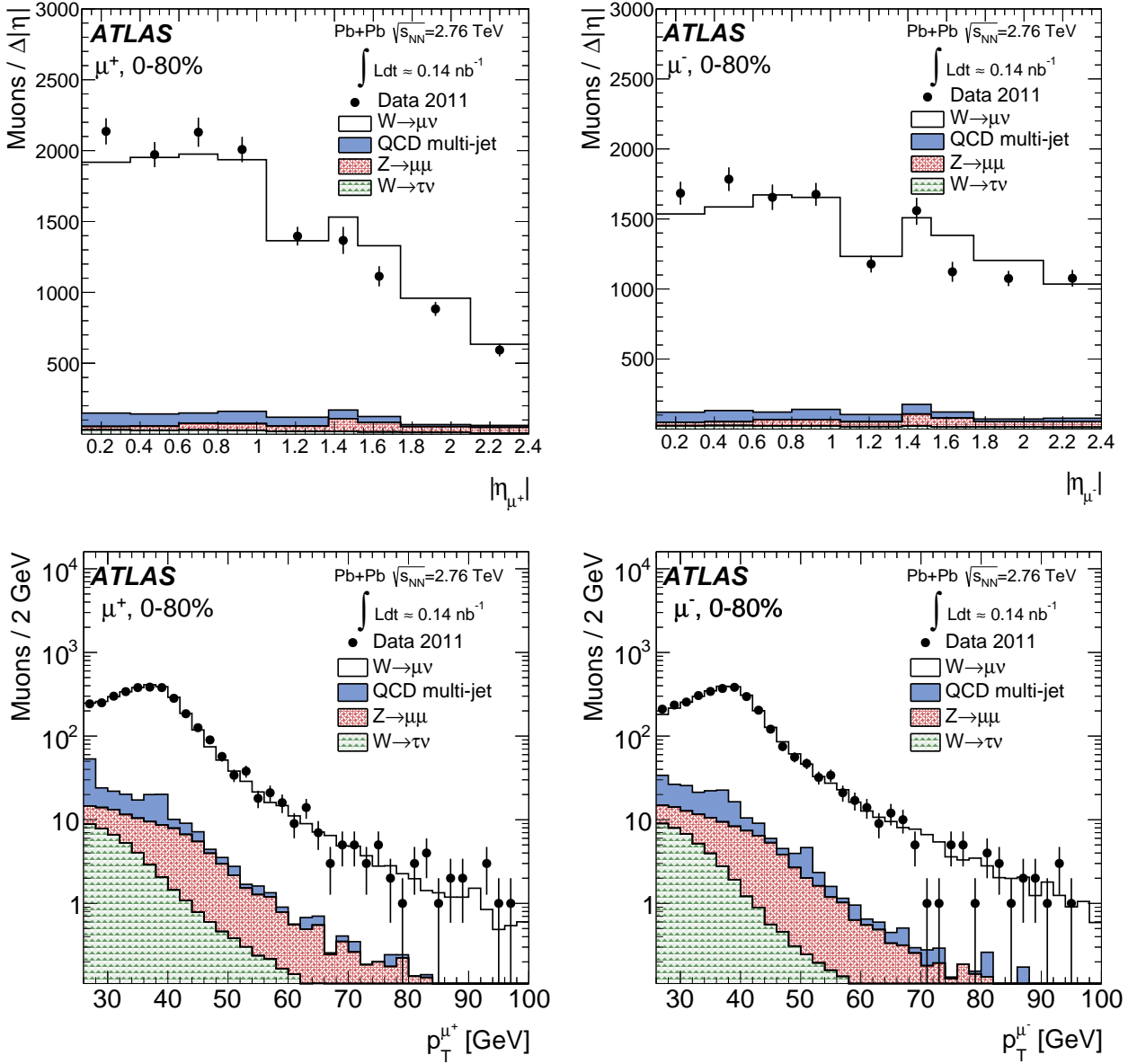


Fig. 2 Measured muon absolute pseudorapidity (top) and transverse momentum (bottom) distributions for $W^+ \rightarrow \mu^+ \nu_\mu$ (left) and $W^- \rightarrow \mu^- \bar{\nu}_\mu$ (right) candidates after applying the complete set of selection requirements in the fiducial region, $p_T^\mu > 25$ GeV, $p_T^{\text{miss}} > 25$ GeV, $m_T > 40$ GeV and $0.1 < |\eta_\mu| < 2.4$. The contributions from electroweak and QCD multi-jet processes are normalised according to their expected number of events. The $W \rightarrow \mu \nu_\mu$ MC events are normalised to the number of background-subtracted events in the data. The background and signal predictions are added sequentially.

ground fraction is also determined separately for μ^+ and μ^- , and no charge dependence is observed. The multi-jet background fraction is estimated to be on average 3.7% of the total number of W^\pm boson candidates, varying from 2.0% to 5.4% as a function of η_μ and centrality.

The estimated number of background events from electroweak processes is determined separately for the $Z \rightarrow \mu^+ \mu^-$ and $W \rightarrow \tau \nu_\tau$ channels. The background from $Z \rightarrow \mu^+ \mu^-$ events is determined in each η_μ interval from MC simulation and scaled to reproduce the actual number

of $Z \rightarrow \mu^+ \mu^-$ events observed in the data [22] in each centrality class. This contribution is on average 2.4% relative to the total number of W boson candidates and ranges from 1.0% at central $|\eta_\mu|$ to 3.2% in the forward region. Background events originating from $W \rightarrow \tau \nu_\tau \rightarrow \mu \nu_\mu \nu_\tau \nu_\tau$ decays are estimated by calculating the ratio of the number of $W \rightarrow \tau \nu_\tau \rightarrow \mu \nu_\mu \nu_\tau \nu_\tau$ and $W \rightarrow \mu \nu_\mu$ events that satisfy the analysis selection in the simulation. This fraction is on average 1.5% in each $|\eta_\mu|$ interval and centrality class and is applied to the number of observed signal candidates.

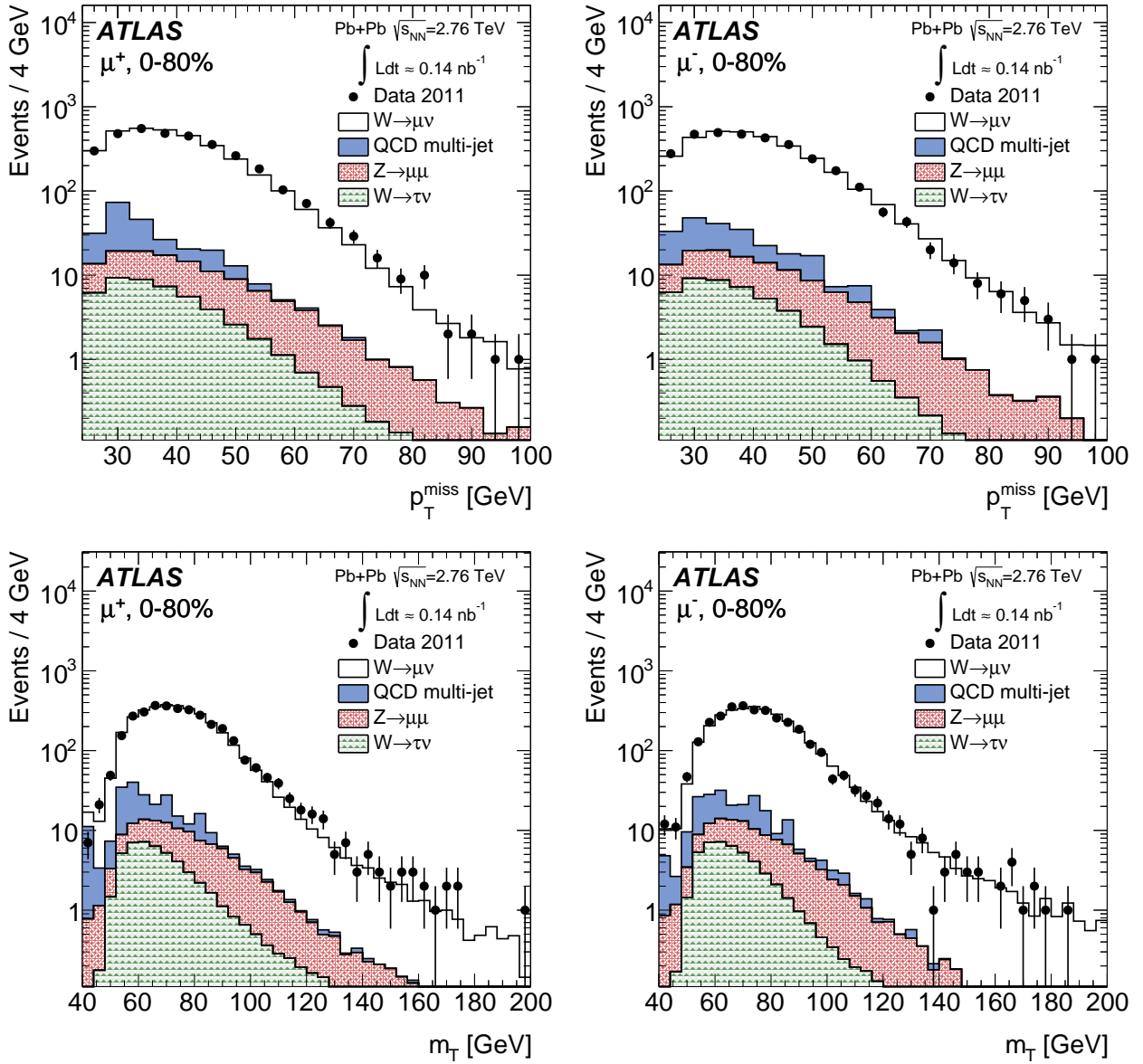


Fig. 3 Measured missing transverse momentum (top) and transverse mass (bottom) distributions for $W^+ \rightarrow \mu^+ \nu_\mu$ (left) and $W^- \rightarrow \mu^- \bar{\nu}_\mu$ (right) candidates after applying the complete set of selection requirements in the fiducial region, $p_T^\mu > 25$ GeV, $p_T^{\text{miss}} > 25$ GeV, $m_T > 40$ GeV and $0.1 < |\eta_\mu| < 2.4$. The contributions from electroweak and QCD multi-jet processes are normalised according to their expected number of events and added sequentially. The $W \rightarrow \mu \nu_\mu$ MC events are normalised to the number of background-subtracted events in the data. The background and signal predictions are added sequentially.

Variations between bins are at the level of 1.3–1.8%. The expected background from all sources in the $W \rightarrow \mu \nu_\mu$ channel amounts to 7.6% of the total number of W boson candidates.

Figure 2 shows the $|\eta_\mu|$ and p_T^μ distributions for positively and negatively charged muons after final event selection. Figure 3 presents the event p_T^{miss} and m_T distributions. In each figure, the data are compared to signal and background distributions from MC simulation in the same phase space. The background distributions are normalised to the

expected number of events, whereas the signal MC distribution is normalised to the number of background-subtracted events in the data. The background and signal predictions in Figs. 2 and 3 are added sequentially, beginning with the contribution from $W \rightarrow \tau \nu_\tau$.

6.2 $W \rightarrow e \nu_e$ channel

A partially data-driven method is used to estimate the QCD multi-jet background observed in $W \rightarrow e \nu_e$ candidate

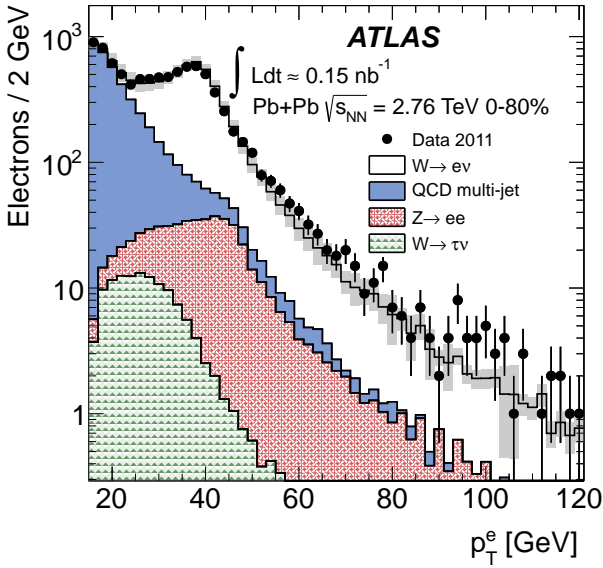


Fig. 4 Electron transverse momentum distribution in the data (points). The p_T distribution of multi-jet events from a data control sample (see text) and of simulated electroweak processes ($W \rightarrow \tau\nu_\tau$ and $Z \rightarrow e^+e^-$) are also shown. The total uncertainties from the fit are shown as solid grey bands.

events. This method involves using a control sample from the data to construct a QCD background template and simulated $W \rightarrow e\nu_e$ events to construct a signal template. The control sample is selected by employing looser electron identification criteria based solely on shower shape information and inverting the isolation requirement. In addition, if the event contains a jet reconstructed at EM scale with $E_T > 25$ GeV, the difference between the azimuthal angle of the jet and p_T^{miss} is required to be greater than $\pi/2$. This condition suppresses events with spurious p_T^{miss} originating from miscalibration of a jet [54]. The nominal p_T^{miss} and m_T criteria are also applied to the control sample. The background and signal templates are fit to the data as a function of p_T^e in the signal region after electroweak background subtraction. A result of the fit is shown in Fig. 4. The fit result slightly underestimates the data at $p_T^e \approx 60$ GeV, but this difference is within the total uncertainty of the fit. A significant contribution to this uncertainty comes from the limited number of events available for determining the QCD multi-jet background. The fitting is performed in all centrality bins and results in a total background estimation of 16.7% of $W \rightarrow e\nu_e$ candidate events in the 0–80% centrality class. As in the muon channel, this background fraction is charge-independent.

The background from electroweak processes with electrons in the final state is estimated from the MC samples listed in Table 1. The nominal selection criteria of this analysis are imposed on each MC sample. The absolute normali-

sation is derived from the W and Z PowHEG cross-sections in pp collisions. These cross-sections are scaled by $\langle N_{\text{coll}} \rangle$ in each centrality bin and normalised to the integrated luminosity of the Pb+Pb data sample. This method gives a valid estimate of the electroweak background in this analysis since ATLAS has recently demonstrated that the $Z \rightarrow e^+e^-$ yields in Pb+Pb collisions at $\sqrt{s_{\text{NN}}} = 2.76$ TeV are consistent with the pp expectation scaled by $\langle T_{AA} \rangle$ to within 3% [22]. The $Z \rightarrow e^+e^-$ background is the dominant electroweak background in this analysis and amounts to 6.5% of the total $W \rightarrow e\nu_e$ candidate events. The background from $W \rightarrow \tau\nu_\tau$ contributes an additional 2.5%. Electrons from $Z \rightarrow \tau\tau$ and $t\bar{t}$ are found to be $<0.3\%$ and $<0.1\%$, respectively. As with the muon channel, the latter two background sources are considered negligible.

Figure 5 shows the $|\eta_e|$ and p_T^e distributions for positively and negatively charged electrons after final event selection. Figure 6 presents the event p_T^{miss} and m_T distributions. In each figure, the data are compared to signal and background distributions from MC simulation in the same phase space. The background distributions are normalised to the expected number of events, whereas the signal MC distribution is normalised to the number of background-subtracted events in the data. The background and signal predictions in Figs. 5 and 6 are added sequentially, beginning with the contribution from $W \rightarrow \tau\nu_\tau$.

7 Yield correction procedure

In order to correct the data for losses attributable to the trigger, reconstruction, and selection efficiencies, a correction factor is applied to the measured yields after background subtraction. This correction factor C_{W^\pm} is defined by the following ratio:

$$C_{W^\pm} = \frac{N_W^{\text{rec}}}{N_W^{\text{gen, fid}}}, \quad (4)$$

where N_W^{rec} represents the number of $W \rightarrow \ell\nu_\ell$ events reconstructed in the fiducial region and satisfying final selection criteria, and $N_W^{\text{gen, fid}}$ signifies the number of $W \rightarrow \ell\nu_\ell$ events in the same phase space at the generator-level. This is calculated separately for each charge, $|\eta_\ell|$ interval, and centrality class. The denominator in Eq. (4) is evaluated directly from the boson decay i.e. Born level; this way of constructing the correction factor accounts for effects due to migration and QED radiation in the final state. Corrections for reconstruction and selection are derived solely from the signal MC simulation, whereas the trigger efficiencies are obtained from the data in each $|\eta_\ell|$ interval and centrality class.

In both the muon and electron channels, the C_{W^\pm} significantly depends on the event centrality and $|\eta_\ell|$. In the muon

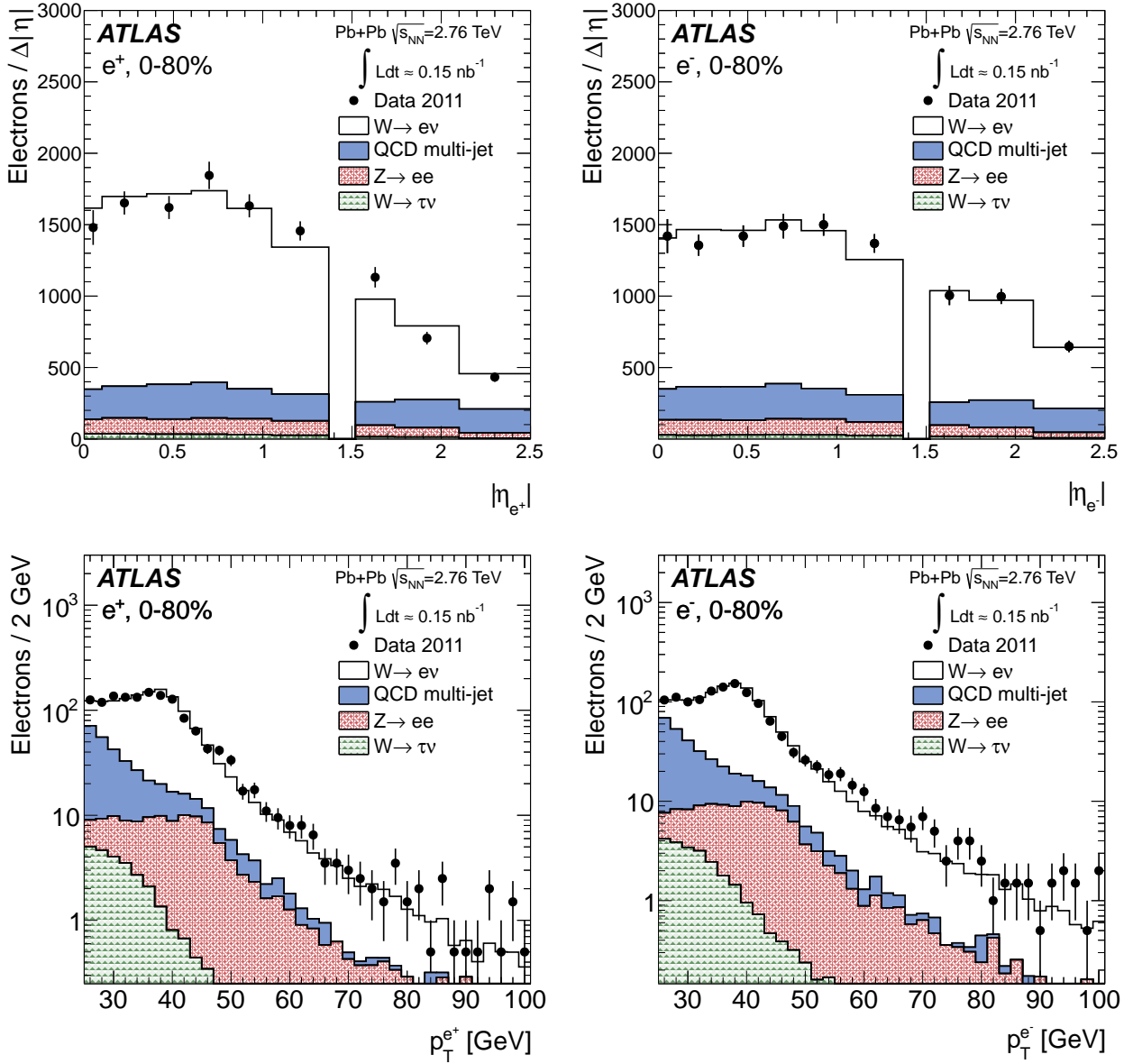


Fig. 5 Measured electron absolute pseudorapidity (top) and transverse momentum (bottom) distributions for $W^+ \rightarrow e^+ \nu_e$ (left) and $W^- \rightarrow e^- \bar{\nu}_e$ (right) candidates after applying the complete set of selection requirements in the fiducial region, $p_T^e > 25$ GeV, $p_T^{\text{miss}} > 25$ GeV, $m_T > 40$ GeV and $|\eta_e| < 2.47$ excluding the transition region ($1.37 < |\eta_e| < 1.52$). The contributions from electroweak and QCD multi-jet processes are normalised according to their expected number of events. The $W \rightarrow e\nu_e$ MC events are normalised to the number of background-subtracted events in the data. The background and signal predictions are added sequentially.

channel, the integrated C_{W^\pm} is $(67.4 \pm 0.2)\%$, ranging from 32% in the most central events in the highest $|\eta_\mu|$ region to 85% in the most peripheral events at mid-pseudorapidity. In the electron channel, the integrated C_{W^\pm} is $(39.2 \pm 0.3)\%$, ranging from 34% in the most central events to 51% in the most peripheral centrality class. The large variations in the C_{W^\pm} are attributable to two main factors: areas of the detector with limited coverage and the centrality dependence of the isolation efficiency and p_T^{miss} resolution.

The differential W boson production yields in the fiducial region are computed as:

$$N_{W^\pm}(|\eta_\ell, \text{centrality}) = \frac{N_{W^\pm}^{\text{obs}} - N^{\text{bkg}}}{C_{W^\pm}}, \quad (5)$$

where $N_{W^\pm}^{\text{obs}}$ signifies the number of candidate events observed in the data and N^{bkg} the number of background events in a given $|\eta_\ell|$ and centrality class.

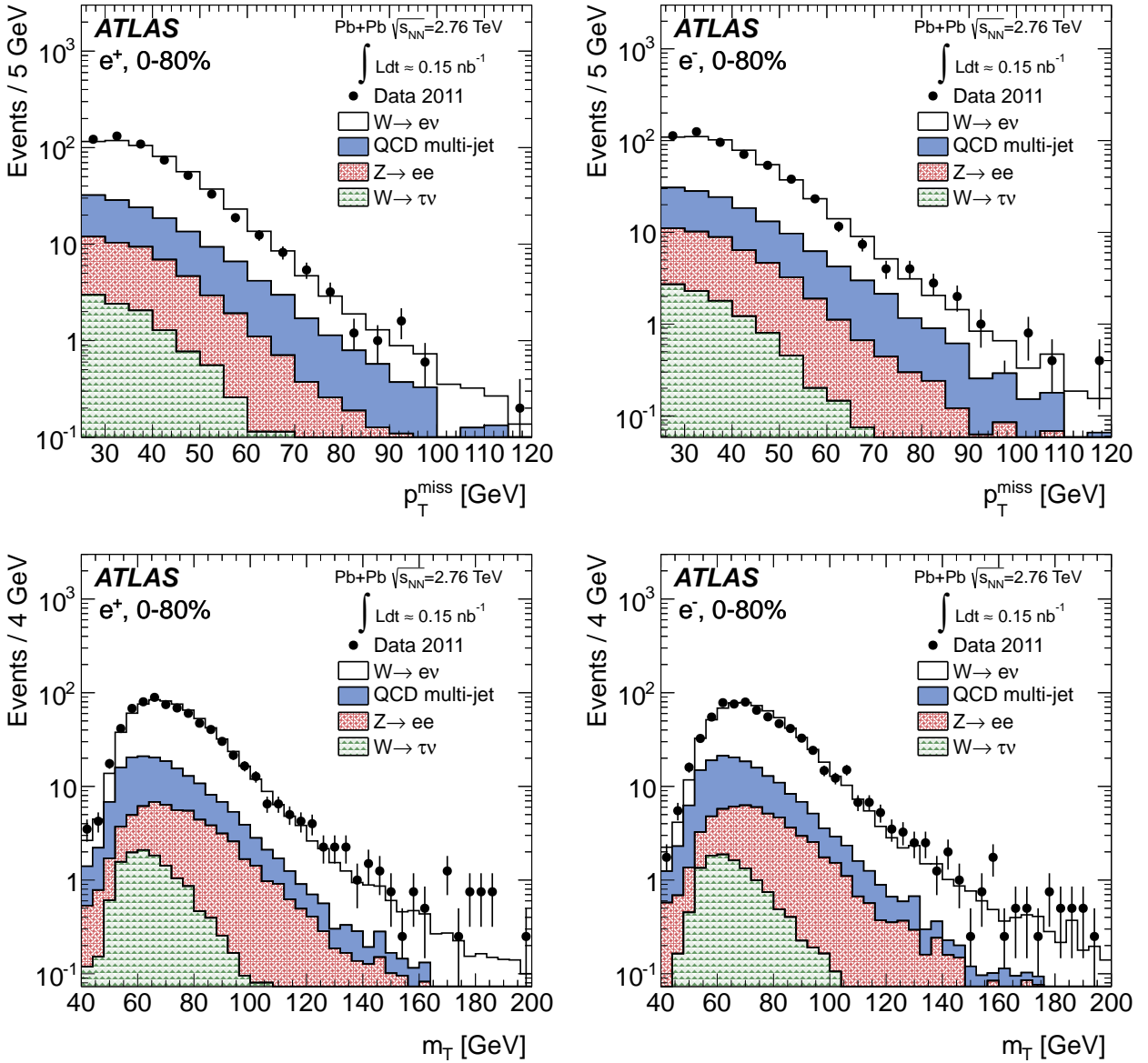


Fig. 6 Measured missing transverse momentum (top) and transverse mass (bottom) distributions for $W^+ \rightarrow e^+ \nu_e$ (left) and $W^- \rightarrow e^- \bar{\nu}_e$ (right) candidates after applying the complete set of selection requirements in the fiducial region, $p_T^\ell > 25$ GeV, $p_T^{\text{miss}} > 25$ GeV, $m_T > 40$ GeV and $|\eta_\ell| < 2.47$ excluding the transition region ($1.37 < |\eta_\ell| < 1.52$). The contributions from electroweak and QCD multi-jet processes are normalised according to their expected number of events. The $W \rightarrow e \nu_e$ MC events are normalised to the number of background-subtracted events in the data. The background and signal predictions are added sequentially.

The combination of the results from each channel are reported both as an integrated result in each centrality class and as a differential measurement as a function of $|\eta_\ell|$. The integrated result requires the extrapolation of each measurement to the full pseudorapidity region, $|\eta_\ell| < 2.5$ – this includes the excluded regions discussed above. Correction factors for this extrapolation are derived from the signal MC simulation and increase the integrated yield for muons by 7.5% and electrons by 6.6%. In the differential measurement as a function of $|\eta_\ell|$, the extrapolation is performed

only in the most forward bin up to $|\eta_\ell| = 2.5$. The correction increases the number of signal candidates in this bin by 28% in the muon channel and 7% in the electron channel.

8 Systematic uncertainties

The systematic uncertainties are studied separately for each charge, $|\eta_\ell|$, and centrality class. The magnitude by which each uncertainty is correlated from bin-to-bin is determined from the change in the corrected yields as a

function of $|\eta_\ell|$ and centrality after applying a systematic variation. The sources of uncertainty considered fully correlated between bins are as follows: the p_T^{miss} resolution, electroweak and QCD multi-jet background estimations, lepton isolation efficiencies, lepton and track reconstruction efficiencies, lepton energy/momentum scales and resolutions, extrapolation corrections and $\langle N_{\text{coll}} \rangle$. The dominant systematic uncertainty in both channels originates from the missing transverse momentum resolution. In the asymmetry and charge ratio measurements, uncertainties correlated between charges largely cancel. This correlation is determined for each source of systematic uncertainty from the variation in the charge ratio measurements with respect to the nominal values.

8.1 Muon channel

The resolution on the p_T^{miss} (described in Sect. 4) worsens with an increasing soft particle contribution to the vector sum of Eq. (2). This in turn depends on the lower track p_T threshold. The variation in the resolution with lower track p_T threshold is attributable to sources of spurious p_T^{miss} – e.g. undetected tracks, limited detector coverage, inactive material, finite detector resolution. These sources become amplified when a larger number of tracks are considered in the vector sum. A larger σ_{miss} in the p_T^{miss} distribution implies a larger uncertainty of the true neutrino p_T . However, setting a lower track p_T threshold too high can also introduce sources of fake p_T^{miss} by vetoing tracks required to balance the transverse energy of the event. Therefore, to optimise the p_T^{miss} calculation, several lower track p_T thresholds were studied in MB events and 3 GeV is considered optimal. To quantify the uncertainty on the optimisation, the p_T threshold of the tracks used in Eq. (2) is varied in both data and MC simulation by ± 1 GeV relative to the nominal track p_T threshold. All background sources, correction factors, and signal yields are recalculated during this procedure, resulting in an estimated uncertainty in the signal yield of 2.0–4.0%.

The uncertainty in the QCD multi-jet background estimation arises primarily from the extrapolation procedure. There are two contributing factors: how well the MC simulation represents the shape of the QCD multi-jet muon p_T distribution – particularly in the high- p_T region – and to what degree this distribution is altered by jet energy-loss in the medium. Both contributions may be accounted for by scaling the muon p_T distribution from simulated QCD multi-jet events by a p_T -dependent nuclear modification factor. The scale factors are calculated according to the procedure from Ref. [15] and are defined as the ratio of the inclusive charged hadron yield per binary collision in a heavy-ion event and the charged hadron yield in a pp collision. This is performed for each centrality class. Since there is little difference between the nuclear modification

factor between heavy-flavour muons and inclusive charged hadrons [15, 56], this scaling procedure is a valid estimation of the extrapolation uncertainty. Applying this factor to each muon p_T bin results in a maximum uncertainty in the QCD multi-jet background of 50% and variations in the final signal yields from 0.4% to 2.0%.

The electroweak background uncertainty is estimated separately for $Z \rightarrow \mu^+\mu^-$ and $W \rightarrow \tau\nu_\tau$. The uncertainty in the Z boson background estimation is determined by scaling the number of Z events in each η_μ interval to the number of events estimated from the MC simulation rather than those observed in the data in each centrality class. The variation in the number of $W \rightarrow \mu\nu_\mu$ events in each $|\eta_\mu|$ or centrality class with respect to the nominal yields is $< 0.1\%$. The systematic error in the τ background estimation is evaluated by assuming that the muon selection efficiencies for the p_T^{miss} and m_T requirements in the $W \rightarrow \tau\nu_\tau \rightarrow \mu\nu_\mu\nu_\tau\nu_\tau$ sample are identical to those in the $W \rightarrow \mu\nu_\mu$ sample for muons with $p_T^\mu > 25$ GeV. Estimating the τ background with these efficiencies from the $W \rightarrow \mu\nu_\mu$ sample results in a variation in the signal yields no larger than 0.1% of the nominal number of signal events in the data. Other sources of background from $Z \rightarrow \tau\tau$ and $t\bar{t}$ events are also included as a systematic uncertainty and result in a signal variation of less than 0.2%.

A systematic uncertainty attributable to the modelling accuracy of the isolation in the MC simulation is assessed by varying the ΔR and $\sum p_T^{\text{ID}}$ requirements in both data and simulation. This uncertainty is estimated by re-evaluating the yields either with a larger ΔR or a larger $\sum p_T^{\text{ID}}$. The ΔR around the muon momentum direction is increased from 0.2 to 0.3, and the requirement on the $\sum p_T^{\text{ID}}$ is increased from 10% to 20% of the muon p_T . This results in a yield variation of 1–2% in each centrality, $|\eta_\mu|$, or charge class.

Systematic uncertainties related to the C_{W^\pm} correction originate from uncertainties in the muon p_T resolution, reconstruction efficiency, and trigger efficiency. These uncertainties were previously evaluated for the 2011 heavy-ion data-taking period in Ref. [22]. A short summary of the methodology used in estimating these uncertainties and their respective contributions to the W analysis is provided below. An uncertainty in the muon p_T resolution due to differences in the detector performance in simulation relative to actual data-taking conditions is estimated by additionally smearing the p_T of muons in the MC simulation in the range allowed by the systematic uncertainties in Ref. [57]. The correction factors are then re-evaluated, and the yield variation is used as the systematic uncertainty. The relative uncertainty from this procedure results in a variation of less than 1.0% in the number of signal events in each η_μ , centrality, and charge class. Uncertainties in the muon reconstruction efficiency are also estimated from $Z \rightarrow \mu^+\mu^-$ events. To estimate this uncertainty, $Z \rightarrow \mu^+\mu^-$ MC events are re-weighted

such that the ratio of the number of muon pairs reconstructed using both the ID and MS components and muon pairs reconstructed using only the MS component – with no restriction on the ID component – agree in data and the MC simulation. The reconstruction efficiencies in the MC simulation are then recalculated and result in an additional 1.0% uncertainty in the number of $W \rightarrow \mu\nu_\mu$ events. Uncertainties in the muon trigger efficiency are determined from differences in the efficiencies calculated using single muons from MB events and a tag-and-probe method applied to a $Z \rightarrow \mu^+\mu^-$ sample. This results in yield variations of 0.4%.

Scaling uncertainties in $\langle N_{\text{coll}} \rangle$ are also applied when reporting the yields per binary collision. These were shown in Table 2 and arise from possible contamination due to photonuclear events and diffractive processes. The procedure for calculating these uncertainties is described in detail in Ref. [49]. This uncertainty is largest in the most peripheral events and amounts to 9.4%. Integrated over all events the $\langle N_{\text{coll}} \rangle$ uncertainty is around 8.5%.

The extrapolation of the yields over $|\eta_\mu| < 2.5$ also introduces a source of systematic uncertainty. This uncertainty is mainly attributable to the PDF uncertainty, which has been studied extensively in pp collisions at the LHC by ATLAS [26] using the same PDF set that this analysis uses to correct the data. The uncertainties are derived from differences in the correction factor using various PDF sets, differences due to the parton-shower modelling, and the PDF error eigenvectors. These individual contributions are added in quadrature and result in uncertainties at the 0.2% level. An uncertainty of 0.3% is associated with the differential production measurement in the highest $|\eta_\mu|$ bin.

Table 3 presents a summary of the maximum values for all systematic uncertainties included in the muon channel. Systematic uncertainties correlated between different centrality or $|\eta_\mu|$ intervals are 3–5%. The bin-uncorrelated systematic uncertainties, which are comprised of statistical uncertainties from the background estimation, trigger efficiency, and correction factors, are 1–3%. These are also included at the bottom of Table 3.

8.2 Electron channel

In the electron channel, the contribution due to the missing transverse momentum resolution is evaluated using the same procedure as in the muon channel. The yield variation is on average 2–5% with a maximum deviation of 10%.

The uncertainty in the QCD multi-jet background estimation arises from the choice of control region used to model the p_T spectrum of fake electrons from QCD multi-jet processes. This uncertainty is assessed by modifying the background composition of the control region in order to test the stability in the fitting procedure under shape changes. In

Table 3 Maximum values of the relative systematic uncertainties in the $W \rightarrow \mu\nu_\mu$ channel on the measured event yield in each $|\eta_\mu|$ interval and centrality class. Correlated uncertainties represent those that are correlated as a function of centrality or $|\eta_\mu|$. Bin-uncorrelated uncertainties represent statistical uncertainties in the background estimation, trigger efficiencies, and yield correction factors.

Source	Uncertainty [%]
p_T^{miss} resolution	4.0
QCD multi-jet background	2.0
Electroweak + $t\bar{t}$ backgrounds	0.2
Muon isolation	2.0
Muon reconstruction	1.0
Muon p_T resolution	1.0
Muon trigger efficiency	0.4
Extrapolation correction	0.3
Total bin-correlated	5.2
$\langle N_{\text{coll}} \rangle$ determination	9.4
Total bin-uncorrelated	3.0

addition, the constraint on the azimuthal separation between a jet – reconstructed at the EM scale with $E_T > 25$ GeV – and the p_T^{miss} vector is loosened or tightened [54]. After applying these modifications, the altered background fractions result in signal yield variations below 5%.

The systematic contribution associated with the electron isolation is evaluated by varying the isolation ratio from 0.2 to 0.3. This results in an average corrected yield variation of 2% with a maximum variation of 4%.

Systematic uncertainties in the electroweak background estimations are obtained from the 5% theoretical uncertainty on each of the W and Z boson production cross-sections. These uncertainties are treated as fully correlated among various W and Z boson production processes. The resulting relative systematic uncertainty is approximately 0.2% with the largest deviation at the level of 0.5%.

The main uncertainty associated with the C_{W^\pm} correction stems from possible discrepancies between data and MC simulation. In general, there are two contributions to this discrepancy: differences in the detector performance description and shortcomings in the physics model of the MC simulation that lead to distortions in the C_{W^\pm} correction given the finite binning used. To account for the first contribution, a result obtained in pp collisions [54] is used. There it was found that the electron identification efficiencies in the data are consistent with those from the MC simulation within a 3% total relative uncertainty, which is applied as a systematic uncertainty for this analysis. The second contribution is estimated by re-weighting the signal MC sample such that the $|\eta_e|$ distribution in the simulation matches the one measured in the data. This systematic variation results in an average relative systematic uncertainty below 1%.

The electron trigger efficiency obtained from the data using a tag-and-probe method is compared to the efficiency

from MC simulation. The efficiencies from both samples are consistent within their statistical uncertainties. The statistical errors in the data are propagated as uncertainties on the event yield, introducing a 0.2% uncertainty.

The systematic uncertainty due to the extrapolation of the yields in the region $|\eta_e| < 2.5$ is attributed to the same factors as in the muon channel (i.e. PDF uncertainties). This introduces an additional 0.2% uncertainty in the yields from the extrapolated $|\eta_e|$ regions. A 0.1% uncertainty is associated with the differential production measurement in the highest $|\eta_e|$ bin.

The charge of leptons from $W \rightarrow e\nu_e$ decays may be misidentified, resulting in possible misrepresentations of charge-dependent observables. The charge misidentification probability is determined from the signal MC sample. It is below 0.2% for $|\eta_e| < 1.37$ and between 1–3% in the highest $|\eta_e|$ region. These values are consistent with data-driven measurements [55] except in the highest $|\eta_e|$ bin, where a disagreement at the level of 50% is found. This percentage is propagated as an uncertainty in the difference between the correction factors of each charge, resulting in a systematic uncertainty of 1.5% and 2.0% in the number of W^- and W^+ boson yields, respectively, in the highest $|\eta_e|$ bin. In all other $|\eta_e|$ regions, the average relative systematic uncertainty is below 1%. The uncertainty in the charge asymmetry measurement is determined by varying the W^- and W^+ boson yields by their respective uncertainties in opposite directions.

Table 4 presents a summary of the maximum values for all systematic uncertainties considered in the electron channel. The bin-correlated systematic uncertainties among different centrality or $|\eta_e|$ bins are 4.0–10.5%. The bin-uncorrelated systematic uncertainties, which are comprised of statistical uncertainties from the background estimation, trigger efficiency, and correction factors, are 3.0–5.8%. These are summarised at the bottom of Table 4.

8.3 Channel combination

The results from the $W \rightarrow \mu\nu_\mu$ and $W \rightarrow e\nu_e$ channels are combined in order to increase the precision of the measurement. Although the two channels share a common kinematic phase space, differences in their geometrical acceptances must be considered in the combination procedure. After verifying that the results are compatible, the two channels are combined using an averaging method with weights proportional to the inverse square of the individual uncertainties. Uncertainties treated as fully correlated between the muon and electron channels include the p_T^{miss} resolution, electroweak background subtraction, and $\langle N_{\text{coll}} \rangle$. All other sources are treated as uncorrelated.

Table 4 Maximum values of the relative systematic uncertainties in the $W \rightarrow e\nu_e$ channel on the measured event yield in each $|\eta_e|$ interval and centrality class. Correlated uncertainties represent those that are correlated as a function of centrality or $|\eta_e|$. Uncorrelated uncertainties represent statistical uncertainties in the background estimation, trigger efficiencies, and yield correction factors.

Source	Uncertainty [%]
p_T^{miss} resolution	10.0
QCD multi-jet background	5.0
Electroweak backgrounds	0.5
Electron isolation	4.0
Electron reconstruction	3.2
Electron trigger efficiency	0.2
Charge misidentification	2.0
Extrapolation correction	0.2
Total bin-correlated	10.5
$\langle N_{\text{coll}} \rangle$ determination	9.4
Total bin-uncorrelated	5.8

8.4 Theoretical predictions

Uncertainties inherent in the PDF and EPS09 nuclear corrections are evaluated using the Hessian method to quantify the relative differences between current experimental uncertainties and central values of the PDF [58]. PDF uncertainties in the Pb nucleus are obtained from the weighted average of free proton and neutron PDF uncertainties. In addition, uncertainties in the renormalisation and factorisation scales are also taken into account by increasing and decreasing each scale by a factor of two and using the maximum variation as the uncertainty in each bin.

9 Results

The total number of background-subtracted and efficiency-corrected events in the fiducial phase space ($p_T^\ell > 25$ GeV, $p_T^{\text{miss}} > 25$ GeV, $m_T > 40$ GeV) and after extrapolation to $|\eta_\ell| < 2.5$ is presented in Table 5 along with the ratio of W^+ and W^- boson production.

The corrected yields from each channel are consistent. Moreover, the contributions from nn and pn collisions are evident. pp collisions alone would result in a ratio of W^+ and W^- bosons significantly above unity, but in Pb+Pb collisions, the larger number of d valence quarks in the neutron increases W^- production, driving the ratio closer to one. This is supported by Fig. 7, which presents the fiducial charge ratio as a function of $\langle N_{\text{part}} \rangle$ for the combined muon and electron channels.

Figure 8 shows a comparison between the differential production yields per binary collision for the muon and electron channels, separately, as a function of $|\eta_\ell|$ for W^+ and W^- . A good agreement is found between the two decay modes. In both decay channels, the distribution from W^+

Table 5 Summary of the number of background-subtracted and efficiency-corrected events for $W \rightarrow \mu\nu_\mu$ and $W \rightarrow e\nu_e$ events. The yields are defined in a fiducial region $p_T^\ell > 25$ GeV, $p_T^{\text{miss}} > 25$ GeV, $m_T > 40$ GeV and are extrapolated to $|\eta_\ell| < 2.5$.

$W \rightarrow \mu\nu_\mu$	
W^+	5870 ± 100 (stat.) ± 90 (syst.)
W^-	5680 ± 100 (stat.) ± 80 (syst.)
W^+/W^-	1.03 ± 0.03 (stat.) ± 0.02 (syst.)
$W \rightarrow e\nu_e$	
W^+	5760 ± 150 (stat.) ± 90 (syst.)
W^-	5650 ± 150 (stat.) ± 110 (syst.)
W^+/W^-	1.02 ± 0.04 (stat.) ± 0.01 (syst.)

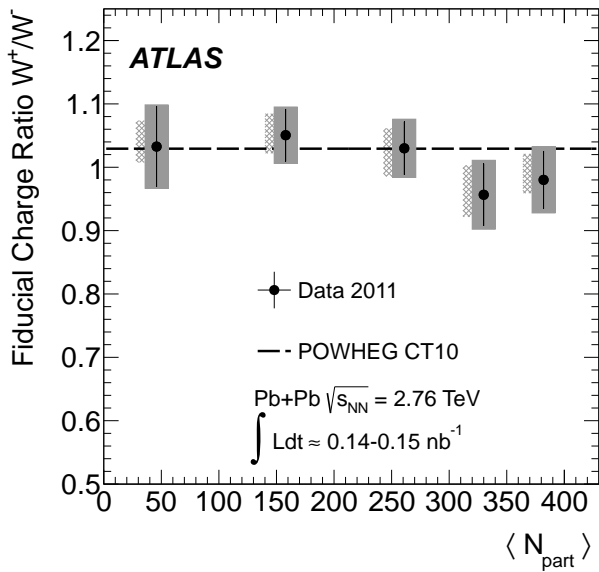


Fig. 7 Ratio of W^+ and W^- candidates (from $W \rightarrow \ell\nu_\ell$) as a function of $\langle N_{\text{part}} \rangle$. The kinematic requirements are $p_T^\ell > 25$ GeV, $p_T^{\text{miss}} > 25$ GeV, $m_T > 40$ GeV, and $|\eta_\ell| < 2.5$. Also shown is a QCD NLO prediction from POWHEG. Statistical uncertainties are shown as black bars. The filled grey boxes represent statistical and bin-uncorrelated systematic uncertainties added in quadrature, whereas the grey-hatched boxes represent bin-correlated uncertainties and are offset for clarity.

bosons steeply falls at large $|\eta_\ell|$, whereas this is not the case for W^- events. This behaviour is understood and is further discussed below in connection to the charge asymmetry.

Figure 9 presents the W boson production yield per binary collision for each charge separately as well as inclusively as a function of $\langle N_{\text{part}} \rangle$ for the combined data. Also shown are comparisons to QCD NLO predictions. The NLO predictions are consistent with the data for both the charge ratio, as shown in Fig. 7, and production yields in Fig. 9.

As with other heavy-ion electroweak boson measurements, W boson production yields per binary nucleon-nucleon collision are independent of centrality. This suggests that the W boson can be used for benchmarking

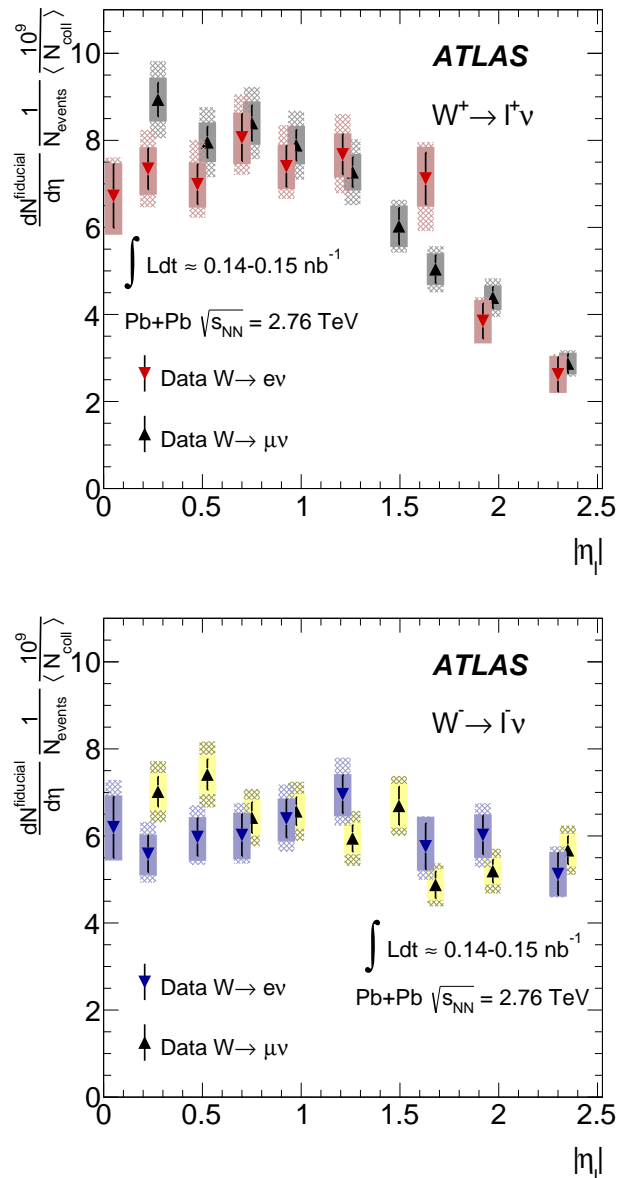


Fig. 8 Differential production yields per binary collision for W^+ (top) and W^- (bottom) events from electron and muon channels. Due to acceptance the first bin in the muon channel and the seventh bin in the electron channel are not covered. Muon points are shifted horizontally for visibility. The kinematic requirements are $p_T^\ell > 25$ GeV, $p_T^{\text{miss}} > 25$ GeV, and $m_T > 40$ GeV. Statistical errors are shown as black bars, whereas bin-uncorrelated systematic and statistical uncertainties added in quadrature are shown as the filled error box. Bin-correlated uncertainties are shown as the hatched boxes. These include uncertainties from $\langle N_{\text{coll}} \rangle$.

energy-loss processes in a QGP. Thus, when produced in association with jets, W boson production introduces an additional avenue for exploring in-medium modifications – energy loss due to multiple scattering and gluon radiation – to energetic partons traversing the heavy-ion medium.

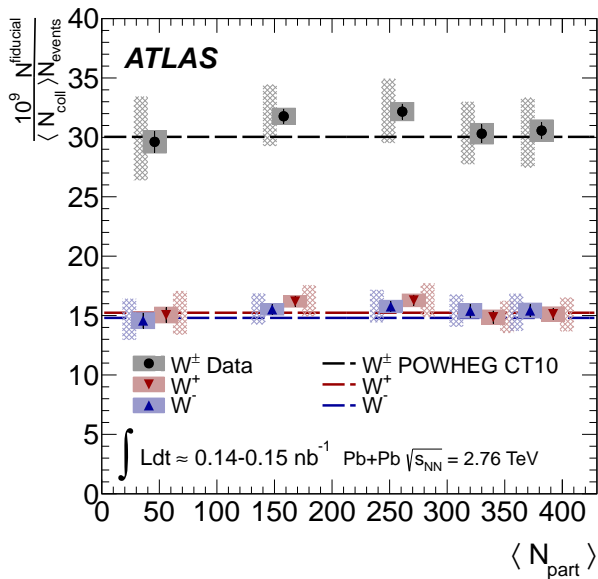


Fig. 9 W boson production yield per binary collision as a function of the mean number of participants $\langle N_{\text{part}} \rangle$ for W^+ , W^- , and W^\pm bosons for combined muon and electron channels. The kinematic requirements are $p_T^\ell > 25$ GeV, $p_T^{\text{miss}} > 25$ GeV, $m_T > 40$ GeV, and $|\eta_\ell| < 2.5$. Statistical errors are shown as black bars, whereas bin–uncorrelated systematic and statistical uncertainties added in quadrature are shown as the filled error box. Bin–correlated uncertainties are shown as the hatched boxes and are offset for clarity. These include uncertainties from $\langle N_{\text{coll}} \rangle$. Also shown is an NLO QCD prediction.

Nuclear modifications to the PDF are explored in Figs. 10 and 11, which present the differential $W \rightarrow \ell \nu_\ell$ production yields per binary nucleon–nucleon collision and the lepton charge asymmetry, respectively, as a function of $|\eta_\ell|$. Each figure includes NLO predictions with the CT10 PDF set, both with and without EPS09 nuclear corrections. The EPS09 corrections incorporate modifications to the PDF that account for contributions from shadowing, anti–shadowing, the EMC–effect, and Fermi–motion [34].

Both the CT10 and CT10+EPS09 predictions in Figs. 10 and 11 describe the data well. Therefore, at the current level of theoretical and experimental precision, this measurement is insensitive to nuclear modifications to the PDF. Fig. 11 also exhibits a sign–change of the charge asymmetry at $|\eta_\ell| \approx 1.5$, behaviour hitherto only observed at $|\eta_\ell| > 3$ in pp measurements at 7 TeV [26, 59]. The negative asymmetry is attributable to the $V-A$ structure of W boson decays, in which the decay angle of the charged lepton is anisotropic and a larger fraction of negatively charged leptons are produced at forward $|\eta_\ell|$. The larger fraction of $W^- \rightarrow \ell^- \bar{\nu}_\ell$ events in Pb+Pb compared to pp collisions results in a sign–change of the asymmetry that can be observed within the $|\eta_\ell|$ acceptance of the measurement. This behaviour is in accordance with the NLO QCD predictions.

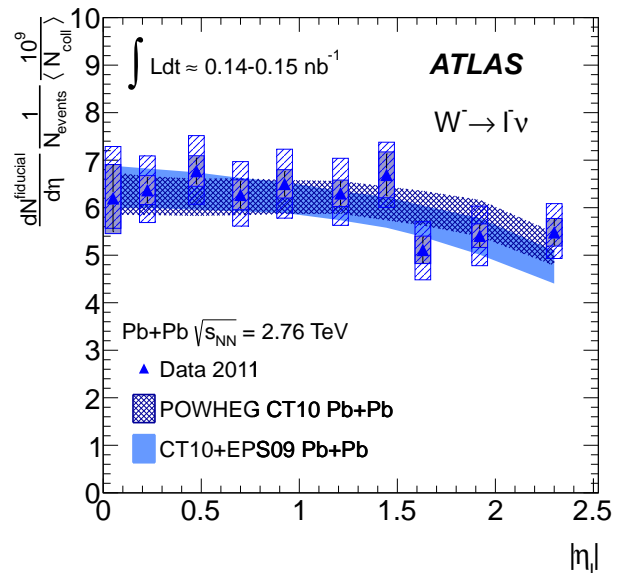
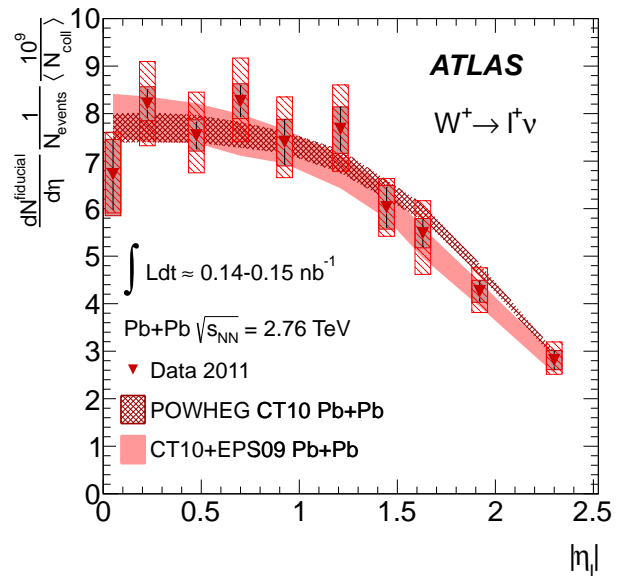


Fig. 10 Differential production yield per binary collision for W^+ (top) and W^- (bottom) events integrated over all centralities and compared to NLO QCD theoretical predictions with (CT10+EPS09) and without (CT10) nuclear corrections. The kinematic requirements are $p_T^\ell > 25$ GeV, $p_T^{\text{miss}} > 25$ GeV, and $m_T > 40$ GeV. Statistical errors are shown as black bars, whereas bin–uncorrelated systematic and statistical uncertainties added in quadrature are shown as the filled error box. Bin–correlated uncertainties are shown as the hatched boxes. These include uncertainties from $\langle N_{\text{coll}} \rangle$. The PDF uncertainties in both the CT10+EPS09 and CT10 predictions are derived from the PDF error eigensets. The total theoretical uncertainty also includes uncertainties in the renormalisation and factorisation scales used in the cross-section calculations.

10 Summary and conclusions

The measurements of W^\pm boson production in Pb+Pb collisions at $\sqrt{s_{\text{NN}}} = 2.76$ TeV are presented using data cor-

responding to an integrated luminosity of $0.14 - 0.15 \text{ nb}^{-1}$ collected with the ATLAS detector at the LHC. The W^\pm boson candidates are selected using muons or electrons in the final state in the fiducial region defined by $p_T^\ell > 25 \text{ GeV}$, $p_T^{\text{miss}} > 25 \text{ GeV}$, $m_T > 40 \text{ GeV}$ and $0.1 < |\eta_\mu| < 2.4$ for muons and $|\eta_e| < 2.47$, excluding the transition region, for electrons. After background subtraction, correction, and extrapolation to a pseudorapidity coverage of $|\eta_\ell| < 2.5$, the numbers of events reported in each channel are consistent.

The W boson production yields are presented as a function of $\langle N_{\text{part}} \rangle$ and $|\eta_\ell|$. These yields, scaled by $1/\langle N_{\text{coll}} \rangle$, are independent of centrality and in agreement with NLO QCD predictions. The lepton charge asymmetry from W^\pm boson decays differs from measurements in pp collisions. This is expected since in Pb+Pb collisions there is an additional neutron component contributing to W boson production. The lepton charge asymmetry agrees well with theoretical predictions using QCD at NLO with CT10 PDF sets with and without EPS09 nuclear corrections. The nuclear corrections account for modifications that are not present in the PDF of free nucleons. However, further improvements in the experimental precision and uncertainties in the theory are needed to establish the existence of nuclear effects. The results presented here clearly indicate that in events associated with a jet, W bosons are an excellent tool for evaluating jet energy-loss in a QGP. Moreover, it was demonstrated that W bosons can be used to study PDFs in multi-nucleon systems. With improved statistical and systematic precision, along with additional data from different colliding systems such as p +Pb, it will be possible to decisively evaluate the extent of nuclear effects on PDFs and to further test theoretical predictions.

Acknowledgements

We thank CERN for the very successful operation of the LHC, as well as the support staff from our institutions without whom ATLAS could not be operated efficiently.

We acknowledge the support of ANPCyT, Argentina; YerPhI, Armenia; ARC, Australia; BMWF and FWF, Austria; ANAS, Azerbaijan; SSTC, Belarus; CNPq and FAPESP, Brazil; NSERC, NRC and CFI, Canada; CERN; CONICYT, Chile; CAS, MOST and NSFC, China; COLCIENCIAS, Colombia; MSMT CR, MPO CR and VSC CR, Czech Republic; DNRF, DNSRC and Lundbeck Foundation, Denmark; EPLANET, ERC and NSRF, European Union; IN2P3-CNRS, CEA-DSM/IRFU, France; GNSF, Georgia; BMBF, DFG, HGF, MPG and AvH Foundation, Germany; GSRT and NSRF, Greece; ISF, MINERVA, GIF, I-CORE and Benoziyo Center, Israel; INFN, Italy; MEXT and JSPS, Japan; CNRST, Morocco; FOM and NWO, Netherlands; BRF and RCN, Norway; MNiSW and NCN, Poland; GRICES and FCT, Portugal; MNE/IFA, Romania;

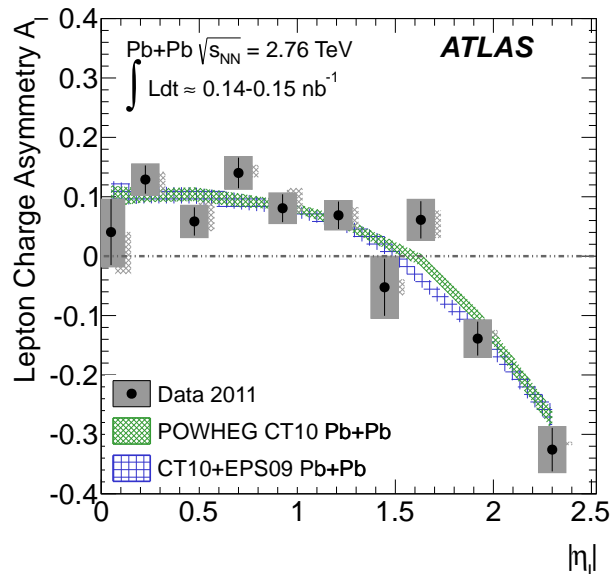


Fig. 11 The lepton charge asymmetry A_ℓ from W^\pm bosons as a function of absolute pseudorapidity compared to theoretical predictions from the CT10 and CT10+EPS09 NLO PDF sets. The kinematic requirements are $p_T^\ell > 25 \text{ GeV}$, $p_T^{\text{miss}} > 25 \text{ GeV}$, and $m_T > 40 \text{ GeV}$. Statistical uncertainties are shown as black bars, whereas bin-uncorrelated systematic and statistical uncertainties added in quadrature are shown as the filled error box. Correlated scaling uncertainties are shown as the hatched boxes and are offset for clarity. The PDF uncertainties in both the CT10+EPS09 and CT10 predictions are derived from the PDF error eigensets. The total theoretical uncertainty also includes uncertainties in the renormalisation and factorisation scales used in the cross-section calculations.

MES of Russia and ROSATOM, Russian Federation; JINR; MSTD, Serbia; MSSR, Slovakia; ARRS and MIZŠ, Slovenia; DST/NRF, South Africa; MINECO, Spain; SRC and Wallenberg Foundation, Sweden; SER, SNSF and Cantons of Bern and Geneva, Switzerland; NSC, Taiwan; TAEK, Turkey; STFC, the Royal Society and Leverhulme Trust, United Kingdom; DOE and NSF, United States of America.

The crucial computing support from all WLCG partners is acknowledged gratefully, in particular from CERN and the ATLAS Tier-1 facilities at TRIUMF (Canada), NDGF (Denmark, Norway, Sweden), CC-IN2P3 (France), KIT/GridKA (Germany), INFN-CNAF (Italy), NL-T1 (Netherlands), PIC (Spain), ASGC (Taiwan), RAL (UK) and BNL (USA) and in the Tier-2 facilities worldwide.

References

1. I. Arsene et al. [BRAHMS Collaboration], Nucl. Phys. **A757**, 1 (2005). [arXiv:nucl-ex/0410020]
2. B.B. Back et al. [PHOBOS Collaboration], Nucl. Phys. **A757**, 28 (2005). [arXiv:nucl-ex/0410022]

3. J. Adams et al. [STAR Collaboration], Nucl. Phys. **A757**, 102 (2005). [arXiv:nucl-ex/0501009]
4. K. Adcox et al. [PHENIX Collaboration], Nucl. Phys. **A757**, 184 (2005). [arXiv:nucl-ex/0410003]
5. ATLAS Collaboration, Phys. Lett. **B710**, 363 (2012). [arXiv:1108.6027]
6. CMS Collaboration, JHEP **1108**, 141 (2011). [arXiv:1107.4800]
7. M.J. Tannenbaum, Rept. Prog. Phys. **69**, 2005 (2006). [arXiv:nucl-ex/0603003]
8. B. Mohanty, Nucl. Phys. **A830**, 899C (2009). [arXiv:0907.4476]
9. K. Fukushima, T. Hatsuda, Rept. Prog. Phys. **74**, 014001 (2011). [arXiv:1005.4814]
10. B. Mohanty, New J. Phys. **13**, 065031 (2011). [arXiv:1102.2495]
11. B. Muller, J. Schukraft, B. Wyslouch, Ann. Rev. Nucl. Part. Sci. **62**, 361 (2012). [arXiv:1202.3233]
12. S.S. Adler et al. [PHENIX Collaboration], Phys. Rev. Lett. **91**, 072301 (2003). [arXiv:nucl-ex/0304022]
13. J. Adams et al. [STAR Collaboration], Phys. Rev. Lett. **91**, 172302 (2003). [arXiv:nucl-ex/0305015]
14. K. Aamodt et al. [ALICE Collaboration], Phys. Lett. **B696**, 30 (2011). [arXiv:1012.1004]
15. CMS Collaboration, Eur. Phys. J. **C72**, 1945 (2012). [arXiv:1202.2554]
16. ATLAS Collaboration, (2014). [arXiv:1406.2979]
17. ATLAS Collaboration, Phys. Lett. **B719**, 220 (2013). [arXiv:1208.1967]
18. ATLAS Collaboration, Phys. Rev. Lett. **105**, 252303 (2010). [arXiv:1011.6182]
19. CMS Collaboration, Phys. Rev. **C84**, 024906 (2011). [arXiv:1102.1957]
20. CMS Collaboration, Phys. Lett. **B712**, 176 (2012). [arXiv:1202.5022]
21. S. Afanasiev et al. [PHENIX Collaboration], Phys. Rev. Lett. **109**, 152302 (2012). [arXiv:1205.5759]
22. ATLAS Collaboration, Phys. Rev. Lett. **110**, 022301 (2013). [arXiv:1210.6486]
23. CMS Collaboration, Phys. Rev. Lett. **106**, 212301 (2011). [arXiv:1102.5435]
24. CMS Collaboration, Phys. Lett. **B710**, 256 (2012). [arXiv:1201.3093]
25. CMS Collaboration, Phys. Lett. **B715**, 66 (2012). [arXiv:1205.6334]
26. ATLAS Collaboration, Phys. Rev. **D85**, 072004 (2012). [arXiv:1109.5141]
27. CMS Collaboration, Phys. Rev. Lett. **109**, 111806 (2012). [arXiv:1206.2598]
28. CMS Collaboration, (2013). Submitted to Phys. Rev. D, [arXiv:1312.6283]
29. T. Aaltonen et al. [CDF Collaboration], Phys. Rev. Lett. **102**, 181801 (2009). [arXiv:0901.2169]
30. V. Abazov et al. [D0 Collaboration], Phys. Rev. **D88**, 091102 (2013). [arXiv:1309.2591]
31. G. Altarelli, R.K. Ellis, G. Martinelli, Nucl.Phys. **B157**, 461 (1979). DOI 10.1016/0550-3213(79)90116-0
32. J. Kubar-Andre, F.E. Paige, Phys.Rev. **D19**, 221 (1979). DOI 10.1103/PhysRevD.19.221
33. J. Kubar, M. Le Bellac, J. Meunier, G. Plaut, Nucl.Phys. **B175**, 251 (1980). DOI 10.1016/0550-3213(80)90053-X
34. H. Paukkunen, C.A. Salgado, JHEP **1103**, 071 (2011). We thank the authors for providing us with their EPS09 predictions., [arXiv:1010.5392]
35. ATLAS Collaboration, JINST **3**, S08003 (2008)
36. ATLAS Collaboration, LHCC-I-016. CERN-LHCC-2007-001 URL <http://cds.cern.ch/record/1009649>
37. ATLAS Collaboration, Eur. Phys. J. **C72**, 1849 (2012). [arXiv:1110.1530]
38. S. Agostinelli, et al., Nucl. Instrum. Meth. **A506**, 250 (2003)
39. ATLAS Collaboration, Eur. Phys. J. **C70**, 823 (2010). [arXiv:1005.4568]
40. X.N. Wang, M. Gyulassy, Phys. Rev. **D44**, 3501 (1991)
41. S. Alioli, P. Nason, C. Oleari, E. Re, JHEP **0807**, 060 (2008). [arXiv:0805.4802]
42. T. Sjostrand, S. Mrenna, P.Z. Skands, Comput. Phys. Commun. **178**, 852 (2008). [arXiv:0710.3820]
43. H.-L. Lai et al., Phys. Rev. **D82**, 074024 (2010). [arXiv:1007.2241]
44. A. Sherstnev, R. Thorne, Eur. Phys. J. **C55**, 553 (2008). [arXiv:0711.2473]
45. S. Jadach, J.H. Kuhn, Z. Was, Comput. Phys. Commun. **64**, 275 (1990)
46. P. Golonka, Z. Was, Eur. Phys. J. **C45**, 97 (2006). [arXiv:hep-ph/0506026]
47. ATLAS Collaboration, Phys. Lett. **B707**, 330 (2012). [arXiv:1108.6018]
48. ATLAS Collaboration, ATLAS-CONF-2012-122 URL <http://cds.cern.ch/record/1473425>
49. M.L. Miller, K. Reygers, S.J. Sanders, P. Steinberg, Ann. Rev. Nucl. Part. Sci. **57**, 205 (2007). [arXiv:nucl-ex/0701025]

50. J. Beringer et al. and Particle Data Group, Phys. Rev. **D86**, 010001 (2012). URL http://pdg.lbl.gov/2013/reviews/contents_sports.html
51. ATLAS Collaboration, ATLAS-CONF-2012-101 URL <http://cds.cern.ch/record/1463915>
52. ATLAS Collaboration, ATLAS-CONF-2010-036 URL <http://cds.cern.ch/record/1277675>
53. ATLAS Collaboration, ATLAS-CONF-2011-003 URL <http://cds.cern.ch/record/1326960>
54. ATLAS Collaboration, Eur. Phys. J. **C72**, 1909 (2012). [arXiv:1110.3174]
55. ATLAS Collaboration, (2014). Submitted to Eur. Phys. J. C, [arXiv:1404.2240]
56. B. Abelev et al. [ALICE Collaboration], Phys. Rev. Lett. **109**, 112301 (2012). [arXiv:1205.6443]
57. ATLAS Collaboration, ATLAS-CONF-2013-088 URL <http://cds.cern.ch/record/1580207>
58. K. Eskola, H. Paukkunen, C. Salgado, JHEP **0904**, 065 (2009). [arXiv:0902.4154]
59. LHCb Collaboration, JHEP **1206**, 058 (2012). DOI 10.1007/JHEP06(2012)058. [arXiv:1204.1620]

The ATLAS Collaboration

G. Aad⁸⁴, B. Abbott¹¹², J. Abdallah¹⁵², S. Abdel Khalek¹¹⁶, O. Abidinov¹¹, R. Aben¹⁰⁶, B. Abi¹¹³, M. Abolins⁸⁹, O.S. AbouZeid¹⁵⁹, H. Abramowicz¹⁵⁴, H. Abreu¹⁵³, R. Abreu³⁰, Y. Abulaiti^{147a,147b}, B.S. Acharya^{165a,165b,a}, L. Adamczyk^{38a}, D.L. Adams²⁵, J. Adelman¹⁷⁷, S. Adomeit⁹⁹, T. Adye¹³⁰, T. Agatonovic-Jovin^{13a}, J.A. Aguilar-Saavedra^{125a,125f}, M. Agustoni¹⁷, S.P. Ahlen²², F. Ahmadov^{64,b}, G. Aielli^{134a,134b}, H. Akerstedt^{147a,147b}, T.P.A. Åkesson⁸⁰, G. Akimoto¹⁵⁶, A.V. Akimov⁹⁵, G.L. Alberghi^{20a,20b}, J. Albert¹⁷⁰, S. Albrand⁵⁵, M.J. Alconada Verzini⁷⁰, M. Aleksa³⁰, I.N. Aleksandrov⁶⁴, C. Alexa^{26a}, G. Alexander¹⁵⁴, G. Alexandre⁴⁹, T. Alexopoulos¹⁰, M. Alhroob^{165a,165c}, G. Alimonti^{90a}, L. Alio⁸⁴, J. Alison³¹, B.M.M. Allbrooke¹⁸, L.J. Allison⁷¹, P.P. Allport⁷³, J. Almond⁸³, A. Aloisio^{103a,103b}, A. Alonso³⁶, F. Alonso⁷⁰, C. Alpigiani⁷⁵, A. Althaiser³⁵, B. Alvarez Gonzalez⁸⁹, M.G. Alviggi^{103a,103b}, K. Amako⁶⁵, Y. Amaral Coutinho^{24a}, C. Amelung²³, D. Amidei⁸⁸, S.P. Amor Dos Santos^{125a,125c}, A. Amorim^{125a,125b}, S. Amoroso⁴⁸, N. Amram¹⁵⁴, G. Amundsen²³, C. Anastopoulos¹⁴⁰, L.S. Ancu⁴⁹, N. Andari³⁰, T. Andeen³⁵, C.F. Anders^{58b}, G. Anders³⁰, K.J. Anderson³¹, A. Andreazza^{90a,90b}, V. Andrei^{58a}, X.S. Anduaga⁷⁰, S. Angelidakis⁹, I. Angelozzi¹⁰⁶, P. Anger⁴⁴, A. Angerami³⁵, F. Anghinolfi³⁰, A.V. Anisenkov¹⁰⁸, N. Anjos^{125a}, A. Annovi⁴⁷, A. Antonaki⁹, M. Antonelli⁴⁷, A. Antonov⁹⁷, J. Antos^{145b}, F. Anulli^{133a}, M. Aoki⁶⁵, L. Aperio Bella¹⁸, R. Apolle^{119,c}, G. Arabidze⁸⁹, I. Aracena¹⁴⁴, Y. Arai⁶⁵, J.P. Araque^{125a}, A.T.H. Arce⁴⁵, J-F. Arguin⁹⁴, S. Argyropoulos⁴², M. Arik^{19a}, A.J. Armbruster³⁰, O. Arnaez³⁰, V. Arnal⁸¹, H. Arnold⁴⁸, M. Arratia²⁸, O. Arslan²¹, A. Artamonov⁹⁶, G. Artoni²³, S. Asai¹⁵⁶, N. Asbah⁴², A. Ashkenazi¹⁵⁴, B. Åsman^{147a,147b}, L. Asquith⁶, K. Assamagan²⁵, R. Astalos^{145a}, M. Atkinson¹⁶⁶, N.B. Atlay¹⁴², B. Auerbach⁶, K. Augsten¹²⁷, M. Aurousseau^{146b}, G. Avolio³⁰, G. Azuelos^{94,d}, Y. Azuma¹⁵⁶, M.A. Baak³⁰, A. Baas^{58a}, C. Bacci^{135a,135b}, H. Bachacou¹³⁷, K. Bachas¹⁵⁵, M. Backes³⁰, M. Backhaus³⁰, J. Backus Mayes¹⁴⁴, E. Badescu^{26a}, P. Bagiachi^{133a,133b}, P. Bagnaia^{133a,133b}, Y. Bai^{33a}, T. Bain³⁵, J.T. Baines¹³⁰, O.K. Baker¹⁷⁷, P. Balek¹²⁸, T. Balestri¹⁴⁹, F. Balli¹³⁷, E. Banas³⁹, Sw. Banerjee¹⁷⁴, A.A.E. Bannoura¹⁷⁶, V. Bansal¹⁷⁰, H.S. Bansil¹⁸, L. Barak¹⁷³, S.P. Baranov⁹⁵, E.L. Barberio⁸⁷, D. Barberis^{50a,50b}, M. Barbero⁸⁴, T. Barillari¹⁰⁰, M. Barisonzi¹⁷⁶, T. Barklow¹⁴⁴, N. Barlow²⁸, B.M. Barnett¹³⁰, R.M. Barnett¹⁵, Z. Barnovska⁵, A. Baroncelli^{135a}, G. Barone⁴⁹, A.J. Barr¹¹⁹, F. Barreiro⁸¹, J. Barreiro Guimarães da Costa⁵⁷, R. Bartoldus¹⁴⁴, A.E. Barton⁷¹, P. Bartos^{145a}, V. Bartsch¹⁵⁰, A. Bassalat¹¹⁶, A. Basye¹⁶⁶, R.L. Bates⁵³, J.R. Batley²⁸, M. Battaglia¹³⁸, M. Battistin³⁰, F. Bauer¹³⁷, H.S. Bawa^{144,e}, M.D. Beattie⁷¹, T. Beau⁷⁹, P.H. Beauchemin¹⁶², R. Beccherle^{123a,123b}, P. Bechtel²¹, H.P. Beck¹⁷, K. Becker¹⁷⁶, S. Becker⁹⁹, M. Beckingham¹⁷¹, C. Becot¹¹⁶, A.J. Beddall^{19c}, A. Beddall^{19c}, S. Bedikian¹⁷⁷, V.A. Bednyakov⁶⁴, C.P. Bee¹⁴⁹, L.J. Beemster¹⁰⁶, T.A. Beermann¹⁷⁶, M. Begel²⁵, K. Behr¹¹⁹, C. Belanger-Champagne⁸⁶, P.J. Bell⁴⁹, W.H. Bell⁴⁹, G. Bella¹⁵⁴, L. Bellagamba^{20a}, A. Bellerive²⁹, M. Bellomo⁸⁵, K. Belotskiy⁹⁷, O. Beltramello³⁰, O. Benary¹⁵⁴, D. Bencheikroun^{136a}, K. Bendtz^{147a,147b}, N. Benekos¹⁶⁶, Y. Benhammou¹⁵⁴, E. Benhar Noccioli⁴⁹, J.A. Benitez Garcia^{160b}, D.P. Benjamin⁴⁵, J.R. Bensinger²³, K. Benslama¹³¹, S. Bentvelsen¹⁰⁶, D. Berge¹⁰⁶, E. Bergeas Kuutmann¹⁶, N. Berger⁵, F. Berghaus¹⁷⁰, J. Beringer¹⁵, C. Bernard²², P. Bernat⁷⁷, C. Bernius⁷⁸, F.U. Bernlochner¹⁷⁰, T. Berry⁷⁶, P. Berta¹²⁸, C. Bertella⁸⁴, G. Bertoli^{147a,147b}, F. Bertolucci^{123a,123b}, C. Bertsche¹¹², D. Bertsche¹¹², M.I. Besana^{90a}, G.J. Besjes¹⁰⁵, O. Bessidskaia^{147a,147b}, M. Bessner⁴², N. Besson¹³⁷, C. Betancourt⁴⁸, S. Bethke¹⁰⁰, W. Bhimji⁴⁶, R.M. Bianchi¹²⁴, L. Bianchini²³, M. Bianco³⁰, O. Biebel⁹⁹, S.P. Bieniek⁷⁷, K. Bierwagen⁵⁴, J. Biesiada¹⁵, M. Biglietti^{135a}, J. Bilbao De Mendizabal⁴⁹, H. Bilokon⁴⁷, M. Bindi⁵⁴, S. Binet¹¹⁶, A. Bingul^{19c}, C. Bini^{133a,133b}, C.W. Black¹⁵¹, J.E. Black¹⁴⁴, K.M. Black²², D. Blackburn¹³⁹, R.E. Blair⁶, J.-B. Blanchard¹³⁷, T. Blazek^{145a}, I. Bloch⁴², C. Blocker²³, W. Blum^{82,*}, U. Blumenschein⁵⁴, G.J. Bobbink¹⁰⁶, V.S. Bobrovnikov¹⁰⁸, S.S. Bocchetta⁸⁰, A. Bocchi⁴⁵, C. Bock⁹⁹, C.R. Boddy¹¹⁹, M. Boehler⁴⁸, T.T. Boek¹⁷⁶, J.A. Bogaerts³⁰, A.G. Bogdanchikov¹⁰⁸, A. Bogouch^{91,*}, C. Bohm^{147a}, J. Bohm¹²⁶, V. Boisvert⁷⁶, T. Bold^{38a}, V. Boldea^{26a}, A.S. Boldyrev⁹⁸, M. Bomben⁷⁹, M. Bona⁷⁵, M. Boonekamp¹³⁷, A. Borisov¹²⁹, G. Borissov⁷¹, M. Borri⁸³, S. Borroni⁴², J. Bortfeldt⁹⁹, V. Bortolotto^{135a,135b}, K. Bos¹⁰⁶, D. Boscherini^{20a}, M. Bosman¹², H. Boterenbrood¹⁰⁶, J. Boudreau¹²⁴, J. Bouffard², E.V. Bouhova-Thacker⁷¹, D. Boumediene³⁴, C. Bourdarios¹¹⁶, N. Bousson¹¹³, S. Boutouil^{136d}, A. Boveia³¹, J. Boyd³⁰, I.R. Boyko⁶⁴, J. Bracinik¹⁸, A. Brandt⁸, G. Brandt¹⁵, O. Brandt^{58a}, U. Bratzler¹⁵⁷, B. Brau⁸⁵, J.E. Brau¹¹⁵, H.M. Braun^{176,*}, S.F. Brazzale^{165a,165c}, B. Brelief¹⁵⁹, K. Brendlinger¹²¹, A.J. Brennan⁸⁷, R. Brenner¹⁶⁷, S. Bressler¹⁷³, K. Bristow^{146c}, T.M. Bristow⁴⁶, D. Britton⁵³, F.M. Brochu²⁸, I. Brock²¹, R. Brock⁸⁹, C. Bromberg⁸⁹, J. Bronner¹⁰⁰, G. Brooijmans³⁵, T. Brooks⁷⁶, W.K. Brooks^{32b}, J. Brosamer¹⁵, E. Brost¹¹⁵, J. Brown⁵⁵, P.A. Bruckman de Renstrom³⁹, D. Bruncko^{145b}, R. Brunelieire⁴⁸, S. Brunet⁶⁰, A. Bruni^{20a}, G. Bruni^{20a}, M. Bruschi^{20a}, L. Bryngemark⁸⁰, T. Buanes¹⁴, Q. Buat¹⁴³, F. Bucci⁴⁹, P. Buchholz¹⁴², R.M. Buckingham¹¹⁹, A.G. Buckley⁵³, S.I. Buda^{26a}, I.A. Budagov⁶⁴, F. Buehrer⁴⁸, L. Bugge¹¹⁸, M.K. Bugge¹¹⁸, O. Bulekov⁹⁷, A.C. Bundock⁷³, H. Burckhart³⁰, S. Burdin⁷³, B. Burghgrave¹⁰⁷, S. Burke¹³⁰, I. Burmeister⁴³, E. Busato³⁴, D. Büscher⁴⁸, V. Büscher⁸², P. Bussey⁵³, C.P. Buszello¹⁶⁷, B. Butler⁵⁷, J.M. Butler²², A.I. Butt³, C.M. Buttar⁵³, J.M. Butterworth⁷⁷, P. Butti¹⁰⁶, W. Buttinger²⁸, A. Buzatu⁵³, M. Byszewski¹⁰,

S. Cabrera Urbán¹⁶⁸, D. Caforio^{20a,20b}, O. Cakir^{4a}, P. Calafiura¹⁵, A. Calandri¹³⁷, G. Calderini⁷⁹, P. Calfayan⁹⁹, R. Calkins¹⁰⁷, L.P. Caloba^{24a}, D. Calvet³⁴, S. Calvet³⁴, R. Camacho Toro⁴⁹, S. Camarda⁴², D. Cameron¹¹⁸, L.M. Caminada¹⁵, R. Caminal Armadans¹², S. Campana³⁰, M. Campanelli⁷⁷, A. Campoverde¹⁴⁹, V. Canale^{103a,103b}, A. Canepa^{160a}, M. Cano Bret⁷⁵, J. Cantero⁸¹, R. Cantrill^{125a}, T. Cao⁴⁰, M.D.M. Capeans Garrido³⁰, I. Caprini^{26a}, M. Caprini^{26a}, M. Capua^{37a,37b}, R. Caputo⁸², R. Cardarelli^{134a}, T. Carli³⁰, G. Carlino^{103a}, L. Carminati^{90a,90b}, S. Caron¹⁰⁵, E. Carquin^{32a}, G.D. Carrillo-Montoya^{146c}, J.R. Carter²⁸, J. Carvalho^{125a,125c}, D. Casadei⁷⁷, M.P. Casado¹², M. Casolino¹², E. Castaneda-Miranda^{146b}, A. Castelli¹⁰⁶, V. Castillo Gimenez¹⁶⁸, N.F. Castro^{125a}, P. Catastini⁵⁷, A. Catinaccio³⁰, J.R. Catmore¹¹⁸, A. Cattai³⁰, G. Cattani^{134a,134b}, S. Caughron⁸⁹, V. Cavaliere¹⁶⁶, D. Cavalli^{90a}, M. Cavalli-Sforza¹², V. Cavasinni^{123a,123b}, F. Ceradini^{135a,135b}, B. Cerio⁴⁵, K. Cerny¹²⁸, A.S. Cerqueira^{24b}, A. Cerri¹⁵⁰, L. Cerrito⁷⁵, F. Cerutti¹⁵, M. Cerv³⁰, A. Cervelli¹⁷, S.A. Cetin^{19b}, A. Chafaq^{136a}, D. Chakraborty¹⁰⁷, I. Chalupkova¹²⁸, P. Chang¹⁶⁶, B. Chapleau⁸⁶, J.D. Chapman²⁸, D. Charfeddine¹¹⁶, D.G. Charlton¹⁸, C.C. Chau¹⁵⁹, C.A. Chavez Barajas¹⁵⁰, S. Cheatham⁸⁶, A. Chegwidan⁸⁹, S. Chekanov⁶, S.V. Chekulaev^{160a}, G.A. Chelkov^{64,f}, M.A. Chelstowska⁸⁸, C. Chen⁶³, H. Chen²⁵, K. Chen¹⁴⁹, L. Chen^{33d,g}, S. Chen^{33c}, X. Chen^{146c}, Y. Chen⁶⁶, Y. Chen³⁵, H.C. Cheng⁸⁸, Y. Cheng³¹, A. Cheplakov⁶⁴, R. Cherkaoui El Moursli^{136e}, V. Chernyatin^{25,*}, E. Cheu⁷, L. Chevalier¹³⁷, V. Chiarella⁴⁷, G. Chiefari^{103a,103b}, J.T. Childers⁶, A. Chilingarov⁷¹, G. Chiodini^{72a}, A.S. Chisholm¹⁸, R.T. Chislett⁷⁷, A. Chitan^{26a}, M.V. Chizhov⁶⁴, S. Chouridou⁹, B.K.B. Chow⁹⁹, D. Chromek-Burckhart³⁰, M.L. Chu¹⁵², J. Chudoba¹²⁶, J.J. Chwastowski³⁹, L. Chytka¹¹⁴, G. Ciapetti^{133a,133b}, A.K. Ciftci^{4a}, R. Ciftci^{4a}, D. Cinca⁵³, V. Cindro⁷⁴, A. Ciocio¹⁵, P. Cirkovic^{13b}, Z.H. Citron¹⁷³, M. Citterio^{90a}, M. Ciubancan^{26a}, A. Clark⁴⁹, P.J. Clark⁴⁶, R.N. Clarke¹⁵, W. Cleland¹²⁴, J.C. Clemens⁸⁴, C. Clement^{147a,147b}, Y. Coadou⁸⁴, M. Cobal^{165a,165c}, A. Coccaro¹³⁹, J. Cochran⁶³, L. Coffey²³, J.G. Cogan¹⁴⁴, J. Coggeshall¹⁶⁶, B. Cole³⁵, S. Cole¹⁰⁷, A.P. Colijn¹⁰⁶, J. Collot⁵⁵, T. Colombo^{58c}, G. Colon⁸⁵, G. Compostella¹⁰⁰, P. Conde Muino^{125a,125b}, E. Coniavitis⁴⁸, M.C. Conidi¹², S.H. Connell^{146b}, I.A. Connelly⁷⁶, S.M. Consonni^{90a,90b}, V. Consorti⁴⁸, S. Constantinescu^{26a}, C. Conta^{120a,120b}, G. Conti⁵⁷, F. Conventi^{103a,h}, M. Cooke¹⁵, B.D. Cooper⁷⁷, A.M. Cooper-Sarkar¹¹⁹, N.J. Cooper-Smith⁷⁶, K. Copic¹⁵, T. Cornelissen¹⁷⁶, M. Corradi^{20a}, F. Corriveau^{86,i}, A. Corso-Radu¹⁶⁴, A. Cortes-Gonzalez¹², G. Cortiana¹⁰⁰, G. Costa^{90a}, M.J. Costa¹⁶⁸, D. Costanzo¹⁴⁰, D. Côté⁸, G. Cottin²⁸, G. Cowan⁷⁶, B.E. Cox⁸³, K. Cranmer¹⁰⁹, G. Cree²⁹, S. Crépe-Renaudin⁵⁵, F. Crescioli⁷⁹, W.A. Cribbs^{147a,147b}, M. Crispin Ortuzar¹¹⁹, M. Cristinziani²¹, V. Croft¹⁰⁵, G. Crosetti^{37a,37b}, C.-M. Cucuc^{26a}, T. Cuhadar Donszelmann¹⁴⁰, J. Cummings¹⁷⁷, M. Curatolo⁴⁷, C. Cuthbert¹⁵¹, H. Czirz¹⁴², P. Czodrowski³, Z. Czynzula¹⁷⁷, S. D'Auria⁵³, M. D'Onofrio⁷³, M.J. Da Cunha Sargedas De Sousa^{125a,125b}, C. Da Via⁸³, W. Dabrowski^{38a}, A. Dafinca¹¹⁹, T. Dai⁸⁸, O. Dale¹⁴, F. Dallaire⁹⁴, C. Dallapiccola⁸⁵, M. Dam³⁶, A.C. Daniells¹⁸, M. Dano Hoffmann¹³⁷, V. Dao⁴⁸, G. Darbo^{50a}, S. Darmora⁸, J.A. Dassoulas⁴², A. Dattagupta⁶⁰, W. Davey²¹, C. David¹⁷⁰, T. Davidek¹²⁸, E. Davies^{119,c}, M. Davies¹⁵⁴, O. Davignon⁷⁹, A.R. Davison⁷⁷, P. Davison⁷⁷, Y. Davygora^{58a}, E. Dawe¹⁴³, I. Dawson¹⁴⁰, R.K. Daya-Ishmukhametova⁸⁵, K. De⁸, R. de Asmundis^{103a}, S. De Castro^{20a,20b}, S. De Cecco⁷⁹, N. De Groot¹⁰⁵, P. de Jong¹⁰⁶, H. De la Torre⁸¹, F. De Lorenzi⁶³, L. De Nooij¹⁰⁶, D. De Pedis^{133a}, A. De Salvo^{133a}, U. De Sanctis^{165a,165b}, A. De Santo¹⁵⁰, J.B. De Vivie De Regie¹¹⁶, W.J. Dearnaley⁷¹, R. Debbé²⁵, C. Debenedetti¹³⁸, B. Dechenaux⁵⁵, D.V. Dedovich⁶⁴, I. Deigaard¹⁰⁶, J. Del Peso⁸¹, T. Del Prete^{123a,123b}, F. Deliot¹³⁷, C.M. Delitzsch⁴⁹, M. Deliyergiyev⁷⁴, A. Dell'Acqua³⁰, L. Dell'Asta²², M. Dell'Orso^{123a,123b}, M. Della Pietra^{103a,h}, D. della Volpe⁴⁹, M. Delmastro⁵, P.A. Delsart⁵⁵, C. Deluca¹⁰⁶, S. Demers¹⁷⁷, M. Demichev⁶⁴, A. Demilly⁷⁹, S.P. Denisov¹²⁹, D. Derendarz³⁹, J.E. Derkaoui^{136d}, F. Derue⁷⁹, P. Dervan⁷³, K. Desch²¹, C. Deterre⁴², P.O. Deviveiros¹⁰⁶, A. Dewhurst¹³⁰, S. Dhaliwal¹⁰⁶, A. Di Ciaccio^{134a,134b}, L. Di Ciaccio⁵, A. Di Domenico^{133a,133b}, C. Di Donato^{103a,103b}, A. Di Girolamo³⁰, B. Di Girolamo³⁰, A. Di Mattia¹⁵³, B. Di Micco^{135a,135b}, R. Di Nardo⁴⁷, A. Di Simone⁴⁸, R. Di Sipio^{20a,20b}, D. Di Valentino²⁹, F.A. Dias⁴⁶, M.A. Diaz^{32a}, E.B. Diehl⁸⁸, J. Dietrich⁴², T.A. Dietzsch^{58a}, S. Diglio⁸⁴, A. Dimitrievska^{13a}, J. Dingfelder²¹, C. Dionisi^{133a,133b}, P. Dita^{26a}, S. Dita^{26a}, F. Dittus³⁰, F. Djama⁸⁴, T. Djobava^{51b}, M.A.B. do Vale^{24c}, A. Do Valle Wemans^{125a,125g}, T.K.O. Doan⁵, D. Dobos³⁰, C. Doglioni⁴⁹, T. Doherty⁵³, T. Dohmae¹⁵⁶, J. Dolejsi¹²⁸, Z. Dolezal¹²⁸, B.A. Dolgoshein^{97,*}, M. Donadelli^{24d}, S. Donati^{123a,123b}, P. Dondero^{120a,120b}, J. Donini³⁴, J. Dopke¹³⁰, A. Doria^{103a}, M.T. Dova⁷⁰, A.T. Doyle⁵³, M. Dris¹⁰, J. Dubbert⁸⁸, S. Dube¹⁵, E. Dubreuil³⁴, E. Duchovni¹⁷³, G. Duckeck⁹⁹, O.A. Ducu^{26a}, D. Duda¹⁷⁶, A. Dudarev³⁰, F. Dudziak⁶³, L. Dufloth¹¹⁶, L. Duguid⁷⁶, M. Dührssen³⁰, M. Dunford^{58a}, H. Duran Yildiz^{4a}, M. Düren⁵², A. Durglishvili^{51b}, M. Dwuznik^{38a}, M. Dyndal^{38a}, J. Ebke⁹⁹, W. Edson², N.C. Edwards⁴⁶, W. Ehrenfeld²¹, T. Eifert¹⁴⁴, G. Eigen¹⁴, K. Einsweiler¹⁵, T. Ekelof¹⁶⁷, M. El Kacimi^{136c}, M. Ellert¹⁶⁷, S. Elles⁵, F. Ellinghaus⁸², N. Ellis³⁰, J. Elmsheuser⁹⁹, M. Elsing³⁰, D. Emelianov¹³⁰, Y. Enari¹⁵⁶, O.C. Endner⁸², M. Endo¹¹⁷, R. Engelmann¹⁴⁹, J. Erdmann¹⁷⁷, A. Ereditato¹⁷, D. Eriksson^{147a}, G. Ernis¹⁷⁶, J. Ernst², M. Ernst²⁵, J. Ernwein¹³⁷, D. Errede¹⁶⁶, S. Errede¹⁶⁶, E. Ertel⁸², M. Escalier¹¹⁶, H. Esch⁴³, C. Escobar¹²⁴, B. Esposito⁴⁷, A.I. Etienne¹³⁷, E. Etzion¹⁵⁴, H. Evans⁶⁰, A. Ezhilov¹²², L. Fabbri^{20a,20b}, G. Facini³¹, R.M. Fakhruddinov¹²⁹, S. Falciano^{133a}, R.J. Falla⁷⁷, J. Faltova¹²⁸, Y. Fang^{33a}, M. Fanti^{90a,90b}, A. Farbin⁸, A. Farilla^{135a}, T. Farooque¹², S. Farrell¹⁵, S.M. Farrington¹⁷¹, P. Farthouat³⁰, F. Fassi^{136e}, P. Fassnacht³⁰, D. Fassouliotis⁹,

A. Favareto^{50a,50b}, L. Fayard¹¹⁶, P. Federic^{145a}, O.L. Fedin^{122,j}, W. Fedorko¹⁶⁹, M. Fehling-Kaschek⁴⁸, S. Feigl³⁰,
 L. Feligioni⁸⁴, C. Feng^{33d}, E.J. Feng⁶, H. Feng⁸⁸, A.B. Fenyuk¹²⁹, S. Fernandez Perez³⁰, S. Ferrag⁵³, J. Ferrando⁵³,
 A. Ferrari¹⁶⁷, P. Ferrari¹⁰⁶, R. Ferrari^{120a}, D.E. Ferreira de Lima⁵³, A. Ferrer¹⁶⁸, D. Ferrere⁴⁹, C. Ferretti⁸⁸,
 A. Ferretto Parodi^{50a,50b}, M. Fiascaris³¹, F. Fiedler⁸², A. Filipčič⁷⁴, M. Filipuzzi⁴², F. Filthaut¹⁰⁵, M. Fincke-Keeler¹⁷⁰,
 K.D. Finelli¹⁵¹, M.C.N. Fiolhais^{125a,125c}, L. Fiorini¹⁶⁸, A. Firan⁴⁰, A. Fischer², J. Fischer¹⁷⁶, W.C. Fisher⁸⁹,
 E.A. Fitzgerald²³, M. Flechl⁴⁸, I. Fleck¹⁴², P. Fleischmann⁸⁸, S. Fleischmann¹⁷⁶, G.T. Fletcher¹⁴⁰, G. Fletcher⁷⁵,
 T. Flick¹⁷⁶, A. Floderus⁸⁰, L.R. Flores Castillo^{174,k}, A.C. Florez Bustos^{160b}, M.J. Flowerdew¹⁰⁰, A. Formica¹³⁷, A. Forti⁸³,
 D. Fortin^{160a}, D. Fournier¹¹⁶, H. Fox⁷¹, S. Fracchia¹², P. Francavilla⁷⁹, M. Franchini^{20a,20b}, S. Franchino³⁰, D. Francis³⁰,
 L. Franconi¹¹⁸, M. Franklin⁵⁷, S. Franz⁶¹, M. Fraternali^{120a,120b}, S.T. French²⁸, C. Friedrich⁴², F. Friedrich⁴⁴,
 D. Froidevaux³⁰, J.A. Frost²⁸, C. Fukunaga¹⁵⁷, E. Fullana Torregrosa⁸², B.G. Fulsom¹⁴⁴, J. Fuster¹⁶⁸, C. Gabaldon⁵⁵,
 O. Gabizon¹⁷³, A. Gabrielli^{20a,20b}, A. Gabrielli^{133a,133b}, S. Gadatsch¹⁰⁶, S. Gadomski⁴⁹, G. Gagliardi^{50a,50b}, P. Gagnon⁶⁰,
 C. Galea¹⁰⁵, B. Galhardo^{125a,125c}, E.J. Gallas¹¹⁹, V. Gallo¹⁷, B.J. Gallop¹³⁰, P. Gallus¹²⁷, G. Galster³⁶, K.K. Gan¹¹⁰,
 R.P. Gandrajula⁶², J. Gao^{33b,g}, Y.S. Gao^{144,e}, F.M. Garay Walls⁴⁶, F. Garberon¹⁷⁷, C. García¹⁶⁸, J.E. García Navarro¹⁶⁸,
 M. Garcia-Sciveres¹⁵, R.W. Gardner³¹, N. Garelli¹⁴⁴, V. Garonne³⁰, C. Gatti⁴⁷, G. Gaudio^{120a}, B. Gaur¹⁴², L. Gauthier⁹⁴,
 P. Gauzzi^{133a,133b}, I.L. Gavrilenko⁹⁵, C. Gay¹⁶⁹, G. Gaycken²¹, E.N. Gazis¹⁰, P. Ge^{33d}, Z. Gecse¹⁶⁹, C.N.P. Gee¹³⁰,
 D.A.A. Geerts¹⁰⁶, Ch. Geich-Gimbel²¹, K. Gellerstedt^{147a,147b}, C. Gemme^{50a}, A. Gemmell⁵³, M.H. Genest⁵⁵,
 S. Gentile^{133a,133b}, M. George⁵⁴, S. George⁷⁶, D. Gerbaudo¹⁶⁴, A. Gershon¹⁵⁴, H. Ghazlane^{136b}, N. Ghodbane³⁴,
 B. Giacobbe^{20a}, S. Giagu^{133a,133b}, V. Giangiobbe¹², P. Giannetti^{123a,123b}, F. Gianotti³⁰, B. Gibbard²⁵, S.M. Gibson⁷⁶,
 M. Gilchriese¹⁵, T.P.S. Gillam²⁸, D. Gillberg³⁰, G. Gilles³⁴, D.M. Gingrich^{3,d}, N. Giokaris⁹, M.P. Giordani^{165a,165c},
 R. Giordano^{103a,103b}, F.M. Giorgi^{20a}, F.M. Giorgi¹⁶, P.F. Giraud¹³⁷, D. Giugni^{90a}, C. Giuliani⁴⁸, M. Giulini^{58b},
 B.K. Gjelsten¹¹⁸, S. Gkaitatzis¹⁵⁵, I. Gkialas^{155,j}, L.K. Gladilin⁹⁸, C. Glasman⁸¹, J. Glatzer³⁰, P.C.F. Glaysher⁴⁶,
 A. Glazov⁴², G.L. Glonti⁶⁴, M. Goblirsch-Kolb¹⁰⁰, J.R. Goddard⁷⁵, J. Godfrey¹⁴³, J. Godlewski³⁰, C. Goeringer⁸²,
 S. Goldfarb⁸⁸, T. Golling¹⁷⁷, D. Golubkov¹²⁹, A. Gomes^{125a,125b,125d}, L.S. Gomez Fajardo⁴², R. Gonçalo^{125a},
 J. Goncalves Pinto Firmino Da Costa¹³⁷, L. Gonella²¹, S. González de la Hoz¹⁶⁸, G. Gonzalez Parra¹²,
 S. Gonzalez-Sevilla⁴⁹, L. Goossens³⁰, P.A. Gorbounov⁹⁶, H.A. Gordon²⁵, I. Gorelov¹⁰⁴, B. Gorini³⁰, E. Gorini^{72a,72b},
 A. Gorišek⁷⁴, E. Gornicki³⁹, A.T. Goshaw⁶, C. Gössling⁴³, M.I. Gostkin⁶⁴, M. Gouighri^{136a}, D. Goujdamy^{136c},
 M.P. Goulette⁴⁹, A.G. Goussiou¹³⁹, C. Goy⁵, S. Gozpinar²³, H.M.X. Grabas¹³⁷, L. Graber⁵⁴, I. Grabowska-Bold^{38a},
 P. Grafström^{20a,20b}, K.-J. Grahn⁴², J. Gramling⁴⁹, E. Gramstad¹¹⁸, S. Grancagnolo¹⁶, V. Grassi¹⁴⁹, V. Gratchev¹²²,
 H.M. Gray³⁰, E. Graziani^{135a}, O.G. Grebenyuk¹²², Z.D. Greenwood^{78,m}, K. Gregersen⁷⁷, I.M. Gregor⁴², P. Grenier¹⁴⁴,
 J. Griffiths⁸, A.A. Grillo¹³⁸, K. Grimm⁷¹, S. Grinstein^{12,n}, Ph. Gris³⁴, Y.V. Grishkevich⁹⁸, J.-F. Grivaz¹¹⁶, J.P. Grohs⁴⁴,
 A. Grohsjean⁴², E. Gross¹⁷³, J. Grosse-Knetter⁵⁴, G.C. Grossi^{134a,134b}, J. Groth-Jensen¹⁷³, Z.J. Grout¹⁵⁰, L. Guan^{33b},
 F. Guescini⁴⁹, D. Guest¹⁷⁷, O. Gueta¹⁵⁴, C. Guicheney³⁴, E. Guido^{50a,50b}, T. Guillemin¹¹⁶, S. Guindon², U. Gul⁵³,
 C. Gumpert⁴⁴, J. Gunther¹²⁷, J. Guo³⁵, S. Gupta¹¹⁹, P. Gutierrez¹¹², N.G. Gutierrez Ortiz⁵³, C. Gutsche⁷⁷, N. Guttman¹⁵⁴,
 C. Guyot¹³⁷, C. Gwenlan¹¹⁹, C.B. Gwilliam⁷³, A. Haas¹⁰⁹, C. Haber¹⁵, H.K. Hadavand⁸, N. Haddad^{136e}, P. Haefner²¹,
 S. Hageböck²¹, Z. Hajduk³⁹, H. Hakobyan¹⁷⁸, M. Haleem⁴², D. Hall¹¹⁹, G. Halladjian⁸⁹, K. Hamacher¹⁷⁶, P. Hamal¹¹⁴,
 K. Hamano¹⁷⁰, M. Hamer⁵⁴, A. Hamilton^{146a}, S. Hamilton¹⁶², G.N. Hamity^{146c}, P.G. Hamnett⁴², L. Han^{33b},
 K. Hanagaki¹¹⁷, K. Hanawa¹⁵⁶, M. Hance¹⁵, P. Hanke^{58a}, R. Hanna¹³⁷, J.B. Hansen³⁶, J.D. Hansen³⁶, P.H. Hansen³⁶,
 K. Hara¹⁶¹, A.S. Hard¹⁷⁴, T. Harenberg¹⁷⁶, F. Hariri¹¹⁶, S. Harkusha⁹¹, D. Harper⁸⁸, R.D. Harrington⁴⁶, O.M. Harris¹³⁹,
 P.F. Harrison¹⁷¹, F. Hartjes¹⁰⁶, M. Hasegawa⁶⁶, S. Hasegawa¹⁰², Y. Hasegawa¹⁴¹, A. Hasib¹¹², S. Hassani¹³⁷, S. Haug¹⁷,
 M. Hauschild³⁰, R. Hauser⁸⁹, M. Havranek¹²⁶, C.M. Hawkes¹⁸, R.J. Hawkins³⁰, A.D. Hawkins⁸⁰, T. Hayashi¹⁶¹,
 D. Hayden⁸⁹, C.P. Hays¹¹⁹, H.S. Hayward⁷³, S.J. Haywood¹³⁰, S.J. Head¹⁸, T. Heck⁸², V. Hedberg⁸⁰, L. Heelan⁸,
 S. Heim¹²¹, T. Heim¹⁷⁶, B. Heinemann¹⁵, L. Heinrich¹⁰⁹, J. Hejbal¹²⁶, L. Helary²², C. Heller⁹⁹, M. Heller³⁰,
 S. Hellman^{147a,147b}, D. Hellmich²¹, C. Hensens³⁰, J. Henderson¹¹⁹, R.C.W. Henderson⁷¹, Y. Heng¹⁷⁴, C. Hengler⁴²,
 A. Henrichs¹⁷⁷, A.M. Henriques Correia³⁰, S. Henrot-Versille¹¹⁶, C. Hensel⁵⁴, G.H. Herbert¹⁶, Y. Hernández Jiménez¹⁶⁸,
 R. Herrberg-Schubert¹⁶, G. Herten⁴⁸, R. Hertenberger⁹⁹, L. Hervas³⁰, G.G. Hesketh⁷⁷, N.P. Hessey¹⁰⁶, R. Hickling⁷⁵,
 E. Higón-Rodríguez¹⁶⁸, E. Hill¹⁷⁰, J.C. Hill²⁸, K.H. Hiller⁴², S. Hillert²¹, S.J. Hillier¹⁸, I. Hinchliffe¹⁵, E. Hines¹²¹,
 M. Hirose¹⁵⁸, D. Hirschbuehl¹⁷⁶, J. Hobbs¹⁴⁹, N. Hod¹⁰⁶, M.C. Hodgkinson¹⁴⁰, P. Hodgson¹⁴⁰, A. Hoecker³⁰,
 M.R. Hoferkamp¹⁰⁴, F. Hoenig⁹⁹, J. Hoffman⁴⁰, D. Hoffmann⁸⁴, J.I. Hofmann^{58a}, M. Hohlfield⁸², T.R. Holmes¹⁵,
 T.M. Hong¹²¹, L. Hooft van Huysduynen¹⁰⁹, J.-Y. Hostachy⁵⁵, S. Hou¹⁵², A. Hoummada^{136a}, J. Howard¹¹⁹, J. Howarth⁴²,
 M. Hrabovsky¹¹⁴, I. Hristova¹⁶, J. Hrivnac¹¹⁶, T. Hryn'ova⁵, C. Hsu^{146c}, P.J. Hsu⁸², S.-C. Hsu¹³⁹, D. Hu³⁵, X. Hu²⁵,
 Y. Huang⁴², Z. Hubacek³⁰, F. Hubaut⁸⁴, F. Huegging²¹, T.B. Huffman¹¹⁹, E.W. Hughes³⁵, G. Hughes⁷¹, M. Huhtinen³⁰,
 T.A. Hülsing⁸², M. Hurwitz¹⁵, N. Huseynov^{64,b}, J. Huston⁸⁹, J. Huth⁵⁷, G. Iacobucci⁴⁹, G. Iakovidis¹⁰, I. Ibragimov¹⁴²,
 L. Iconomidou-Fayard¹¹⁶, E. Ideal¹⁷⁷, P. Iengo^{103a}, O. Igonkina¹⁰⁶, T. Iizawa¹⁷², Y. Ikegami⁶⁵, K. Ikematsu¹⁴², M. Ikeno⁶⁵,

Y. Ilchenko^{31,o}, D. Iliadis¹⁵⁵, N. Ilic¹⁵⁹, Y. Inamaru⁶⁶, T. Ince¹⁰⁰, P. Ioannou⁹, M. Iodice^{135a}, K. Iordanidou⁹, V. Ippolito⁵⁷, A. Irlles Quiles¹⁶⁸, C. Isaksson¹⁶⁷, M. Ishino⁶⁷, M. Ishitsuka¹⁵⁸, R. Ishmukhametov¹¹⁰, C. Issever¹¹⁹, S. Istin^{19a}, J.M. Iturbe Ponce⁸³, R. Iuppa^{134a,134b}, J. Ivarsson⁸⁰, W. Iwanski³⁹, H. Iwasaki⁶⁵, J.M. Izen⁴¹, V. Izzo^{103a}, B. Jackson¹²¹, M. Jackson⁷³, P. Jackson¹, M.R. Jaekel³⁰, V. Jain², K. Jakobs⁴⁸, S. Jakobsen³⁰, T. Jakoubek¹²⁶, J. Jakubek¹²⁷, D.O. Jamin¹⁵², D.K. Jana⁷⁸, E. Jansen⁷⁷, H. Jansen³⁰, J. Janssen²¹, M. Janus¹⁷¹, G. Jarlskog⁸⁰, N. Javadov^{64,b}, T. Javůrek⁴⁸, L. Jeanty¹⁵, J. Jejelava^{51a,p}, G.-Y. Jeng¹⁵¹, D. Jennens⁸⁷, P. Jenni^{48,q}, J. Jentsch⁴³, C. Jeske¹⁷¹, S. Jézéquel⁵, H. Ji¹⁷⁴, J. Jia¹⁴⁹, Y. Jiang^{33b}, M. Jimenez Belenguer⁴², S. Jin^{33a}, A. Jinaru^{26a}, O. Jinnouchi¹⁵⁸, M.D. Joergensen³⁶, K.E. Johansson^{147a,147b}, P. Johansson¹⁴⁰, K.A. Johns⁷, K. Jon-And^{147a,147b}, G. Jones¹⁷¹, R.W.L. Jones⁷¹, T.J. Jones⁷³, J. Jongmanns^{58a}, P.M. Jorge^{125a,125b}, K.D. Joshi⁸³, J. Jovicevic¹⁴⁸, X. Ju¹⁷⁴, C.A. Jung⁴³, R.M. Jungst³⁰, P. Jussel⁶¹, A. Juste Rozas^{12,n}, M. Kaci¹⁶⁸, A. Kaczmarska³⁹, M. Kado¹¹⁶, H. Kagan¹¹⁰, M. Kagan¹⁴⁴, E. Kajomovitz⁴⁵, C.W. Kalderon¹¹⁹, S. Kama⁴⁰, A. Kamenshchikov¹²⁹, N. Kanaya¹⁵⁶, M. Kaneda³⁰, S. Kaneti²⁸, V.A. Kantsеров⁹⁷, J. Kanzaki⁶⁵, B. Kaplan¹⁰⁹, A. Kapliy³¹, D. Kar⁵³, K. Karakostas¹⁰, N. Karastathis¹⁰, M. Karnevskiy⁸², S.N. Karpov⁶⁴, Z.M. Karpova⁶⁴, K. Karthik¹⁰⁹, V. Kartvelishvili⁷¹, A.N. Karyukhin¹²⁹, L. Kashif¹⁷⁴, G. Kasieczka^{58b}, R.D. Kass¹¹⁰, A. Kastanas¹⁴, Y. Kataoka¹⁵⁶, A. Katre⁴⁹, J. Katzy⁴², V. Kaushik⁷, K. Kawagoe⁶⁹, T. Kawamoto¹⁵⁶, G. Kawamura⁵⁴, S. Kazama¹⁵⁶, V.F. Kazanin¹⁰⁸, M.Y. Kazarinov⁶⁴, R. Keeler¹⁷⁰, R. Kehoe⁴⁰, M. Keil⁵⁴, J.S. Keller⁴², J.J. Kempster⁷⁶, H. Keoshkerian⁵, O. Kepka¹²⁶, B.P. Kerševan⁷⁴, S. Kersten¹⁷⁶, K. Kessoku¹⁵⁶, J. Keung¹⁵⁹, F. Khalil-zada¹¹, H. Khandanyan^{147a,147b}, A. Khanov¹¹³, A. Khodinov⁹⁷, A. Khomich^{58a}, T.J. Khoo²⁸, G. Khoraiuli²¹, A. Khoroshilov¹⁷⁶, V. Khovanskii⁹⁶, E. Khramov⁶⁴, J. Khubua^{51b}, H.Y. Kim⁸, H. Kim^{147a,147b}, S.H. Kim¹⁶¹, N. Kimura¹⁷², O. Kind¹⁶, B.T. King⁷³, M. King¹⁶⁸, R.S.B. King¹¹⁹, S.B. King¹⁶⁹, J. Kirk¹³⁰, A.E. Kiryunin¹⁰⁰, T. Kishimoto⁶⁶, D. Kisielewska^{38a}, F. Kiss⁴⁸, T. Kittelmann¹²⁴, K. Kiuchi¹⁶¹, E. Kladiva^{145b}, M. Klein⁷³, U. Klein⁷³, K. Kleinknecht⁸², P. Klimek^{147a,147b}, A. Klimentov²⁵, R. Klingenberg⁴³, J.A. Klinger⁸³, T. Klioutchnikova³⁰, P.F. Klok¹⁰⁵, E.-E. Kluge^{58a}, P. Kluit¹⁰⁶, S. Kluth¹⁰⁰, E. Kneringer⁶¹, E.B.F.G. Knoops⁸⁴, A. Knue⁵³, D. Kobayashi¹⁵⁸, T. Kobayashi¹⁵⁶, M. Kobel⁴⁴, M. Kocian¹⁴⁴, P. Kodys¹²⁸, P. Koevesarki²¹, T. Koffas²⁹, E. Koffeman¹⁰⁶, L.A. Kogan¹¹⁹, S. Kohlmann¹⁷⁶, Z. Kohout¹²⁷, T. Kohriki⁶⁵, T. Koi¹⁴⁴, H. Kolanoski¹⁶, I. Koletsou⁵, J. Koll⁸⁹, A.A. Komar^{95,*}, Y. Komori¹⁵⁶, T. Kondo⁶⁵, N. Kondrashova⁴², K. Köneke⁴⁸, A.C. König¹⁰⁵, S. König⁸², T. Kono^{65,r}, R. Konoplich^{109,s}, N. Konstantinidis⁷⁷, R. Kopeliansky¹⁵³, S. Koperny^{38a}, L. Köpke⁸², A.K. Kopp⁴⁸, K. Korcyl³⁹, K. Kordas¹⁵⁵, A. Korn⁷⁷, A.A. Korol^{108,t}, I. Korolkov¹², E.V. Korolkova¹⁴⁰, V.A. Korotkov¹²⁹, O. Kortner¹⁰⁰, S. Kortner¹⁰⁰, V.V. Kostyukhin²¹, V.M. Kotov⁶⁴, A. Kotwal⁴⁵, C. Kourkoumelis⁹, V. Kouskoura¹⁵⁵, A. Koutsman^{160a}, R. Kowalewski¹⁷⁰, T.Z. Kowalski^{38a}, W. Kozanecki¹³⁷, A.S. Kozhin¹²⁹, V. Kral¹²⁷, V.A. Kramarenko⁹⁸, G. Kramberger⁷⁴, D. Krasnopevtsev⁹⁷, M.W. Krasny⁷⁹, A. Krasznahorkay³⁰, J.K. Kraus²¹, A. Kravchenko²⁵, S. Kreiss¹⁰⁹, M. Kretz^{58c}, J. Kretzschmar⁷³, K. Kreutzfeldt⁵², P. Krieger¹⁵⁹, K. Kroeninger⁵⁴, H. Kroha¹⁰⁰, J. Kroll¹²¹, J. Kroseberg²¹, J. Krstic^{13a}, U. Kruchonak⁶⁴, H. Krüger²¹, T. Kruker¹⁷, N. Krumnack⁶³, Z.V. Krumshteyn⁶⁴, A. Kruse¹⁷⁴, M.C. Kruse⁴⁵, M. Kruskal²², T. Kubota⁸⁷, S. Kудay^{4a}, S. Kuehn⁴⁸, A. Kugel^{58c}, A. Kuhl¹³⁸, T. Kuhl⁴², V. Kukhtin⁶⁴, Y. Kulchitsky⁹¹, S. Kuleshov^{32b}, M. Kuna^{133a,133b}, J. Kunkle¹²¹, A. Kupco¹²⁶, H. Kurashige⁶⁶, Y.A. Kurochkin⁹¹, R. Kurumida⁶⁶, V. Kus¹²⁶, E.S. Kuwertz¹⁴⁸, M. Kuze¹⁵⁸, J. Kvita¹¹⁴, A. La Rosa⁴⁹, L. La Rotonda^{37a,37b}, C. Lacasta¹⁶⁸, F. Lacava^{133a,133b}, J. Lacey²⁹, H. Lacker¹⁶, D. Lacour⁷⁹, V.R. Lacuesta¹⁶⁸, E. Ladygin⁶⁴, R. Lafaye⁵, B. Laforge⁷⁹, T. Lagouri¹⁷⁷, S. Lai⁴⁸, H. Laier^{58a}, L. Lambourne⁷⁷, S. Lammers⁶⁰, C.L. Lampen⁷, W. Lampl⁷, E. Lançon¹³⁷, U. Landgraf⁴⁸, M.P.J. Landon⁷⁵, V.S. Lang^{58a}, A.J. Lankford¹⁶⁴, F. Lanni²⁵, K. Lantzsch³⁰, S. Laplace⁷⁹, C. Lapoire²¹, J.F. Laporte¹³⁷, T. Lari^{90a}, M. Lassnig³⁰, P. Laurelli⁴⁷, W. Lavrijsen¹⁵, A.T. Law¹³⁸, P. Laycock⁷³, O. Le Dortz⁷⁹, E. Le Guirriec⁸⁴, E. Le Menedeu¹², T. LeCompte⁶, F. Ledroit-Guillon⁵⁵, C.A. Lee¹⁵², H. Lee¹⁰⁶, J.S.H. Lee¹¹⁷, S.C. Lee¹⁵², L. Lee¹⁷⁷, G. Lefebvre⁷⁹, M. Lefebvre¹⁷⁰, F. Legger⁹⁹, C. Leggett¹⁵, A. Lehan⁷³, M. Lehmann²¹, G. Lehmann Miotto³⁰, X. Lei⁷, W.A. Leight²⁹, A. Leisos¹⁵⁵, A.G. Leister¹⁷⁷, M.A.L. Leite^{24d}, R. Leitner¹²⁸, D. Lellouch¹⁷³, B. Lemmer⁵⁴, K.J.C. Leney⁷⁷, T. Lenz²¹, G. Lenzen¹⁷⁶, B. Lenzi³⁰, R. Leone⁷, S. Leone^{123a,123b}, K. Leonhardt⁴⁴, C. Leonidopoulos⁴⁶, S. Leontsinis¹⁰, C. Leroy⁹⁴, C.G. Lester²⁸, C.M. Lester¹²¹, M. Levchenko¹²², J. Levêque⁵, D. Levin⁸⁸, L.J. Levinson¹⁷³, M. Levy¹⁸, A. Lewis¹¹⁹, G.H. Lewis¹⁰⁹, A.M. Leyko²¹, M. Leyton⁴¹, B. Li^{33b,u}, B. Li⁸⁴, H. Li¹⁴⁹, H.L. Li³¹, L. Li⁴⁵, L. Li^{33e}, S. Li⁴⁵, Y. Li^{33c,v}, Z. Liang¹³⁸, H. Liao³⁴, B. Liberti^{134a}, P. Lichard³⁰, K. Lie¹⁶⁶, J. Liebal²¹, W. Liebig¹⁴, C. Limbach²¹, A. Limosani⁸⁷, S.C. Lin^{152,w}, T.H. Lin⁸², F. Linde¹⁰⁶, B.E. Lindquist¹⁴⁹, J.T. Linnemann⁸⁹, E. Lipeles¹²¹, A. Lipniacka¹⁴, M. Lisovsky⁴², T.M. Liss¹⁶⁶, D. Lissauer²⁵, A. Lister¹⁶⁹, A.M. Litke¹³⁸, B. Liu¹⁵², D. Liu¹⁵², J.B. Liu^{33b}, K. Liu^{33b,x}, L. Liu⁸⁸, M. Liu⁴⁵, M. Liu^{33b}, Y. Liu^{33b}, M. Livan^{120a,120b}, S.S.A. Livermore¹¹⁹, A. Lleres⁵⁵, J. Llorente Merino⁸¹, S.L. Lloyd⁷⁵, F. Lo Sterzo¹⁵², E. Lobodzinska⁴², P. Loch⁷, W.S. Lockman¹³⁸, T. Loddenkoetter²¹, F.K. Loebinger⁸³, A.E. Loevschall-Jensen³⁶, A. Loginov¹⁷⁷, T. Lohse¹⁶, K. Lohwasser⁴², M. Lokajicek¹²⁶, V.P. Lombardo⁵, B.A. Long²², J.D. Long⁸⁸, R.E. Long⁷¹, L. Lopes^{125a}, D. Lopez Mateos⁵⁷, B. Lopez Paredes¹⁴⁰, I. Lopez Paz¹², J. Lorenz⁹⁹, N. Lorenzo Martinez⁶⁰, M. Losada¹⁶³, P. Loscutoff¹⁵, X. Lou⁴¹, A. Lounis¹¹⁶, J. Love⁶, P.A. Love⁷¹, A.J. Lowe^{144,e}, F. Lu^{33a}, N. Lu⁸⁸, H.J. Lubatti¹³⁹,

C. Luci^{133a,133b}, A. Lucotte⁵⁵, F. Luehring⁶⁰, W. Lukas⁶¹, L. Luminari^{133a}, O. Lundberg^{147a,147b}, B. Lund-Jensen¹⁴⁸, M. Lungwitz⁸², D. Lynn²⁵, R. Lysak¹²⁶, E. Lytken⁸⁰, H. Ma²⁵, L.L. Ma^{33d}, G. Maccarrone⁴⁷, A. Macchiolo¹⁰⁰, J. Machado Miguens^{125a,125b}, D. Macina³⁰, D. Madaffari⁸⁴, R. Madar⁴⁸, H.J. Maddocks⁷¹, W.F. Mader⁴⁴, A. Madsen¹⁶⁷, M. Maeno⁸, T. Maeno²⁵, E. Magradze⁵⁴, K. Mahboubi⁴⁸, J. Mahlstedt¹⁰⁶, S. Mahmoud⁷³, C. Maiani¹³⁷, C. Maidantchik^{24a}, A.A. Maier¹⁰⁰, A. Maio^{125a,125b,125d}, S. Majewski¹¹⁵, Y. Makida⁶⁵, N. Makovec¹¹⁶, P. Mal^{137,y}, B. Malaescu⁷⁹, Pa. Malecki³⁹, V.P. Maleev¹²², F. Malek⁵⁵, U. Mallik⁶², D. Malon⁶, C. Malone¹⁴⁴, S. Maltezos¹⁰, V.M. Malyshev¹⁰⁸, S. Malyukov³⁰, J. Mamuzic^{13b}, B. Mandelli³⁰, L. Mandelli^{90a}, I. Mandić⁷⁴, R. Mandrysch⁶², J. Maneira^{125a,125b}, A. Manfredini¹⁰⁰, L. Manhaes de Andrade Filho^{24b}, J.A. Manjarres Ramos^{160b}, A. Mann⁹⁹, P.M. Manning¹³⁸, A. Manousakis-Katsikakis⁹, B. Mansoulie¹³⁷, R. Mantifel⁸⁶, L. Mapelli³⁰, L. March¹⁶⁸, J.F. Marchand²⁹, G. Marchiori⁷⁹, M. Marcisovsky¹²⁶, C.P. Marino¹⁷⁰, M. Marjanovic^{13a}, C.N. Marques^{125a}, F. Marroquim^{24a}, S.P. Marsden⁸³, Z. Marshall¹⁵, L.F. Marti¹⁷, S. Marti-Garcia¹⁶⁸, B. Martin³⁰, B. Martin⁸⁹, T.A. Martin¹⁷¹, V.J. Martin⁴⁶, B. Martin dit Latour¹⁴, H. Martinez¹³⁷, M. Martinez^{12,n}, S. Martin-Haugh¹³⁰, A.C. Martyniuk⁷⁷, M. Marx¹³⁹, F. Marzano^{133a}, A. Marzin³⁰, L. Masetti⁸², T. Mashimo¹⁵⁶, R. Mashinistov⁹⁵, J. Masik⁸³, A.L. Maslennikov¹⁰⁸, I. Massa^{20a,20b}, L. Massa^{20a,20b}, N. Massol⁵, P. Mastrandrea¹⁴⁹, A. Mastroberardino^{37a,37b}, T. Masubuchi¹⁵⁶, P. Mättig¹⁷⁶, J. Mattmann⁸², J. Maurer^{26a}, S.J. Maxfield⁷³, D.A. Maximov^{108,t}, R. Mazini¹⁵², L. Mazzaferro^{134a,134b}, G. Mc Goldrick¹⁵⁹, S.P. Mc Kee⁸⁸, A. McCarn⁸⁸, R.L. McCarthy¹⁴⁹, T.G. McCarthy²⁹, N.A. McCubbin¹³⁰, K.W. McFarlane^{56,*}, J.A. McFayden⁷⁷, G. Mchedlidze⁵⁴, S.J. McMahon¹³⁰, R.A. McPherson^{170,i}, A. Meade⁸⁵, J. Mechnich¹⁰⁶, M. Medinnis⁴², S. Meehan³¹, S. Mehlhase⁹⁹, A. Mehta⁷³, K. Meier^{58a}, C. Meineck⁹⁹, B. Meirose⁸⁰, C. Melachrinou³¹, B.R. Mellado Garcia^{146c}, F. Meloni¹⁷, A. Mengarelli^{20a,20b}, S. Menke¹⁰⁰, E. Meoni¹⁶², K.M. Mercurio⁵⁷, S. Mergelmeyer²¹, N. Meric¹³⁷, P. Mermod⁴⁹, L. Merola^{103a,103b}, C. Meroni^{90a}, F.S. Merritt³¹, H. Merritt¹¹⁰, A. Messina^{30,z}, J. Metcalfe²⁵, A.S. Mete¹⁶⁴, C. Meyer⁸², C. Meyer¹²¹, J.-P. Meyer¹³⁷, J. Meyer³⁰, R.P. Middleton¹³⁰, S. Migas⁷³, L. Mijović²¹, G. Mikenberg¹⁷³, M. Mikestikova¹²⁶, M. Mikuž⁷⁴, A. Milic³⁰, D.W. Miller³¹, C. Mills⁴⁶, A. Milov¹⁷³, D.A. Milstead^{147a,147b}, D. Milstein¹⁷³, A.A. Minaenko¹²⁹, I.A. Minashvili⁶⁴, A.I. Mincer¹⁰⁹, B. Mindur^{38a}, M. Mineev⁶⁴, Y. Ming¹⁷⁴, L.M. Mir¹², G. Mirabelli^{133a}, T. Mitani¹⁷², J. Mitrevski⁹⁹, V.A. Mitsou¹⁶⁸, S. Mitsui⁶⁵, A. Miucci⁴⁹, P.S. Miyagawa¹⁴⁰, J.U. Mjörnmark⁸⁰, T. Moa^{147a,147b}, K. Mochizuki⁸⁴, S. Mohapatra³⁵, W. Mohr⁴⁸, S. Molander^{147a,147b}, R. Moles-Valls¹⁶⁸, K. Mönig⁴², C. Monini⁵⁵, J. Monk³⁶, E. Monnier⁸⁴, J. Montejo Berlingen¹², F. Monticelli⁷⁰, S. Monzani^{133a,133b}, R.W. Moore³, A. Moraes⁵³, N. Morange⁶², D. Moreno⁸², M. Moreno Llácer⁵⁴, P. Morettini^{50a}, M. Morgenstern⁴⁴, M. Morii⁵⁷, S. Moritz⁸², A.K. Morley¹⁴⁸, G. Mornacchi³⁰, J.D. Morris⁷⁵, L. Morvaj¹⁰², H.G. Moser¹⁰⁰, M. Mosidze^{51b}, J. Moss¹¹⁰, K. Motohashi¹⁵⁸, R. Mount¹⁴⁴, E. Mountricha²⁵, S.V. Mouraviev^{95,*}, E.J.W. Moyses⁸⁵, S. Muanza⁸⁴, R.D. Mudd¹⁸, F. Mueller^{58a}, J. Mueller¹²⁴, K. Mueller²¹, T. Mueller²⁸, T. Mueller⁸², D. Muenstermann⁴⁹, Y. Munwes¹⁵⁴, J.A. Murillo Quijada¹⁸, W.J. Murray^{171,130}, H. Musheghyan⁵⁴, E. Musto¹⁵³, A.G. Myagkov^{129,aa}, M. Myska¹²⁷, O. Nackenhorst⁵⁴, J. Nadal⁵⁴, K. Nagai⁶¹, R. Nagai¹⁵⁸, Y. Nagai⁸⁴, K. Nagano⁶⁵, A. Nagarkar¹¹⁰, Y. Nagasaka⁵⁹, M. Nagel¹⁰⁰, A.M. Nairz³⁰, Y. Nakahama³⁰, K. Nakamura⁶⁵, T. Nakamura¹⁵⁶, I. Nakano¹¹¹, H. Namasivayam⁴¹, G. Nanava²¹, R. Narayan^{58b}, T. Nattermann²¹, T. Naumann⁴², G. Navarro¹⁶³, R. Nayyar⁷, H.A. Neal⁸⁸, P.Yu. Nechaeva⁹⁵, T.J. Neep⁸³, P.D. Nef¹⁴⁴, A. Negri^{120a,120b}, G. Negri³⁰, M. Negrini^{20a}, S. Nektarijevic⁴⁹, A. Nelson¹⁶⁴, T.K. Nelson¹⁴⁴, S. Nemecek¹²⁶, P. Nemethy¹⁰⁹, A.A. Nepomuceno^{24a}, M. Nessi^{30,ab}, M.S. Neubauer¹⁶⁶, M. Neumann¹⁷⁶, R.M. Neves¹⁰⁹, P. Nevski²⁵, P.R. Newman¹⁸, D.H. Nguyen⁶, R.B. Nickerson¹¹⁹, R. Nicolaidou¹³⁷, B. Nicquevert³⁰, J. Nielsen¹³⁸, N. Nikiforou³⁵, A. Nikiforov¹⁶, V. Nikolaenko^{129,aa}, I. Nikolic-Audit⁷⁹, K. Nikolics⁴⁹, K. Nikolopoulos¹⁸, P. Nilsson⁸, Y. Ninomiya¹⁵⁶, A. Nisati^{133a}, R. Nisius¹⁰⁰, T. Nobe¹⁵⁸, L. Nodulman⁶, M. Nomachi¹¹⁷, I. Nomidis²⁹, S. Norberg¹¹², M. Nordberg³⁰, O. Novgorodova⁴⁴, S. Nowak¹⁰⁰, M. Nozaki⁶⁵, L. Nozka¹¹⁴, K. Ntekas¹⁰, G. Nunes Hanninger⁸⁷, T. Nunnemann⁹⁹, E. Nurse⁷⁷, F. Nuti⁸⁷, B.J. O'Brien⁴⁶, F. O'grady⁷, D.C. O'Neil¹⁴³, V. O'Shea⁵³, F.G. Oakham^{29,d}, H. Oberlack¹⁰⁰, T. Obermann²¹, J. Ocariz⁷⁹, A. Ochi⁶⁶, M.I. Ochoa⁷⁷, S. Oda⁶⁹, S. Odaka⁶⁵, H. Ogren⁶⁰, A. Oh⁸³, S.H. Oh⁴⁵, C.C. Ohm¹⁵, H. Ohman¹⁶⁷, W. Okamura¹¹⁷, H. Okawa²⁵, Y. Okumura³¹, T. Okuyama¹⁵⁶, A. Olariu^{26a}, A.G. Olchevski⁶⁴, S.A. Olivares Pino⁴⁶, D. Oliveira Damazio²⁵, E. Oliver Garcia¹⁶⁸, A. Olszewski³⁹, J. Olszowska³⁹, A. Onofre^{125a,125e}, P.U.E. Onyisi^{31,o}, C.J. Oram^{160a}, M.J. Oreglia³¹, Y. Oren¹⁵⁴, D. Orestano^{135a,135b}, N. Orlando^{72a,72b}, C. Oropeza Barrera⁵³, R.S. Ori¹⁵⁹, B. Osculati^{50a,50b}, R. Ospanov¹²¹, G. Otero y Garzon²⁷, H. Otono⁶⁹, M. Ouchrif^{136d}, E.A. Ouellette¹⁷⁰, F. Ould-Saada¹¹⁸, A. Ouraou¹³⁷, K.P. Oussoren¹⁰⁶, Q. Ouyang^{33a}, A. Ovcharova¹⁵, M. Owen⁸³, V.E. Ozcan^{19a}, N. Ozturk⁸, K. Pachal¹¹⁹, A. Pacheco Pages¹², C. Padilla Aranda¹², M. Pagáčová⁴⁸, S. Pagan Griso¹⁵, E. Paganis¹⁴⁰, C. Pahl¹⁰⁰, F. Paige²⁵, P. Pais⁸⁵, K. Pajchel¹¹⁸, G. Palacino^{160b}, S. Palestini³⁰, M. Palka^{38b}, D. Pallin³⁴, A. Palma^{125a,125b}, J.D. Palmer¹⁸, Y.B. Pan¹⁷⁴, E. Panagiotopoulou¹⁰, J.G. Panduro Vazquez⁷⁶, P. Pani¹⁰⁶, N. Panikashvili⁸⁸, S. Panitkin²⁵, D. Pantea^{26a}, L. Paolozzi^{134a,134b}, Th.D. Papadopoulou¹⁰, K. Papageorgiou^{155,l}, A. Paramonov⁶, D. Paredes Hernandez³⁴, M.A. Parker²⁸, F. Parodi^{50a,50b}, J.A. Parsons³⁵, U. Parzefall⁴⁸, E. Pasqualucci^{133a}, S. Passaggio^{50a}, A. Passeri^{135a}, F. Pastore^{135a,135b,*}, Fr. Pastore⁷⁶, G. Pásztor²⁹, S. Pataraja¹⁷⁶, N.D. Patel¹⁵¹, J.R. Pater⁸³, S. Patricelli^{103a,103b}, T. Pauly³⁰, J. Pearce¹⁷⁰,

M. Pedersen¹¹⁸, S. Pedraza Lopez¹⁶⁸, R. Pedro^{125a,125b}, S.V. Peleganchuk¹⁰⁸, D. Pelikan¹⁶⁷, H. Peng^{33b}, B. Penning³¹, J. Penwell⁶⁰, D.V. Perepelitsa²⁵, E. Perez Codina^{160a}, M.T. Pérez García-Estañ¹⁶⁸, V. Perez Reale³⁵, L. Perini^{90a,90b}, H. Pernegger³⁰, R. Perrino^{72a}, R. Peschke⁴², V.D. Peshekhonov⁶⁴, K. Peters³⁰, R.F.Y. Peters⁸³, B.A. Petersen³⁰, T.C. Petersen³⁶, E. Petit⁴², A. Petridis^{147a,147b}, C. Petridou¹⁵⁵, E. Petrolo^{133a}, F. Petrucci^{135a,135b}, N.E. Pettersson¹⁵⁸, R. Pezoa^{32b}, P.W. Phillips¹³⁰, G. Piacquadio¹⁴⁴, E. Pianori¹⁷¹, A. Picazio⁴⁹, E. Piccaro⁷⁵, M. Piccinini^{20a,20b}, R. Piegaia²⁷, D.T. Pignotti¹¹⁰, J.E. Pilcher³¹, A.D. Pilkington⁷⁷, J. Pina^{125a,125b,125d}, M. Pinamonti^{165a,165c,ac}, A. Pinder¹¹⁹, J.L. Pinfold³, A. Pingel³⁶, B. Pinto^{125a}, S. Pires⁷⁹, M. Pitt¹⁷³, C. Pizio^{90a,90b}, L. Plazak^{145a}, M.-A. Pleier²⁵, V. Pleskot¹²⁸, E. Plotnikova⁶⁴, P. Plucinski^{147a,147b}, S. Poddar^{58a}, F. Podlyski³⁴, R. Poettgen⁸², L. Poggioli¹¹⁶, D. Pohl²¹, M. Pohl⁴⁹, G. Polesello^{120a}, A. Policicchio^{37a,37b}, R. Polifka¹⁵⁹, A. Polini^{20a}, C.S. Pollard⁴⁵, V. Polychronakos²⁵, K. Pommès³⁰, L. Pontecorvo^{133a}, B.G. Pope⁸⁹, G.A. Popeneciu^{26b}, D.S. Popovic^{13a}, A. Poppleton³⁰, X. Portell Bueso¹², S. Pospisil¹²⁷, K. Potamianos¹⁵, I.N. Potrap⁶⁴, C.J. Potter¹⁵⁰, C.T. Potter¹¹⁵, G. Poulard³⁰, J. Poveda⁶⁰, V. Pozdnyakov⁶⁴, P. Pralavorio⁸⁴, A. Pranko¹⁵, S. Prasad³⁰, R. Pravahan⁸, S. Prell⁶³, D. Price⁸³, J. Price⁷³, L.E. Price⁶, D. Prieur¹²⁴, M. Primavera^{72a}, M. Proissl⁴⁶, K. Prokofiev⁴⁷, F. Prokoshin^{32b}, E. Protopapadaki¹³⁷, S. Protopopescu²⁵, J. Proudfoot⁶, M. Przybycien^{38a}, H. Przysiezniak⁵, E. Ptacek¹¹⁵, D. Puddu^{135a,135b}, E. Pueschel⁸⁵, D. Puldron¹⁴⁹, M. Purohit^{25,ad}, P. Puzo¹¹⁶, J. Qian⁸⁸, G. Qin⁵³, Y. Qin⁸³, A. Quadt⁵⁴, D.R. Quarrie¹⁵, W.B. Quayle^{165a,165b}, M. Queitsch-Maitland⁸³, D. Quilty⁵³, A. Qureshi^{160b}, V. Radeka²⁵, V. Radescu⁴², S.K. Radhakrishnan¹⁴⁹, P. Radloff¹¹⁵, P. Rados⁸⁷, F. Ragusa^{90a,90b}, G. Rahal¹⁷⁹, S. Rajagopalan²⁵, M. Rammensee³⁰, A.S. Randle-Conde⁴⁰, C. Rangel-Smith¹⁶⁷, K. Rao¹⁶⁴, F. Rauscher⁹⁹, T.C. Rave⁴⁸, T. Ravenscroft⁵³, M. Raymond³⁰, A.L. Read¹¹⁸, N.P. Readioff⁷³, D.M. Rebuffi^{120a,120b}, A. Redelbach¹⁷⁵, G. Redlinger²⁵, R. Reece¹³⁸, K. Reeves⁴¹, L. Rehnisch¹⁶, H. Reisin²⁷, M. Relich¹⁶⁴, C. Rembser³⁰, H. Ren^{33a}, Z.L. Ren¹⁵², A. Renaud¹¹⁶, M. Rescigno^{133a}, S. Resconi^{90a}, O.L. Rezanova^{108,t}, P. Reznicek¹²⁸, R. Rezvani⁹⁴, R. Richter¹⁰⁰, M. Ridel⁷⁹, P. Rieck¹⁶, J. Rieger⁵⁴, M. Rijssenbeek¹⁴⁹, A. Rimoldi^{120a,120b}, L. Rinaldi^{20a}, E. Ritsch⁶¹, I. Riu¹², F. Rizatdinova¹¹³, E. Rizvi⁷⁵, S.H. Robertson^{86,i}, A. Robichaud-Veronneau⁸⁶, D. Robinson²⁸, J.E.M. Robinson⁸³, A. Robson⁵³, C. Roda^{123a,123b}, L. Rodrigues³⁰, S. Roe³⁰, O. Røhne¹¹⁸, S. Rolli¹⁶², A. Romaniouk⁹⁷, M. Romano^{20a,20b}, E. Romero Adam¹⁶⁸, N. Rompotis¹³⁹, M. Ronzani⁴⁸, L. Roos⁷⁹, E. Ros¹⁶⁸, S. Rosati^{133a}, K. Rosbach⁴⁹, M. Rose⁷⁶, P. Rose¹³⁸, P.L. Rosendahl¹⁴, O. Rosenthal¹⁴², V. Rossetti^{147a,147b}, E. Rossi^{103a,103b}, L.P. Rossi^{50a}, R. Rosten¹³⁹, M. Rotaru^{26a}, I. Roth¹⁷³, J. Rothberg¹³⁹, D. Rousseau¹¹⁶, C.R. Royon¹³⁷, A. Rozanov⁸⁴, Y. Rozen¹⁵³, X. Ruan^{146c}, F. Rubbo¹², I. Rubinsky⁴², V.I. Rud⁹⁸, C. Rudolph⁴⁴, M.S. Rudolph¹⁵⁹, F. Rühr⁴⁸, A. Ruiz-Martinez³⁰, Z. Rurikova⁴⁸, N.A. Rusakovich⁶⁴, A. Ruschke⁹⁹, J.P. Rutherford⁷, N. Ruthmann⁴⁸, Y.F. Ryabov¹²², M. Rybar¹²⁸, G. Rybkin¹¹⁶, N.C. Ryder¹¹⁹, A.F. Saavedra¹⁵¹, S. Sacerdoti²⁷, A. Saddique³, I. Sadeh¹⁵⁴, H.F.W. Sadrozinski¹³⁸, R. Sadykov⁶⁴, F. Safai Tehrani^{133a}, H. Sakamoto¹⁵⁶, Y. Sakurai¹⁷², G. Salamanna^{135a,135b}, A. Salamon^{134a}, M. Saleem¹¹², D. Salek¹⁰⁶, P.H. Sales De Bruin¹³⁹, D. Salihagic¹⁰⁰, A. Salnikov¹⁴⁴, J. Salt¹⁶⁸, D. Salvatore^{37a,37b}, F. Salvatore¹⁵⁰, A. Salvucci¹⁰⁵, A. Salzburger³⁰, D. Sampsonidis¹⁵⁵, A. Sanchez^{103a,103b}, J. Sánchez¹⁶⁸, V. Sanchez Martinez¹⁶⁸, H. Sandaker¹⁴, R.L. Sandbach⁷⁵, H.G. Sander⁸², M.P. Sanders⁹⁹, M. Sandhoff¹⁷⁶, T. Sandoval²⁸, C. Sandoval¹⁶³, R. Sandstroem¹⁰⁰, D.P.C. Sankey¹³⁰, A. Sansoni⁴⁷, C. Santoni³⁴, R. Santonico^{134a,134b}, H. Santos^{125a}, I. Santoyo Castillo¹⁵⁰, K. Sapp¹²⁴, A. Sapronov⁶⁴, J.G. Saraiva^{125a,125d}, B. Sarrazin²¹, G. Sartisohn¹⁷⁶, O. Sasaki⁶⁵, Y. Sasaki¹⁵⁶, G. Sauvage^{5,*}, E. Sauvan⁵, P. Savard^{159,d}, D.O. Savu³⁰, C. Sawyer¹¹⁹, L. Sawyer^{78,m}, D.H. Saxon⁵³, J. Saxon¹²¹, C. Sbarra^{20a}, A. Sbrizzi³, T. Scanlon⁷⁷, D.A. Scannicchio¹⁶⁴, M. Scarcella¹⁵¹, V. Scarfone^{37a,37b}, J. Schaarschmidt¹⁷³, P. Schacht¹⁰⁰, D. Schaefer³⁰, R. Schaefer⁴², S. Schaepe²¹, S. Schatzel^{58b}, U. Schäfer⁸², A.C. Schaffer¹¹⁶, D. Schaile⁹⁹, R.D. Schamberger¹⁴⁹, V. Scharf^{58a}, V.A. Schegelsky¹²², D. Scheirich¹²⁸, M. Schernau¹⁶⁴, M.I. Scherzer³⁵, C. Schiavi^{50a,50b}, J. Schieck⁹⁹, C. Schillo⁴⁸, M. Schioppa^{37a,37b}, S. Schlenker³⁰, E. Schmidt⁴⁸, K. Schmieden³⁰, C. Schmitt⁸², S. Schmitt^{58b}, B. Schneider¹⁷, Y.J. Schnellbach⁷³, U. Schnoor⁴⁴, L. Schoeffel¹³⁷, A. Schoening^{58b}, B.D. Schoenrock⁸⁹, A.L.S. Schorlemmer⁵⁴, M. Schott⁸², D. Schouten^{160a}, J. Schovancova²⁵, S. Schramm¹⁵⁹, M. Schreyer¹⁷⁵, C. Schroeder⁸², N. Schuh⁸², M.J. Schultens²¹, H.-C. Schultz-Coulon^{58a}, H. Schulz¹⁶, M. Schumacher⁴⁸, B.A. Schumm¹³⁸, Ph. Schune¹³⁷, C. Schwanenberger⁸³, A. Schwartzman¹⁴⁴, Ph. Schwegler¹⁰⁰, Ph. Schwemling¹³⁷, R. Schwienhorst⁸⁹, J. Schwindling¹³⁷, T. Schwindt²¹, M. Schwoerer⁵, F.G. Sciacca¹⁷, E. Scifo¹¹⁶, G. Sciolla²³, W.G. Scott¹³⁰, F. Scuri^{123a,123b}, F. Scutti²¹, J. Searcy⁸⁸, G. Sedov⁴², E. Sedykh¹²², S.C. Seidel¹⁰⁴, A. Seiden¹³⁸, F. Seifert¹²⁷, J.M. Seixas^{24a}, G. Sekhniaidze^{103a}, S.J. Sekula⁴⁰, K.E. Selbach⁴⁶, D.M. Seliverstov^{122,*}, G. Sellers⁷³, N. Semprini-Cesari^{20a,20b}, C. Serfon³⁰, L. Serin¹¹⁶, L. Serkin⁵⁴, T. Serre⁸⁴, R. Seuster^{160a}, H. Severini¹¹², T. Sfiligoj⁷⁴, F. Sforza¹⁰⁰, A. Sfyrla³⁰, E. Shabalina⁵⁴, M. Shamim¹¹⁵, L.Y. Shan^{33a}, R. Shang¹⁶⁶, J.T. Shank²², M. Shapiro¹⁵, P.B. Shatalov⁹⁶, K. Shaw^{165a,165b}, C.Y. Shehu¹⁵⁰, P. Sherwood⁷⁷, L. Shi^{152,ae}, S. Shimizu⁶⁶, C.O. Shimmin¹⁶⁴, M. Shimojima¹⁰¹, M. Shiyakova⁶⁴, A. Shmeleva⁹⁵, M.J. Shochet³¹, D. Short¹¹⁹, S. Shrestha⁶³, E. Shulga⁹⁷, M.A. Shupe⁷, S. Shushkevich⁴², P. Sicho¹²⁶, O. Sidiropoulou¹⁵⁵, D. Sidorov¹¹³, A. Sidoti^{133a}, F. Siegert⁴⁴, Dj. Sijacki^{13a}, J. Silva^{125a,125d}, Y. Silver¹⁵⁴, D. Silverstein¹⁴⁴, S.B. Silverstein^{147a}, V. Simak¹²⁷, O. Simard⁵, Lj. Simic^{13a}, S. Simion¹¹⁶, E. Simioni⁸², B. Simmons⁷⁷, R. Simoniello^{90a,90b}, M. Simonyan³⁶, P. Sinervo¹⁵⁹, N.B. Sinev¹¹⁵,

V. Sipica¹⁴², G. Siragusa¹⁷⁵, A. Sircar⁷⁸, A.N. Sisakyan^{64,*}, S.Yu. Sivoklokov⁹⁸, J. Sjölin^{147a,147b}, T.B. Sjurksen¹⁴, H.P. Skottowe⁵⁷, K.Yu. Skovpen¹⁰⁸, P. Skubic¹¹², M. Slater¹⁸, T. Slavicek¹²⁷, K. Sliwa¹⁶², V. Smakhtin¹⁷³, B.H. Smart⁴⁶, L. Smestad¹⁴, S.Yu. Smirnov⁹⁷, Y. Smirnov⁹⁷, L.N. Smirnova^{98,af}, O. Smirnova⁸⁰, K.M. Smith⁵³, M. Smizanska⁷¹, K. Smolek¹²⁷, A.A. Snesarev⁹⁵, G. Snidero⁷⁵, S. Snyder²⁵, R. Sobie^{170,i}, F. Socher⁴⁴, A. Soffer¹⁵⁴, D.A. Soh^{152,ae}, C.A. Solans³⁰, M. Solar¹²⁷, J. Solc¹²⁷, E.Yu. Soldatov⁹⁷, U. Soldevila¹⁶⁸, A.A. Solodkov¹²⁹, A. Soloshenko⁶⁴, O.V. Solovyanov¹²⁹, V. Solovyev¹²², P. Sommer⁴⁸, H.Y. Song^{33b}, N. Soni¹, A. Sood¹⁵, A. Sopczak¹²⁷, B. Sopko¹²⁷, V. Sopko¹²⁷, V. Sorin¹², M. Sosebee⁸, R. Soualah^{165a,165c}, P. Soueid⁹⁴, A.M. Soukharev¹⁰⁸, D. South⁴², S. Spagnolo^{72a,72b}, F. Spanò⁷⁶, W.R. Spearman⁵⁷, F. Spettel¹⁰⁰, R. Spighi^{20a}, G. Spigo³⁰, L.A. Spiller⁸⁷, M. Spousta¹²⁸, T. Spreitzer¹⁵⁹, B. Spurlock⁸, R.D. St. Denis^{53,*}, S. Staerz⁴⁴, J. Stahlman¹²¹, R. Stamen^{58a}, S. Stamm¹⁶, E. Stanecka³⁹, R.W. Stanek⁶, C. Stanescu^{135a}, M. Stanescu-Bellu⁴², M.M. Stanitzki⁴², S. Stapnes¹¹⁸, E.A. Starchenko¹²⁹, J. Stark⁵⁵, P. Staroba¹²⁶, P. Starovoitov⁴², R. Staszewski³⁹, P. Stavina^{145a,*}, P. Steinberg²⁵, B. Stelzer¹⁴³, H.J. Stelzer³⁰, O. Stelzer-Chilton^{160a}, H. Stenzel⁵², S. Stern¹⁰⁰, G.A. Stewart⁵³, J.A. Stillings²¹, M.C. Stockton⁸⁶, M. Stoebe⁸⁶, G. Stoicica^{26a}, P. Stolte⁵⁴, S. Stonjek¹⁰⁰, A.R. Stradling⁸, A. Straessner⁴⁴, M.E. Stramaglia¹⁷, J. Strandberg¹⁴⁸, S. Strandberg^{147a,147b}, A. Strandlie¹¹⁸, E. Strauss¹⁴⁴, M. Strauss¹¹², P. Strizenc^{145b}, R. Ströhmer¹⁷⁵, D.M. Strom¹¹⁵, R. Stroynowski⁴⁰, S.A. Stucci¹⁷, B. Stugu¹⁴, N.A. Styles⁴², D. Su¹⁴⁴, J. Su¹²⁴, R. Subramaniam⁷⁸, A. Succurro¹², Y. Sugaya¹¹⁷, C. Suhr¹⁰⁷, M. Suk¹²⁷, V.V. Sulin⁹⁵, S. Sultansoy^{4c}, T. Sumida⁶⁷, S. Sun⁵⁷, X. Sun^{33a}, J.E. Sundermann⁴⁸, K. Suruliz¹⁴⁰, G. Susinno^{37a,37b}, M.R. Sutton¹⁵⁰, Y. Suzuki⁶⁵, M. Svatos¹²⁶, S. Swedish¹⁶⁹, M. Swiatlowski¹⁴⁴, I. Sykora^{145a}, T. Sykora¹²⁸, D. Ta⁸⁹, C. Taccini^{135a,135b}, K. Tackmann⁴², J. Taenzer¹⁵⁹, A. Taffard¹⁶⁴, R. Tafirout^{160a}, N. Taiblum¹⁵⁴, H. Takai²⁵, R. Takashima⁶⁸, H. Takeda⁶⁶, T. Takeshita¹⁴¹, Y. Takubo⁶⁵, M. Talby⁸⁴, A.A. Talyshv^{108,t}, J.Y.C. Tam¹⁷⁵, K.G. Tan⁸⁷, J. Tanaka¹⁵⁶, R. Tanaka¹¹⁶, S. Tanaka¹³², S. Tanaka⁶⁵, A.J. Tanasijczuk¹⁴³, B.B. Tannenwald¹¹⁰, N. Tannoury²¹, S. Tapprogge⁸², S. Tarem¹⁵³, F. Tarrade²⁹, G.F. Tartarelli^{90a}, P. Tas¹²⁸, M. Tasevsky¹²⁶, T. Tashiro⁶⁷, E. Tassi^{37a,37b}, A. Tavares Delgado^{125a,125b}, Y. Tayalati^{136d}, F.E. Taylor⁹³, G.N. Taylor⁸⁷, W. Taylor^{160b}, F.A. Teischinger³⁰, M. Teixeira Dias Castanheira⁷⁵, P. Teixeira-Dias⁷⁶, K.K. Temming⁴⁸, H. Ten Kate³⁰, P.K. Teng¹⁵², J.J. Teoh¹¹⁷, S. Terada⁶⁵, K. Terashi¹⁵⁶, J. Terron⁸¹, S. Terzo¹⁰⁰, M. Testa⁴⁷, R.J. Teuscher^{159,i}, J. Therhaag²¹, T. Theveneaux-Pelzer³⁴, J.P. Thomas¹⁸, J. Thomas-Wilsker⁷⁶, E.N. Thompson³⁵, P.D. Thompson¹⁸, P.D. Thompson¹⁵⁹, R.J. Thompson⁸³, A.S. Thompson⁵³, L.A. Thomsen³⁶, E. Thomson¹²¹, M. Thomson²⁸, W.M. Thong⁸⁷, R.P. Thun^{88,*}, F. Tian³⁵, M.J. Tibbetts¹⁵, V.O. Tikhomirov^{95,ag}, Yu.A. Tikhonov^{108,t}, S. Timoshenko⁹⁷, E. Tiouchichine⁸⁴, P. Tipton¹⁷⁷, S. Tisserant⁸⁴, T. Todorov⁵, S. Todorova-Nova¹²⁸, B. Toggerson⁷, J. Tojo⁶⁹, S. Tokár^{145a}, K. Tokushuku⁶⁵, K. Tollefson⁸⁹, L. Tomlinson⁸³, M. Tomoto¹⁰², L. Tompkins³¹, K. Toms¹⁰⁴, N.D. Topilin⁶⁴, E. Torrence¹¹⁵, H. Torres¹⁴³, E. Torró Pastor¹⁶⁸, J. Toth^{84,ah}, F. Touchard⁸⁴, D.R. Tovey¹⁴⁰, H.L. Tran¹¹⁶, T. Trefzger¹⁷⁵, L. Tremblet³⁰, A. Tricoli³⁰, I.M. Trigger^{160a}, S. Trincaz-Duvoid⁷⁹, M.F. Tripiana¹², W. Trischuk¹⁵⁹, B. Trocmé⁵⁵, C. Troncon^{90a}, M. Trotter-McDonald¹⁴³, M. Trovatelli^{135a,135b}, P. True⁸⁹, M. Trzebinski³⁹, A. Trzupek³⁹, C. Tsarouchas³⁰, J.C.-L. Tseng¹¹⁹, P.V. Tsiareshka⁹¹, D. Tsionou¹³⁷, G. Tsipolitis¹⁰, N. Tsirintanis⁹, S. Tsiskaridze¹², V. Tsiskaridze⁴⁸, E.G. Tskhadadze^{51a}, I.I. Tsukerman⁹⁶, V. Tsulaia¹⁵, S. Tsuno⁶⁵, D. Tsybychev¹⁴⁹, A. Tudorache^{26a}, V. Tudorache^{26a}, A.N. Tuna¹²¹, S.A. Tuppuri^{20a,20b}, S. Turchikhin^{98,af}, D. Turecek¹²⁷, I. Turk Cakir^{4d}, R. Turra^{90a,90b}, P.M. Tuts³⁵, A. Tykhonov⁴⁹, M. Tylmad^{147a,147b}, M. Tyndel¹³⁰, K. Uchida²¹, I. Ueda¹⁵⁶, R. Ueno²⁹, M. Ughetto⁸⁴, M. Uglan¹⁴, M. Uhlenbrock²¹, F. Ukegawa¹⁶¹, G. Unal³⁰, A. Undrus²⁵, G. Unel¹⁶⁴, F.C. Ungaro⁴⁸, Y. Unno⁶⁵, C. Unverdorben⁹⁹, D. Urbaniec³⁵, P. Urquijo⁸⁷, G. Usai⁸, A. Usanova⁶¹, L. Vacavant⁸⁴, V. Vacek¹²⁷, B. Vachon⁸⁶, N. Valencic¹⁰⁶, S. Valentini^{20a,20b}, A. Valero¹⁶⁸, L. Valery³⁴, S. Valkar¹²⁸, E. Valladolid Gallego¹⁶⁸, S. Vallecorsa⁴⁹, J.A. Valls Ferrer¹⁶⁸, W. Van Den Wollenberg¹⁰⁶, P.C. Van Der Deijl¹⁰⁶, R. van der Geer¹⁰⁶, H. van der Graaf¹⁰⁶, R. Van Der Leeuw¹⁰⁶, D. van der Ster³⁰, N. van Eldik³⁰, P. van Gemmeren⁶, J. Van Nieuwkoop¹⁴³, I. van Vulpen¹⁰⁶, M.C. van Woerden³⁰, M. Vanadia^{133a,133b}, W. Vandelli³⁰, R. Vanguri¹²¹, A. Vaniachine⁶, P. Vankov⁴², F. Vannucci⁷⁹, G. Vardanyan¹⁷⁸, R. Vari^{133a}, E.W. Varnes⁷, T. Varol⁸⁵, D. Varouchas⁷⁹, A. Vartapetian⁸, K.E. Varvell¹⁵¹, F. Vazeille³⁴, T. Vazquez Schroeder⁵⁴, J. Veatch⁷, F. Veloso^{125a,125c}, S. Veneziano^{133a}, A. Ventura^{72a,72b}, D. Ventura⁸⁵, M. Venturi¹⁷⁰, N. Venturi¹⁵⁹, A. Venturini²³, V. Vercesi^{120a}, M. Verducci^{133a,133b}, W. Verkerke¹⁰⁶, J.C. Vermeulen¹⁰⁶, A. Vest⁴⁴, M.C. Vetterli^{143,d}, O. Viazlo⁸⁰, I. Vichou¹⁶⁶, T. Vickey^{146c,ai}, O.E. Vickey Boeriu^{146c}, G.H.A. Viehhauser¹¹⁹, S. Viel¹⁶⁹, R. Vigne³⁰, M. Villa^{20a,20b}, M. Villaplana Perez^{90a,90b}, E. Vilucchi⁴⁷, M.G. Vincker²⁹, V.B. Vinogradov⁶⁴, J. Virzi¹⁵, I. Vivarelli¹⁵⁰, F. Vives Vaque³, S. Vlachos¹⁰, D. Vladoiu⁹⁹, M. Vlasak¹²⁷, A. Vogel²¹, M. Vogel^{32a}, P. Vokac¹²⁷, G. Volpi^{123a,123b}, M. Volpi⁸⁷, H. von der Schmitt¹⁰⁰, H. von Radziewski⁴⁸, E. von Toerne²¹, V. Vorobel¹²⁸, K. Vorobev⁹⁷, M. Vos¹⁶⁸, R. Voss³⁰, J.H. Vossebeld⁷³, N. Vranjes¹³⁷, M. Vranjes Milosavljevic¹⁰⁶, V. Vrba¹²⁶, M. Vreeswijk¹⁰⁶, T. Vu Anh⁴⁸, R. Vuillemer³⁰, I. Vukotic³¹, Z. Vykydal¹²⁷, P. Wagner²¹, W. Wagner¹⁷⁶, H. Wahlberg⁷⁰, S. Wahrmund⁴⁴, J. Wakabayashi¹⁰², J. Walder⁷¹, R. Walker⁹⁹, W. Walkowiak¹⁴², R. Wall¹⁷⁷, P. Waller⁷³, B. Walsh¹⁷⁷, C. Wang^{152,aj}, C. Wang⁴⁵, F. Wang¹⁷⁴, H. Wang¹⁵, H. Wang⁴⁰, J. Wang⁴², J. Wang^{33a}, K. Wang⁸⁶, R. Wang¹⁰⁴, S.M. Wang¹⁵², T. Wang²¹, X. Wang¹⁷⁷, C. Wanotayaroj¹¹⁵, A. Warburton⁸⁶, C.P. Ward²⁸, D.R. Wardrope⁷⁷, M. Warsinsky⁴⁸, A. Washbrook⁴⁶,

C. Wasicki⁴², P.M. Watkins¹⁸, A.T. Watson¹⁸, I.J. Watson¹⁵¹, M.F. Watson¹⁸, G. Watts¹³⁹, S. Watts⁸³, B.M. Waugh⁷⁷, S. Webb⁸³, M.S. Weber¹⁷, S.W. Weber¹⁷⁵, J.S. Webster³¹, A.R. Weidberg¹¹⁹, P. Weigell¹⁰⁰, B. Weinert⁶⁰, J. Weingarten⁵⁴, C. Weiser⁴⁸, H. Weits¹⁰⁶, P.S. Wells³⁰, T. Wenaus²⁵, D. Wendland¹⁶, Z. Weng^{152,ae}, T. Wengler³⁰, S. Wenig³⁰, N. Vermes²¹, M. Werner⁴⁸, P. Werner³⁰, M. Wessels^{58a}, J. Wetter¹⁶², K. Whalen²⁹, A. White⁸, M.J. White¹, R. White^{32b}, S. White^{123a,123b}, D. Whiteson¹⁶⁴, D. Wicke¹⁷⁶, F.J. Wickens¹³⁰, W. Wiedenmann¹⁷⁴, M. Wielers¹³⁰, P. Wienemann²¹, C. Wiglesworth³⁶, L.A.M. Wiik-Fuchs²¹, P.A. Wijeratne⁷⁷, A. Wildauer¹⁰⁰, M.A. Wildt^{42,ak}, H.G. Wilkens³⁰, J.Z. Will⁹⁹, H.H. Williams¹²¹, S. Williams²⁸, C. Willis⁸⁹, S. Willocq⁸⁵, A. Wilson⁸⁸, J.A. Wilson¹⁸, I. Wingerter-Seez⁵, F. Winklmeier¹¹⁵, B.T. Winter²¹, M. Wittgen¹⁴⁴, T. Wittig⁴³, J. Wittkowski⁹⁹, S.J. Wollstadt⁸², M.W. Wolter³⁹, H. Wolters^{125a,125c}, B.K. Wosiek³⁹, J. Wotschack³⁰, M.J. Woudstra⁸³, K.W. Wozniak³⁹, M. Wright⁵³, M. Wu⁵⁵, S.L. Wu¹⁷⁴, X. Wu⁴⁹, Y. Wu⁸⁸, E. Wulf³⁵, T.R. Wyatt⁸³, B.M. Wynne⁴⁶, S. Xella³⁶, M. Xiao¹³⁷, D. Xu^{33a}, L. Xu^{33b,al}, B. Yabsley¹⁵¹, S. Yacoob^{146b,am}, R. Yakabe⁶⁶, M. Yamada⁶⁵, H. Yamaguchi¹⁵⁶, Y. Yamaguchi¹¹⁷, A. Yamamoto⁶⁵, K. Yamamoto⁶³, S. Yamamoto¹⁵⁶, T. Yamamura¹⁵⁶, T. Yamanaka¹⁵⁶, K. Yamauchi¹⁰², Y. Yamazaki⁶⁶, Z. Yan²², H. Yang^{33e}, H. Yang¹⁷⁴, U.K. Yang⁸³, Y. Yang¹¹⁰, S. Yanush⁹², L. Yao^{33a}, W-M. Yao¹⁵, Y. Yasu⁶⁵, E. Yatsenko⁴², K.H. Yau Wong²¹, J. Ye⁴⁰, S. Ye²⁵, I. Yeletsikh⁶⁴, A.L. Yen⁵⁷, E. Yildirim⁴², M. Yilmaz^{4b}, R. Yoosofmiya¹²⁴, K. Yorita¹⁷², R. Yoshida⁶, K. Yoshihara¹⁵⁶, C. Young¹⁴⁴, C.J.S. Young³⁰, S. Youssef²², D.R. Yu¹⁵, J. Yu⁸, J.M. Yu⁸⁸, J. Yu¹¹³, L. Yuan⁶⁶, A. Yurkewicz¹⁰⁷, I. Yusuff^{28,an}, B. Zabinski³⁹, R. Zaidan⁶², A.M. Zaitsev^{129,aa}, A. Zaman¹⁴⁹, S. Zambito²³, L. Zanello^{133a,133b}, D. Zanzi¹⁰⁰, C. Zeitnitz¹⁷⁶, M. Zeman¹²⁷, A. Zemla^{38a}, K. Zengel²³, O. Zenin¹²⁹, T. Ženiš^{145a}, D. Zerwas¹¹⁶, G. Zevi della Porta⁵⁷, D. Zhang⁸⁸, F. Zhang¹⁷⁴, H. Zhang⁸⁹, J. Zhang⁶, L. Zhang¹⁵², X. Zhang^{33d}, Z. Zhang¹¹⁶, Z. Zhao^{33b}, A. Zhemchugov⁶⁴, J. Zhong¹¹⁹, B. Zhou⁸⁸, L. Zhou³⁵, N. Zhou¹⁶⁴, C.G. Zhu^{33d}, H. Zhu^{33a}, J. Zhu⁸⁸, Y. Zhu^{33b}, X. Zhuang^{33a}, K. Zhukov⁹⁵, A. Zibell¹⁷⁵, D. Zieminska⁶⁰, N.I. Zimine⁶⁴, C. Zimmermann⁸², R. Zimmermann²¹, S. Zimmermann²¹, S. Zimmermann⁴⁸, Z. Zinonos⁵⁴, M. Ziolkowski¹⁴², G. Zobernig¹⁷⁴, A. Zoccoli^{20a,20b}, M. zur Nedden¹⁶, G. Zurzolo^{103a,103b}, V. Zutshi¹⁰⁷, L. Zwalinski³⁰.

¹ Department of Physics, University of Adelaide, Adelaide, Australia

² Physics Department, SUNY Albany, Albany NY, United States of America

³ Department of Physics, University of Alberta, Edmonton AB, Canada

⁴ (a) Department of Physics, Ankara University, Ankara; (b) Department of Physics, Gazi University, Ankara; (c) Division of Physics, TOBB University of Economics and Technology, Ankara; (d) Turkish Atomic Energy Authority, Ankara, Turkey

⁵ LAPP, CNRS/IN2P3 and Université de Savoie, Annecy-le-Vieux, France

⁶ High Energy Physics Division, Argonne National Laboratory, Argonne IL, United States of America

⁷ Department of Physics, University of Arizona, Tucson AZ, United States of America

⁸ Department of Physics, The University of Texas at Arlington, Arlington TX, United States of America

⁹ Physics Department, University of Athens, Athens, Greece

¹⁰ Physics Department, National Technical University of Athens, Zografou, Greece

¹¹ Institute of Physics, Azerbaijan Academy of Sciences, Baku, Azerbaijan

¹² Institut de Física d'Altes Energies and Departament de Física de la Universitat Autònoma de Barcelona, Barcelona, Spain

¹³ (a) Institute of Physics, University of Belgrade, Belgrade; (b) Vinca Institute of Nuclear Sciences, University of Belgrade, Belgrade, Serbia

¹⁴ Department for Physics and Technology, University of Bergen, Bergen, Norway

¹⁵ Physics Division, Lawrence Berkeley National Laboratory and University of California, Berkeley CA, United States of America

¹⁶ Department of Physics, Humboldt University, Berlin, Germany

¹⁷ Albert Einstein Center for Fundamental Physics and Laboratory for High Energy Physics, University of Bern, Bern, Switzerland

¹⁸ School of Physics and Astronomy, University of Birmingham, Birmingham, United Kingdom

¹⁹ (a) Department of Physics, Bogazici University, Istanbul; (b) Department of Physics, Dogus University, Istanbul; (c)

Department of Physics Engineering, Gaziantep University, Gaziantep, Turkey

²⁰ (a) INFN Sezione di Bologna; (b) Dipartimento di Fisica e Astronomia, Università di Bologna, Bologna, Italy

²¹ Physikalisches Institut, University of Bonn, Bonn, Germany

²² Department of Physics, Boston University, Boston MA, United States of America

²³ Department of Physics, Brandeis University, Waltham MA, United States of America

- ²⁴ ^(a) Universidade Federal do Rio De Janeiro COPPE/EE/IF, Rio de Janeiro; ^(b) Federal University of Juiz de Fora (UFJF), Juiz de Fora; ^(c) Federal University of Sao Joao del Rei (UFSJ), Sao Joao del Rei; ^(d) Instituto de Fisica, Universidade de Sao Paulo, Sao Paulo, Brazil
- ²⁵ Physics Department, Brookhaven National Laboratory, Upton NY, United States of America
- ²⁶ ^(a) National Institute of Physics and Nuclear Engineering, Bucharest; ^(b) National Institute for Research and Development of Isotopic and Molecular Technologies, Physics Department, Cluj Napoca; ^(c) University Politehnica Bucharest, Bucharest; ^(d) West University in Timisoara, Timisoara, Romania
- ²⁷ Departamento de Física, Universidad de Buenos Aires, Buenos Aires, Argentina
- ²⁸ Cavendish Laboratory, University of Cambridge, Cambridge, United Kingdom
- ²⁹ Department of Physics, Carleton University, Ottawa ON, Canada
- ³⁰ CERN, Geneva, Switzerland
- ³¹ Enrico Fermi Institute, University of Chicago, Chicago IL, United States of America
- ³² ^(a) Departamento de Física, Pontificia Universidad Católica de Chile, Santiago; ^(b) Departamento de Física, Universidad Técnica Federico Santa María, Valparaíso, Chile
- ³³ ^(a) Institute of High Energy Physics, Chinese Academy of Sciences, Beijing; ^(b) Department of Modern Physics, University of Science and Technology of China, Anhui; ^(c) Department of Physics, Nanjing University, Jiangsu; ^(d) School of Physics, Shandong University, Shandong; ^(e) Physics Department, Shanghai Jiao Tong University, Shanghai, China
- ³⁴ Laboratoire de Physique Corpusculaire, Clermont Université and Université Blaise Pascal and CNRS/IN2P3, Clermont-Ferrand, France
- ³⁵ Nevis Laboratory, Columbia University, Irvington NY, United States of America
- ³⁶ Niels Bohr Institute, University of Copenhagen, Kobenhavn, Denmark
- ³⁷ ^(a) INFN Gruppo Collegato di Cosenza, Laboratori Nazionali di Frascati; ^(b) Dipartimento di Fisica, Università della Calabria, Rende, Italy
- ³⁸ ^(a) AGH University of Science and Technology, Faculty of Physics and Applied Computer Science, Krakow; ^(b) Marian Smoluchowski Institute of Physics, Jagiellonian University, Krakow, Poland
- ³⁹ The Henryk Niewodniczanski Institute of Nuclear Physics, Polish Academy of Sciences, Krakow, Poland
- ⁴⁰ Physics Department, Southern Methodist University, Dallas TX, United States of America
- ⁴¹ Physics Department, University of Texas at Dallas, Richardson TX, United States of America
- ⁴² DESY, Hamburg and Zeuthen, Germany
- ⁴³ Institut für Experimentelle Physik IV, Technische Universität Dortmund, Dortmund, Germany
- ⁴⁴ Institut für Kern- und Teilchenphysik, Technische Universität Dresden, Dresden, Germany
- ⁴⁵ Department of Physics, Duke University, Durham NC, United States of America
- ⁴⁶ SUPA - School of Physics and Astronomy, University of Edinburgh, Edinburgh, United Kingdom
- ⁴⁷ INFN Laboratori Nazionali di Frascati, Frascati, Italy
- ⁴⁸ Fakultät für Mathematik und Physik, Albert-Ludwigs-Universität, Freiburg, Germany
- ⁴⁹ Section de Physique, Université de Genève, Geneva, Switzerland
- ⁵⁰ ^(a) INFN Sezione di Genova; ^(b) Dipartimento di Fisica, Università di Genova, Genova, Italy
- ⁵¹ ^(a) E. Andronikashvili Institute of Physics, Iv. Javakhishvili Tbilisi State University, Tbilisi; ^(b) High Energy Physics Institute, Tbilisi State University, Tbilisi, Georgia
- ⁵² II Physikalisches Institut, Justus-Liebig-Universität Giessen, Giessen, Germany
- ⁵³ SUPA - School of Physics and Astronomy, University of Glasgow, Glasgow, United Kingdom
- ⁵⁴ II Physikalisches Institut, Georg-August-Universität, Göttingen, Germany
- ⁵⁵ Laboratoire de Physique Subatomique et de Cosmologie, Université Grenoble-Alpes, CNRS/IN2P3, Grenoble, France
- ⁵⁶ Department of Physics, Hampton University, Hampton VA, United States of America
- ⁵⁷ Laboratory for Particle Physics and Cosmology, Harvard University, Cambridge MA, United States of America
- ⁵⁸ ^(a) Kirchhoff-Institut für Physik, Ruprecht-Karls-Universität Heidelberg, Heidelberg; ^(b) Physikalisches Institut, Ruprecht-Karls-Universität Heidelberg, Heidelberg; ^(c) ZITI Institut für technische Informatik, Ruprecht-Karls-Universität Heidelberg, Mannheim, Germany
- ⁵⁹ Faculty of Applied Information Science, Hiroshima Institute of Technology, Hiroshima, Japan
- ⁶⁰ Department of Physics, Indiana University, Bloomington IN, United States of America
- ⁶¹ Institut für Astro- und Teilchenphysik, Leopold-Franzens-Universität, Innsbruck, Austria
- ⁶² University of Iowa, Iowa City IA, United States of America
- ⁶³ Department of Physics and Astronomy, Iowa State University, Ames IA, United States of America

- ⁶⁴ Joint Institute for Nuclear Research, JINR Dubna, Dubna, Russia
- ⁶⁵ KEK, High Energy Accelerator Research Organization, Tsukuba, Japan
- ⁶⁶ Graduate School of Science, Kobe University, Kobe, Japan
- ⁶⁷ Faculty of Science, Kyoto University, Kyoto, Japan
- ⁶⁸ Kyoto University of Education, Kyoto, Japan
- ⁶⁹ Department of Physics, Kyushu University, Fukuoka, Japan
- ⁷⁰ Instituto de Física La Plata, Universidad Nacional de La Plata and CONICET, La Plata, Argentina
- ⁷¹ Physics Department, Lancaster University, Lancaster, United Kingdom
- ⁷² ^(a) INFN Sezione di Lecce; ^(b) Dipartimento di Matematica e Fisica, Università del Salento, Lecce, Italy
- ⁷³ Oliver Lodge Laboratory, University of Liverpool, Liverpool, United Kingdom
- ⁷⁴ Department of Physics, Jožef Stefan Institute and University of Ljubljana, Ljubljana, Slovenia
- ⁷⁵ School of Physics and Astronomy, Queen Mary University of London, London, United Kingdom
- ⁷⁶ Department of Physics, Royal Holloway University of London, Surrey, United Kingdom
- ⁷⁷ Department of Physics and Astronomy, University College London, London, United Kingdom
- ⁷⁸ Louisiana Tech University, Ruston LA, United States of America
- ⁷⁹ Laboratoire de Physique Nucléaire et de Hautes Energies, UPMC and Université Paris-Diderot and CNRS/IN2P3, Paris, France
- ⁸⁰ Fysiska institutionen, Lunds universitet, Lund, Sweden
- ⁸¹ Departamento de Física Teórica C-15, Universidad Autónoma de Madrid, Madrid, Spain
- ⁸² Institut für Physik, Universität Mainz, Mainz, Germany
- ⁸³ School of Physics and Astronomy, University of Manchester, Manchester, United Kingdom
- ⁸⁴ CPPM, Aix-Marseille Université and CNRS/IN2P3, Marseille, France
- ⁸⁵ Department of Physics, University of Massachusetts, Amherst MA, United States of America
- ⁸⁶ Department of Physics, McGill University, Montreal QC, Canada
- ⁸⁷ School of Physics, University of Melbourne, Victoria, Australia
- ⁸⁸ Department of Physics, The University of Michigan, Ann Arbor MI, United States of America
- ⁸⁹ Department of Physics and Astronomy, Michigan State University, East Lansing MI, United States of America
- ⁹⁰ ^(a) INFN Sezione di Milano; ^(b) Dipartimento di Fisica, Università di Milano, Milano, Italy
- ⁹¹ B.I. Stepanov Institute of Physics, National Academy of Sciences of Belarus, Minsk, Republic of Belarus
- ⁹² National Scientific and Educational Centre for Particle and High Energy Physics, Minsk, Republic of Belarus
- ⁹³ Department of Physics, Massachusetts Institute of Technology, Cambridge MA, United States of America
- ⁹⁴ Group of Particle Physics, University of Montreal, Montreal QC, Canada
- ⁹⁵ P.N. Lebedev Institute of Physics, Academy of Sciences, Moscow, Russia
- ⁹⁶ Institute for Theoretical and Experimental Physics (ITEP), Moscow, Russia
- ⁹⁷ Moscow Engineering and Physics Institute (MEPhI), Moscow, Russia
- ⁹⁸ D.V.Skobeltzyn Institute of Nuclear Physics, M.V.Lomonosov Moscow State University, Moscow, Russia
- ⁹⁹ Fakultät für Physik, Ludwig-Maximilians-Universität München, München, Germany
- ¹⁰⁰ Max-Planck-Institut für Physik (Werner-Heisenberg-Institut), München, Germany
- ¹⁰¹ Nagasaki Institute of Applied Science, Nagasaki, Japan
- ¹⁰² Graduate School of Science and Kobayashi-Maskawa Institute, Nagoya University, Nagoya, Japan
- ¹⁰³ ^(a) INFN Sezione di Napoli; ^(b) Dipartimento di Fisica, Università di Napoli, Napoli, Italy
- ¹⁰⁴ Department of Physics and Astronomy, University of New Mexico, Albuquerque NM, United States of America
- ¹⁰⁵ Institute for Mathematics, Astrophysics and Particle Physics, Radboud University Nijmegen/Nikhef, Nijmegen, Netherlands
- ¹⁰⁶ Nikhef National Institute for Subatomic Physics and University of Amsterdam, Amsterdam, Netherlands
- ¹⁰⁷ Department of Physics, Northern Illinois University, DeKalb IL, United States of America
- ¹⁰⁸ Budker Institute of Nuclear Physics, SB RAS, Novosibirsk, Russia
- ¹⁰⁹ Department of Physics, New York University, New York NY, United States of America
- ¹¹⁰ Ohio State University, Columbus OH, United States of America
- ¹¹¹ Faculty of Science, Okayama University, Okayama, Japan
- ¹¹² Homer L. Dodge Department of Physics and Astronomy, University of Oklahoma, Norman OK, United States of America
- ¹¹³ Department of Physics, Oklahoma State University, Stillwater OK, United States of America

- 114 Palacký University, RCPTM, Olomouc, Czech Republic
- 115 Center for High Energy Physics, University of Oregon, Eugene OR, United States of America
- 116 LAL, Université Paris-Sud and CNRS/IN2P3, Orsay, France
- 117 Graduate School of Science, Osaka University, Osaka, Japan
- 118 Department of Physics, University of Oslo, Oslo, Norway
- 119 Department of Physics, Oxford University, Oxford, United Kingdom
- 120 ^(a) INFN Sezione di Pavia; ^(b) Dipartimento di Fisica, Università di Pavia, Pavia, Italy
- 121 Department of Physics, University of Pennsylvania, Philadelphia PA, United States of America
- 122 Petersburg Nuclear Physics Institute, Gatchina, Russia
- 123 ^(a) INFN Sezione di Pisa; ^(b) Dipartimento di Fisica E. Fermi, Università di Pisa, Pisa, Italy
- 124 Department of Physics and Astronomy, University of Pittsburgh, Pittsburgh PA, United States of America
- 125 ^(a) Laboratório de Instrumentação e Física Experimental de Partículas - LIP, Lisboa; ^(b) Faculdade de Ciências, Universidade de Lisboa, Lisboa; ^(c) Department of Physics, University of Coimbra, Coimbra; ^(d) Centro de Física Nuclear da Universidade de Lisboa, Lisboa; ^(e) Departamento de Física, Universidade do Minho, Braga; ^(f) Departamento de Física Teórica y del Cosmos and CAFPE, Universidad de Granada, Granada (Spain); ^(g) Dep Física and CEFITEC of Faculdade de Ciências e Tecnologia, Universidade Nova de Lisboa, Caparica, Portugal
- 126 Institute of Physics, Academy of Sciences of the Czech Republic, Praha, Czech Republic
- 127 Czech Technical University in Prague, Praha, Czech Republic
- 128 Faculty of Mathematics and Physics, Charles University in Prague, Praha, Czech Republic
- 129 State Research Center Institute for High Energy Physics, Protvino, Russia
- 130 Particle Physics Department, Rutherford Appleton Laboratory, Didcot, United Kingdom
- 131 Physics Department, University of Regina, Regina SK, Canada
- 132 Ritsumeikan University, Kusatsu, Shiga, Japan
- 133 ^(a) INFN Sezione di Roma; ^(b) Dipartimento di Fisica, Sapienza Università di Roma, Roma, Italy
- 134 ^(a) INFN Sezione di Roma Tor Vergata; ^(b) Dipartimento di Fisica, Università di Roma Tor Vergata, Roma, Italy
- 135 ^(a) INFN Sezione di Roma Tre; ^(b) Dipartimento di Matematica e Fisica, Università Roma Tre, Roma, Italy
- 136 ^(a) Faculté des Sciences Ain Chock, Réseau Universitaire de Physique des Hautes Energies - Université Hassan II, Casablanca; ^(b) Centre National de l'Energie des Sciences Techniques Nucleaires, Rabat; ^(c) Faculté des Sciences Semlalia, Université Cadi Ayyad, LPHEA-Marrakech; ^(d) Faculté des Sciences, Université Mohamed Premier and LPTPM, Oujda; ^(e) Faculté des sciences, Université Mohammed V-Agdal, Rabat, Morocco
- 137 DSM/IRFU (Institut de Recherches sur les Lois Fondamentales de l'Univers), CEA Saclay (Commissariat à l'Energie Atomique et aux Energies Alternatives), Gif-sur-Yvette, France
- 138 Santa Cruz Institute for Particle Physics, University of California Santa Cruz, Santa Cruz CA, United States of America
- 139 Department of Physics, University of Washington, Seattle WA, United States of America
- 140 Department of Physics and Astronomy, University of Sheffield, Sheffield, United Kingdom
- 141 Department of Physics, Shinshu University, Nagano, Japan
- 142 Fachbereich Physik, Universität Siegen, Siegen, Germany
- 143 Department of Physics, Simon Fraser University, Burnaby BC, Canada
- 144 SLAC National Accelerator Laboratory, Stanford CA, United States of America
- 145 ^(a) Faculty of Mathematics, Physics & Informatics, Comenius University, Bratislava; ^(b) Department of Subnuclear Physics, Institute of Experimental Physics of the Slovak Academy of Sciences, Kosice, Slovak Republic
- 146 ^(a) Department of Physics, University of Cape Town, Cape Town; ^(b) Department of Physics, University of Johannesburg, Johannesburg; ^(c) School of Physics, University of the Witwatersrand, Johannesburg, South Africa
- 147 ^(a) Department of Physics, Stockholm University; ^(b) The Oskar Klein Centre, Stockholm, Sweden
- 148 Physics Department, Royal Institute of Technology, Stockholm, Sweden
- 149 Departments of Physics & Astronomy and Chemistry, Stony Brook University, Stony Brook NY, United States of America
- 150 Department of Physics and Astronomy, University of Sussex, Brighton, United Kingdom
- 151 School of Physics, University of Sydney, Sydney, Australia
- 152 Institute of Physics, Academia Sinica, Taipei, Taiwan
- 153 Department of Physics, Technion: Israel Institute of Technology, Haifa, Israel
- 154 Raymond and Beverly Sackler School of Physics and Astronomy, Tel Aviv University, Tel Aviv, Israel
- 155 Department of Physics, Aristotle University of Thessaloniki, Thessaloniki, Greece

- ¹⁵⁶ International Center for Elementary Particle Physics and Department of Physics, The University of Tokyo, Tokyo, Japan
- ¹⁵⁷ Graduate School of Science and Technology, Tokyo Metropolitan University, Tokyo, Japan
- ¹⁵⁸ Department of Physics, Tokyo Institute of Technology, Tokyo, Japan
- ¹⁵⁹ Department of Physics, University of Toronto, Toronto ON, Canada
- ¹⁶⁰ ^(a) TRIUMF, Vancouver BC; ^(b) Department of Physics and Astronomy, York University, Toronto ON, Canada
- ¹⁶¹ Faculty of Pure and Applied Sciences, University of Tsukuba, Tsukuba, Japan
- ¹⁶² Department of Physics and Astronomy, Tufts University, Medford MA, United States of America
- ¹⁶³ Centro de Investigaciones, Universidad Antonio Narino, Bogota, Colombia
- ¹⁶⁴ Department of Physics and Astronomy, University of California Irvine, Irvine CA, United States of America
- ¹⁶⁵ ^(a) INFN Gruppo Collegato di Udine, Sezione di Trieste, Udine; ^(b) ICTP, Trieste; ^(c) Dipartimento di Chimica, Fisica e Ambiente, Università di Udine, Udine, Italy
- ¹⁶⁶ Department of Physics, University of Illinois, Urbana IL, United States of America
- ¹⁶⁷ Department of Physics and Astronomy, University of Uppsala, Uppsala, Sweden
- ¹⁶⁸ Instituto de Física Corpuscular (IFIC) and Departamento de Física Atómica, Molecular y Nuclear and Departamento de Ingeniería Electrónica and Instituto de Microelectrónica de Barcelona (IMB-CNM), University of Valencia and CSIC, Valencia, Spain
- ¹⁶⁹ Department of Physics, University of British Columbia, Vancouver BC, Canada
- ¹⁷⁰ Department of Physics and Astronomy, University of Victoria, Victoria BC, Canada
- ¹⁷¹ Department of Physics, University of Warwick, Coventry, United Kingdom
- ¹⁷² Waseda University, Tokyo, Japan
- ¹⁷³ Department of Particle Physics, The Weizmann Institute of Science, Rehovot, Israel
- ¹⁷⁴ Department of Physics, University of Wisconsin, Madison WI, United States of America
- ¹⁷⁵ Fakultät für Physik und Astronomie, Julius-Maximilians-Universität, Würzburg, Germany
- ¹⁷⁶ Fachbereich C Physik, Bergische Universität Wuppertal, Wuppertal, Germany
- ¹⁷⁷ Department of Physics, Yale University, New Haven CT, United States of America
- ¹⁷⁸ Yerevan Physics Institute, Yerevan, Armenia
- ¹⁷⁹ Centre de Calcul de l'Institut National de Physique Nucléaire et de Physique des Particules (IN2P3), Villeurbanne, France
- ^a Also at Department of Physics, King's College London, London, United Kingdom
- ^b Also at Institute of Physics, Azerbaijan Academy of Sciences, Baku, Azerbaijan
- ^c Also at Particle Physics Department, Rutherford Appleton Laboratory, Didcot, United Kingdom
- ^d Also at TRIUMF, Vancouver BC, Canada
- ^e Also at Department of Physics, California State University, Fresno CA, United States of America
- ^f Also at Tomsk State University, Tomsk, Russia
- ^g Also at CPPM, Aix-Marseille Université and CNRS/IN2P3, Marseille, France
- ^h Also at Università di Napoli Parthenope, Napoli, Italy
- ⁱ Also at Institute of Particle Physics (IPP), Canada
- ^j Also at Department of Physics, St. Petersburg State Polytechnical University, St. Petersburg, Russia
- ^k Also at Chinese University of Hong Kong, China
- ^l Also at Department of Financial and Management Engineering, University of the Aegean, Chios, Greece
- ^m Also at Louisiana Tech University, Ruston LA, United States of America
- ⁿ Also at Institutio Catalana de Recerca i Estudis Avancats, ICREA, Barcelona, Spain
- ^o Also at Department of Physics, The University of Texas at Austin, Austin TX, United States of America
- ^p Also at Institute of Theoretical Physics, Ilia State University, Tbilisi, Georgia
- ^q Also at CERN, Geneva, Switzerland
- ^r Also at Ochadai Academic Production, Ochanomizu University, Tokyo, Japan
- ^s Also at Manhattan College, New York NY, United States of America
- ^t Also at Novosibirsk State University, Novosibirsk, Russia
- ^u Also at Institute of Physics, Academia Sinica, Taipei, Taiwan
- ^v Also at LAL, Université Paris-Sud and CNRS/IN2P3, Orsay, France
- ^w Also at Academia Sinica Grid Computing, Institute of Physics, Academia Sinica, Taipei, Taiwan
- ^x Also at Laboratoire de Physique Nucléaire et de Hautes Energies, UPMC and Université Paris-Diderot and CNRS/IN2P3, Paris, France

-
- ^y Also at School of Physical Sciences, National Institute of Science Education and Research, Bhubaneswar, India
- ^z Also at Dipartimento di Fisica, Sapienza Università di Roma, Roma, Italy
- ^{aa} Also at Moscow Institute of Physics and Technology State University, Dolgoprudny, Russia
- ^{ab} Also at Section de Physique, Université de Genève, Geneva, Switzerland
- ^{ac} Also at International School for Advanced Studies (SISSA), Trieste, Italy
- ^{ad} Also at Department of Physics and Astronomy, University of South Carolina, Columbia SC, United States of America
- ^{ae} Also at School of Physics and Engineering, Sun Yat-sen University, Guangzhou, China
- ^{af} Also at Faculty of Physics, M.V.Lomonosov Moscow State University, Moscow, Russia
- ^{ag} Also at Moscow Engineering and Physics Institute (MEPhI), Moscow, Russia
- ^{ah} Also at Institute for Particle and Nuclear Physics, Wigner Research Centre for Physics, Budapest, Hungary
- ^{ai} Also at Department of Physics, Oxford University, Oxford, United Kingdom
- ^{aj} Also at Department of Physics, Nanjing University, Jiangsu, China
- ^{ak} Also at Institut für Experimentalphysik, Universität Hamburg, Hamburg, Germany
- ^{al} Also at Department of Physics, The University of Michigan, Ann Arbor MI, United States of America
- ^{am} Also at Discipline of Physics, University of KwaZulu-Natal, Durban, South Africa
- ^{an} Also at University of Malaya, Department of Physics, Kuala Lumpur, Malaysia
- * Deceased